olivier.sandre@u-bordeaux.fr
@olive_free

MAGNETIC NANOPARTICLES: SYNTHESIS, PROPERTIES AND BIOMEDICAL APPLICATIONS

Olivier Sandre, senior CNRS researcher at Univ. Bordeaux, France

Magnetic nanoparticles (MNPs) Part 2: Biological applications

- Introduction: why combining polymers and magnetic nanoparticles?
- Magnetic polymer vesicles: tumor homing, MRI and magnetic drug-delivery
- Magnetic polymer micelles: magnetic cyto-toxicity and the puzzle of “cold hyperthermia” $\rightarrow$ Need of analysis method at sub-cellular scales (µm, nm…)
- Magnetic hyperthermia to induce bio-luminescence $\leftrightarrow$ thermal dose
- Grafting of thermosensitive polymers onto iron oxide: synthetic or “biomimetic” polymers (recombinant elastin-like peptides)
- Use to probe temperature by the MRI (positive) contrast

Part 2 (Biological applications): MNPs as MRI contrast agents

- Basic principles of Magnetic Resonance Imaging
- Proton relaxing properties of individual nanoparticles (USPIOs)
- Proton relaxing properties of MNPs clustered by polymer chains (SPIONs) : Applications for magnetic guiding and MRI contrast enhancement
- Relaxivity of more complex shapes: rodlike (magnetic 'nanoworms', magnetic nanogels, magnetic micelles or vesicles (polymersomes)…

Applications of MNPs to Magnetic Resonance Imaging

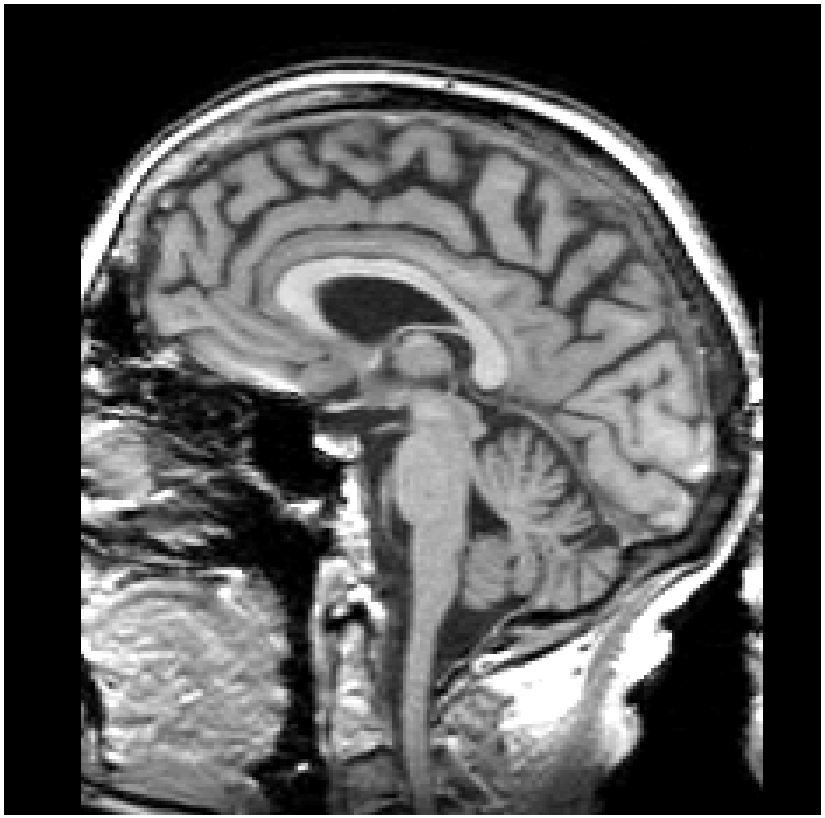

→ NMR : Purcell et Bloch (1946)
→ First NMR Images using gradients: Lauterbur & Mansfield (1973)
→ First Human Head (1979)
→ Nobel Prize in Medecine (2003): Lauterbur & Mansfield

"Negative" Contrast Agents

Microscopic outer sphere theory

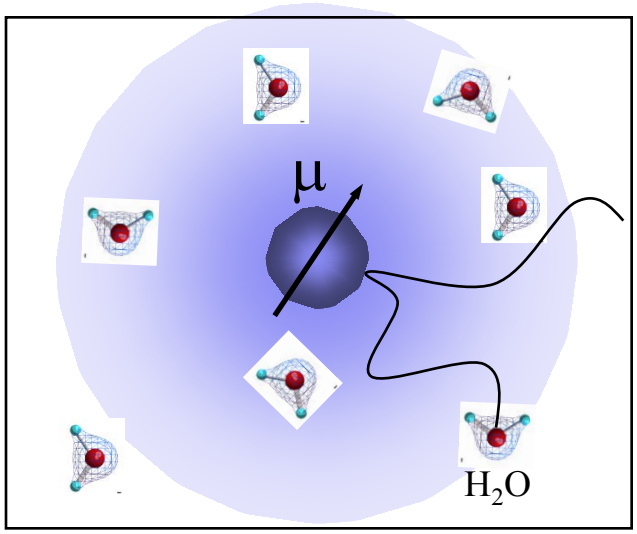

Diffusion of water molecules around magnetic particles

$$\frac{1}{T_{1,2}} = \frac{1}{T_{1,2}^{int}} + R_{1,2}[Conc.]$$

T_1 : longitudinal relax. time
T_2 : transverse relax. time
$R_{1,2}$: relaxivity

(Gillis, Koenig, *Magn. Res. Med.* 1987)

MRI enables to see inside your brain!

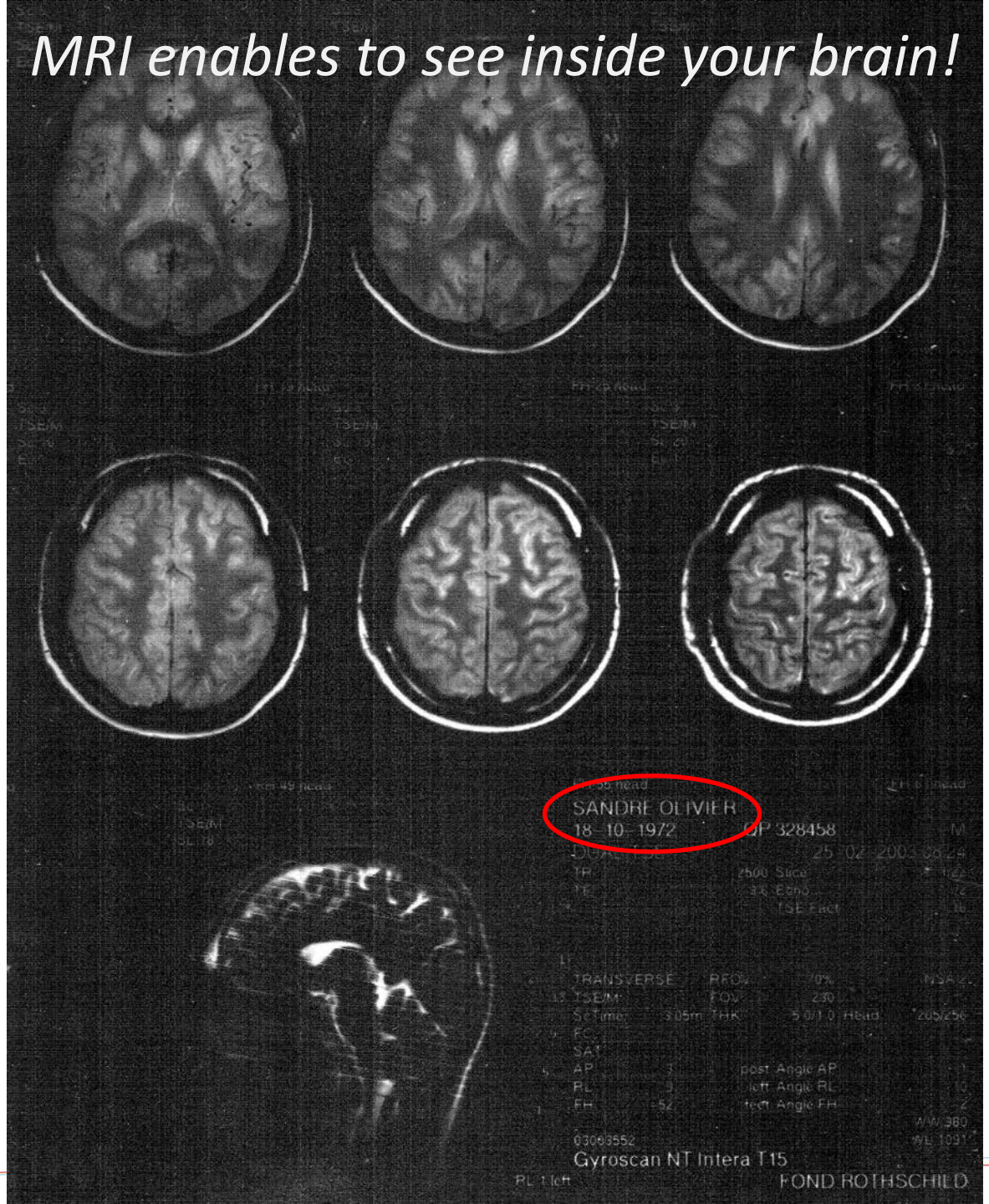

Magnetic Resonance Imaging

MRI images originate from differences in relaxation times of protons in tissues
Contrast depends on the RF pulses sequence (T_2 *vs* T_1-weighting)

T_2(*)-weighted
T_E>120ms, T_R>2.5s

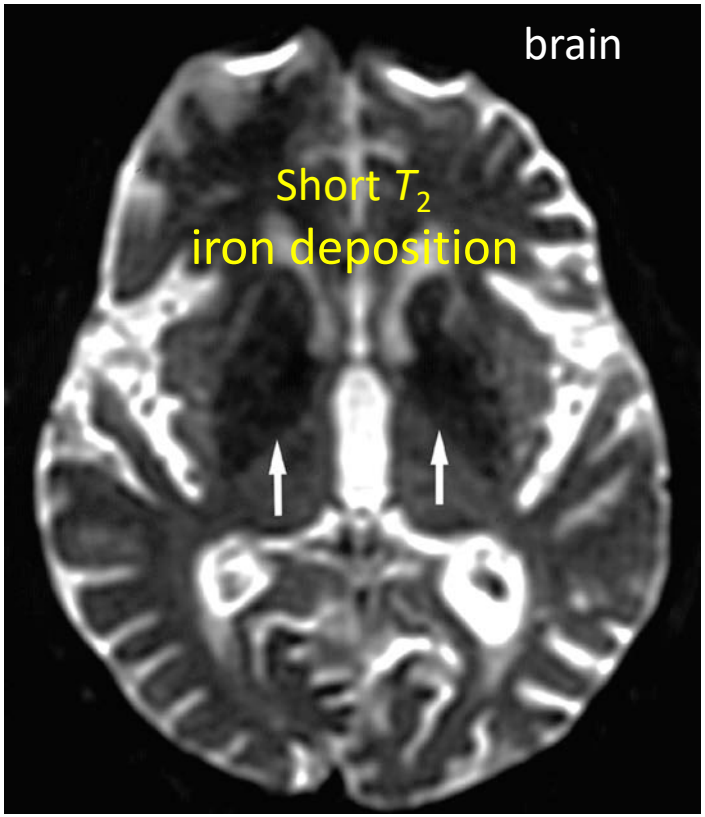

T_1-weighted
T_E<20ms, T_R<600ms

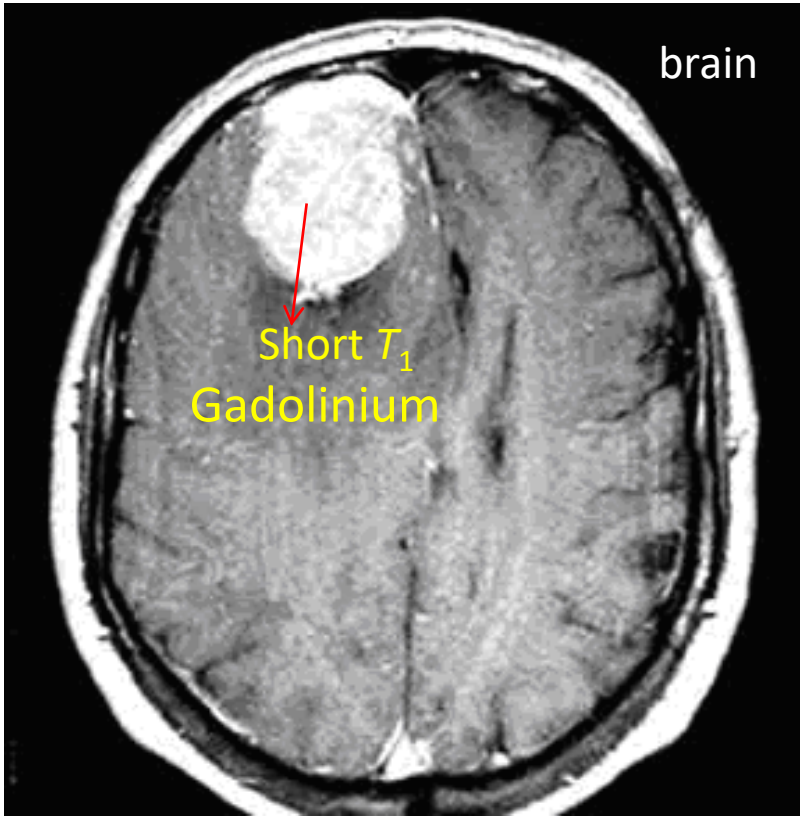

Hiwatashi A et al. *Am J Roentgenol* 2003; **181**: 1705–1709.

Magnetic NPs as MRI positive/negative contrast agents

University of MONS (Belgium) molecular NMR and biophysics labs

Y. Gossuin et al., *WIRE Nanomed Nanobiotech.* **2008,** *1*, 299; S. Laurent et al. *Chem. Rev.* **2008,** 108, 2064

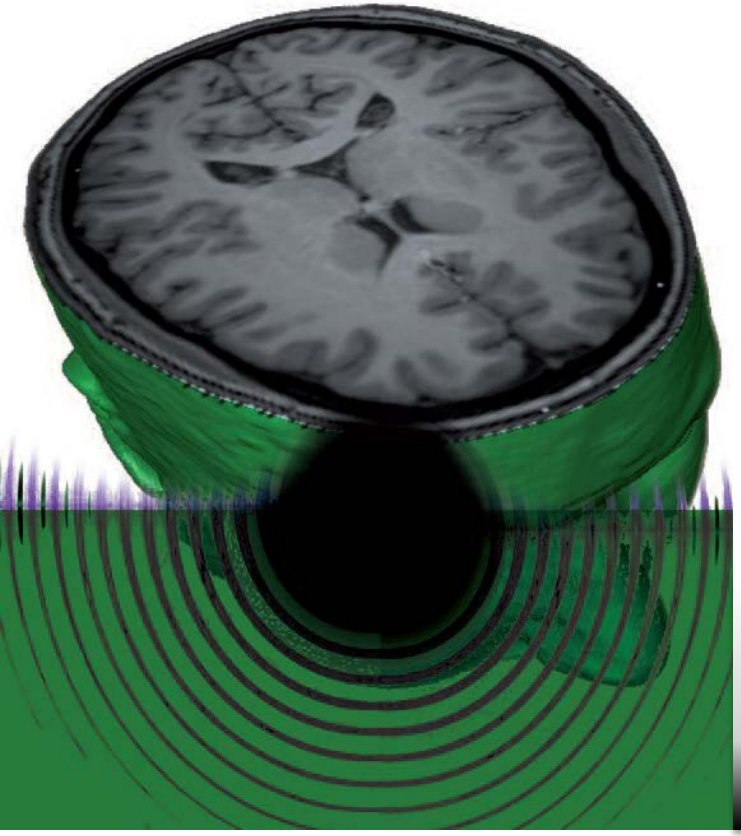

r_2/r_1

T_2 c.a. >10

T_1 c.a. ~ 1-2

"Outer Sphere" model:

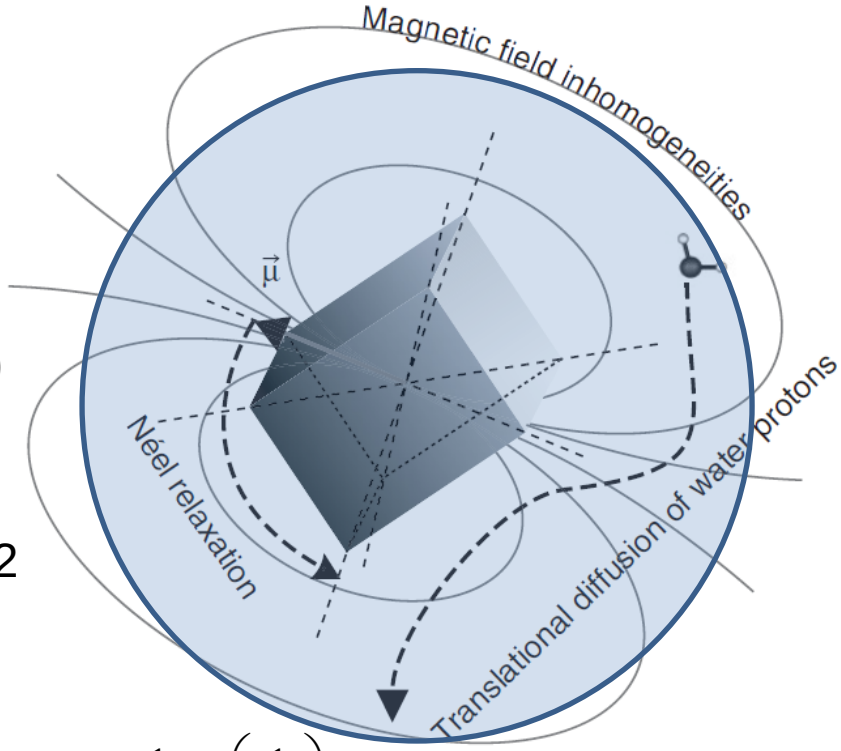

MRI based on the spin-echo sequence:

$$S_{\mathrm{MRI}} \propto \rho_{\mathrm{H}} \left(1 - e^{-TR/T_1}\right) \cdot e^{-TE/T_2}$$

T_1-weighted: *TR*=100 ms *TE*=2.8 ms flip angle =70°
T_2-weighted: *TR*=300 ms *TE*=12 ms

$$R_2 = \frac{1}{T_2} = \left(\frac{1}{T_2}\right)_0 \times \left(1 + r_2 \cdot [\mathrm{Fe}]\right)$$

$s^{-1} \cdot mM_{Fe}^{-1}$

→ relaxometric experiments to predict MRI contrast

Signal in MRI: recall of NMR basics

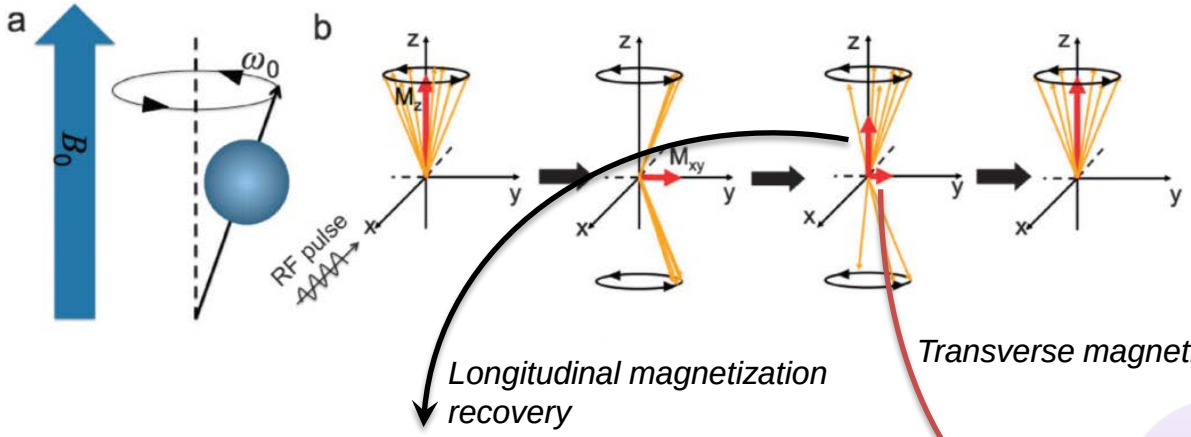

- Applied B_1 radio frequency pulse at ω_0
- Energy supply creates excitation which flips Mz from the z-axis towards the xy-plane

T_1 relaxation

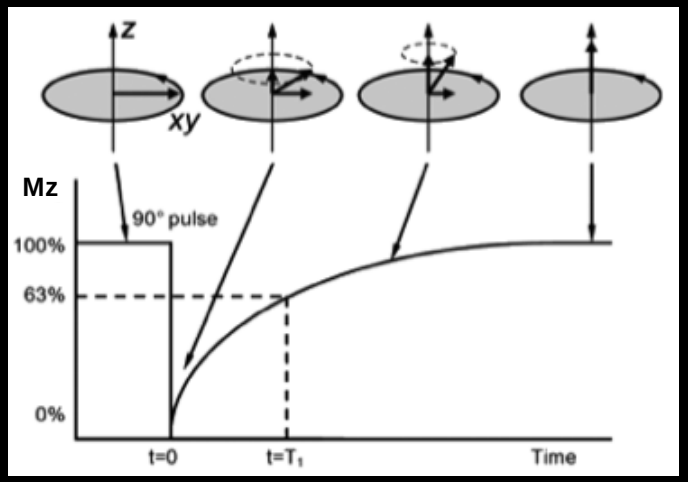

T_1 (spin–lattice) relaxation time = measure of the time required to regain longitudinal magnetization

T_2 relaxation

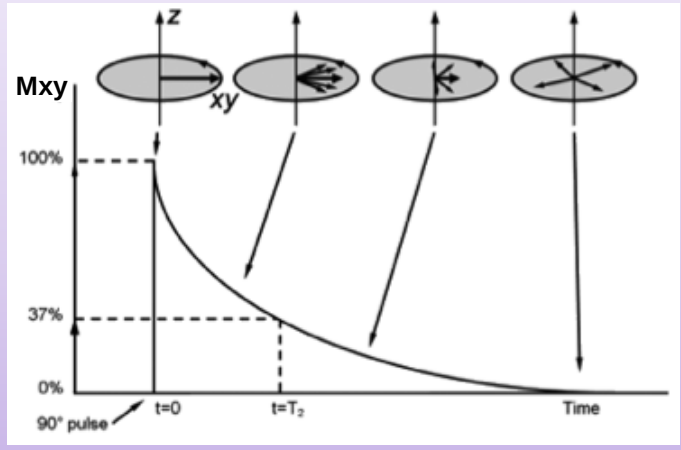

T_2 (spin–spin) relaxation time = measure of the time required to regain decoherence of the transverse nuclear spin magnetization

HA Sharma, Acta Neuropsychiatrica 2009: 21:200-201

Simplest MRI sequence: spin-echo

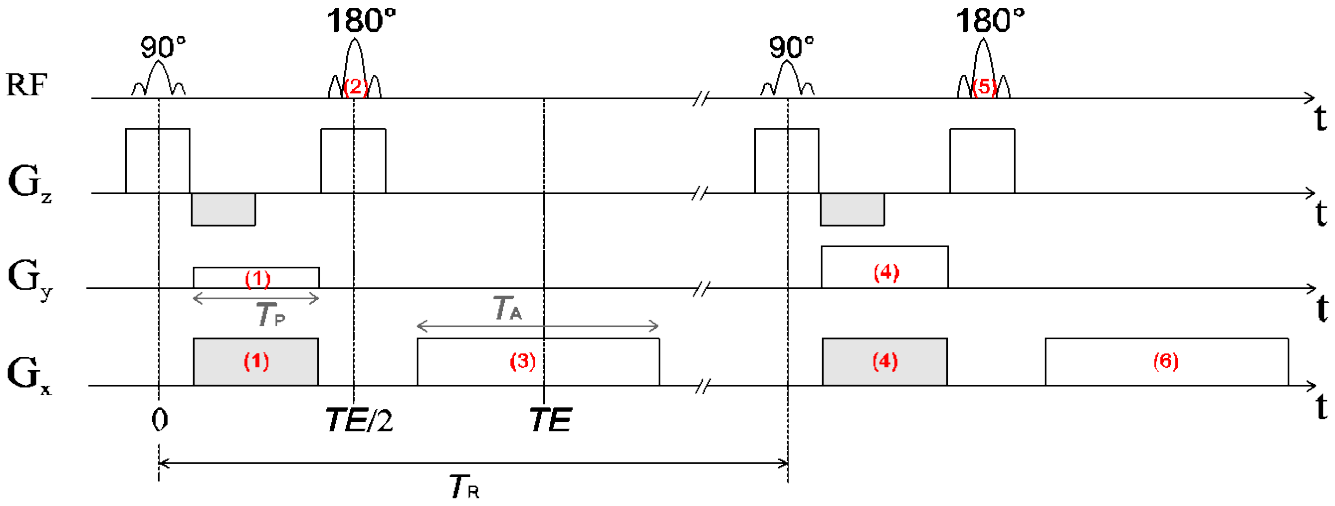

SPIN ECHO

$$I = M_0 \left[1 - exp\left(-\frac{TR}{T_1}\right)\right] exp\left(-\frac{TE}{T_2}\right)$$

T_1-weighted image → short TR (typically < 500ms)

T_2-weighted image → long TE (typically > 60ms)

(U)SPIOs as MRI contrast agents

"Outer Sphere" model:

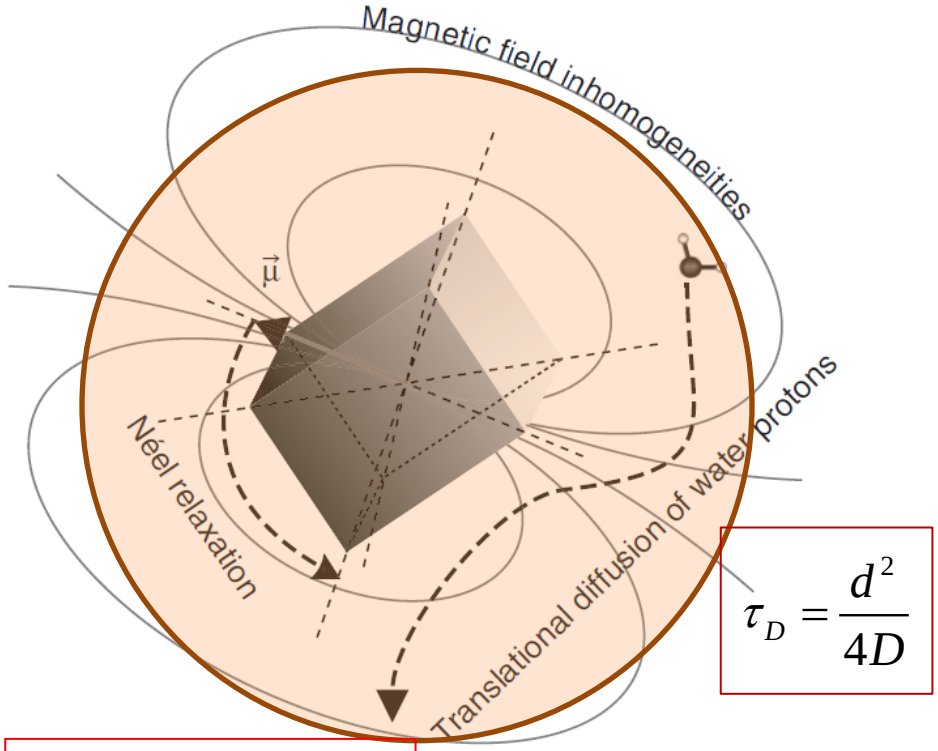

$$\tau_D = \frac{d^2}{4D}$$

$$R_2 = \frac{16}{45}\tau_D f(\Delta\omega)^2$$

$$\Delta\omega = \frac{\gamma \mu_0 M_v}{3}$$

$$\Delta\omega\tau_D < 1$$

Signal for a spin-echo sequence:

$$S_{MRI} \propto \rho_H \left(1 - e^{-TR/T_1}\right) \cdot e^{-TE/T_2}$$

r_2/r_1

T_2 c.a. >10

T_1 c.a. ~ 1-2

$$R_2 = \frac{1}{T_2} = \left(\frac{1}{T_2}\right)_0 \times (1 + r_2 \cdot [Fe])$$

$s^{-1} \cdot mM_{Fe}^{-1}$

→ relaxometric experiments to predict MRI contrast

Y. Gossuin, P. Gillis, A. Hocq, Q. L Vuong, A. Roch **(U Mons, Belgium)** *WIRE Nanomed. Nanobiotech.* 2008, *1*, 299

T_2 relaxivity as a function of magnetic core size for USPIOs

Collaboration with Lam Vuong & Yves Gossuin, Mons, Belgium

$$\frac{r_2}{m_s^2}$$

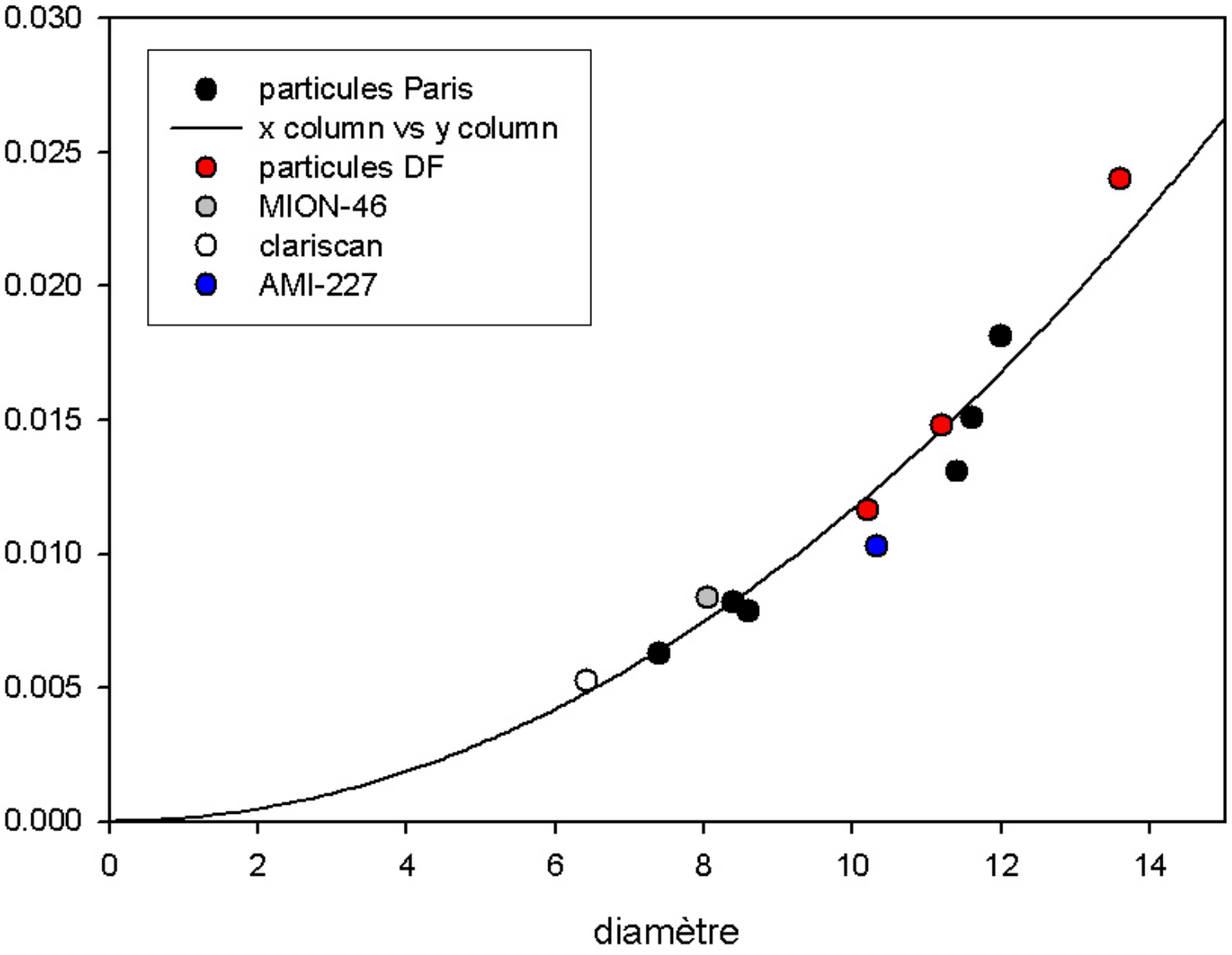

Can one predict T_2 relaxivity of clustered USPIOs (SPIOs)?

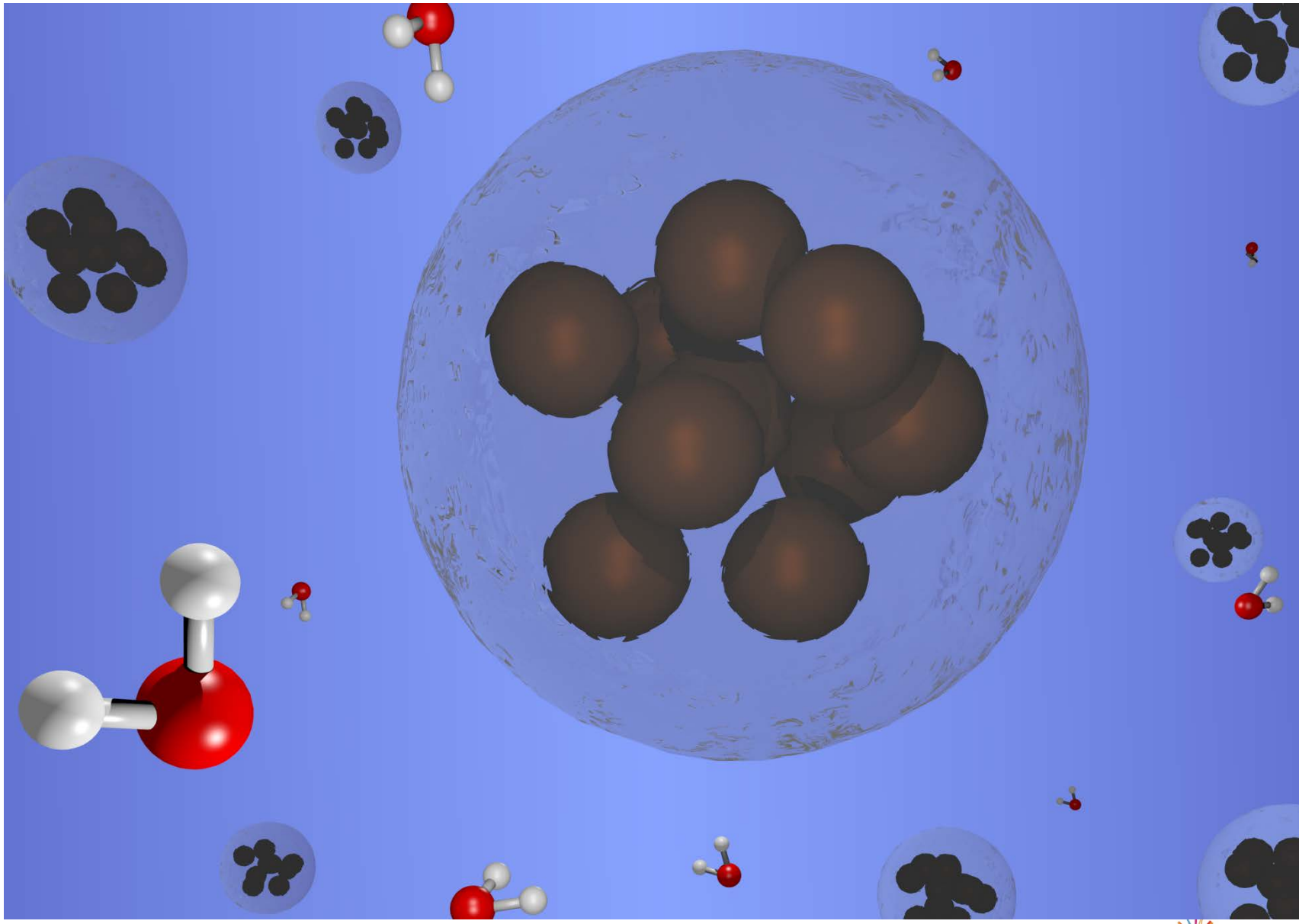

Scaling laws vs. exact laws…

- Analytic solutions of equations in Physics or phenomenological (empirical) laws in engineering sciences → very precise but only in their validity range

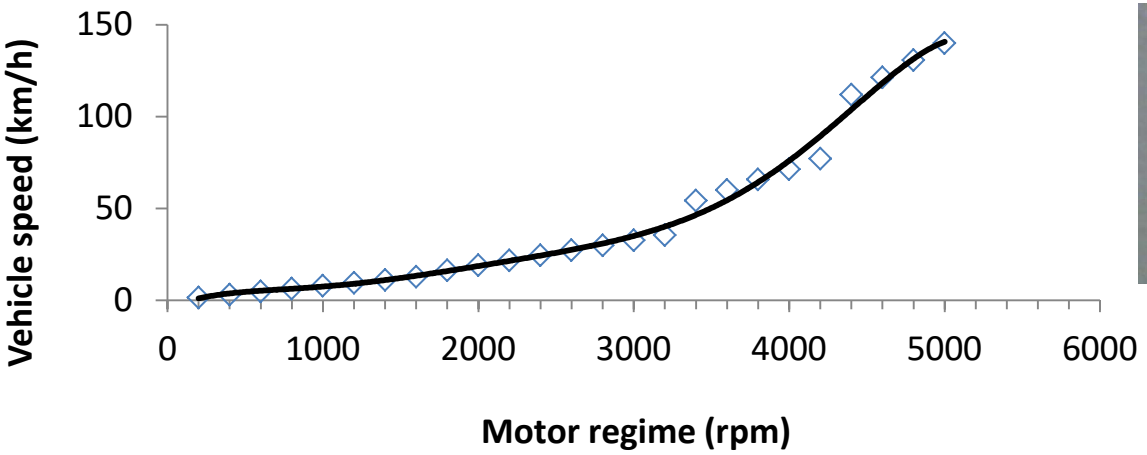

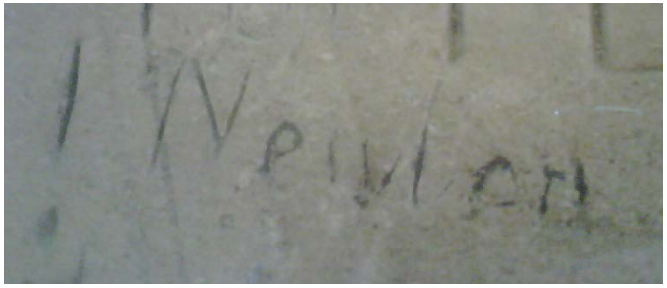

Isaac NEWTON (1687),
Philosophiae Naturalis Principia Mathematica

- Numerous examples of scaling law in polymer science, *eg.* lamellar period for diblock copolymers → approximate but predictive over a wide range

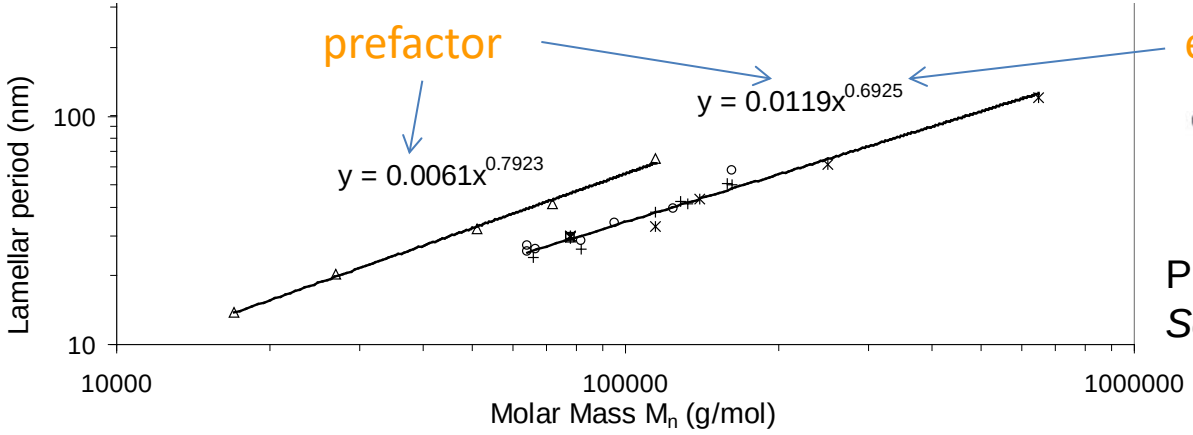

Pierre-Gilles de GENNES (1979)
Scaling concepts in polymer physics

Correct normalization of relaxometric data

in the "Motional Averaging Regime"

$$R_2 = \frac{16}{45}\tau_D f(\Delta\omega)^2 \qquad \Delta\omega\tau_D < 1$$

$$\tau_D = \frac{d^2}{4D} \qquad \Delta\omega = \frac{\gamma\mu_0 M_v}{3}$$

volume fraction (no unit)

$$\frac{f}{[Fe]} = v_{mat} = \frac{M_{MO\cdot Fe_2O_3}}{3\rho_{MO\cdot Fe_2O_3}} \approx 1.5\times10^{-5}\ m^3\cdot mol^{-1}$$

$(mmol_{Fe}\cdot L^{-1})^{-1}$

$$\frac{r_2\times\phi_{intra}}{M_v^2} = a_{theory}\ d^2 = 6\times10^{-12}\ d^2$$

$$a_{theory} == \frac{2}{405}\frac{M_{Fe2O3}}{\rho_{Fe2O3}}\frac{\gamma^2\mu_0{}^2}{D}$$

with $D_{H2O}=3\times10^{-9}\ m^2\cdot s^{-1}$ at 37°C

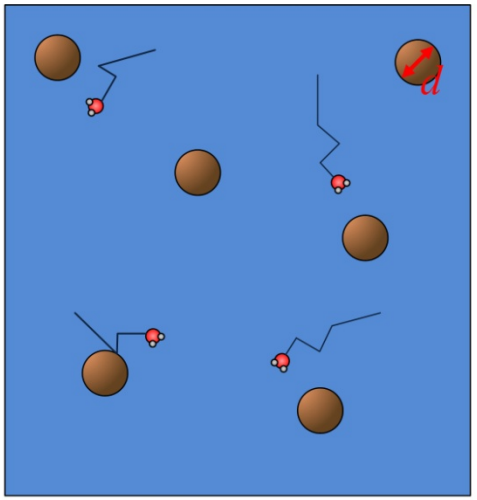

(a)

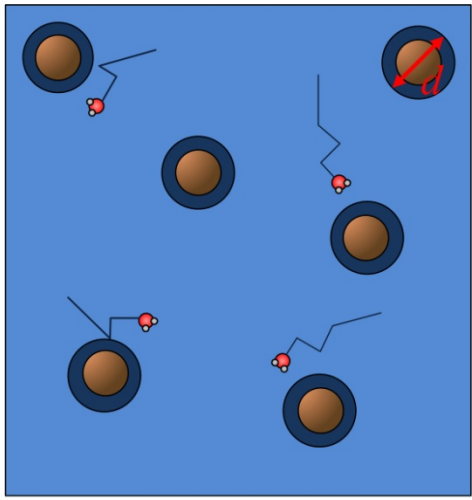

(b)

USPIO

Geometrical parameters: *d* and ϕ_{intra}

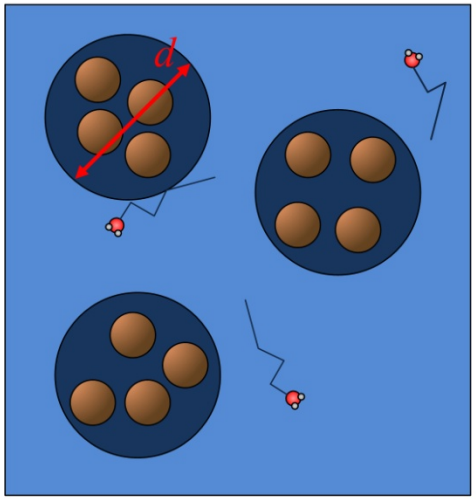

(c)

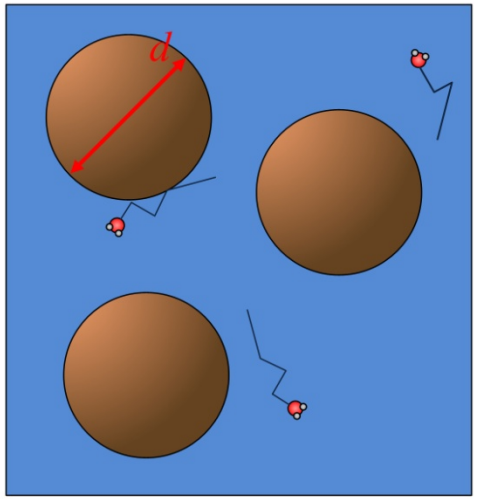

(d)

SPIO

Building USPIOs' assemblies by "brick and mortar" concept

electrostatic clusters (coacervates) with double hydrophilic block copolymers (DHBC)

Poly(trimethylammonium ethylacrylate) (PTEA)

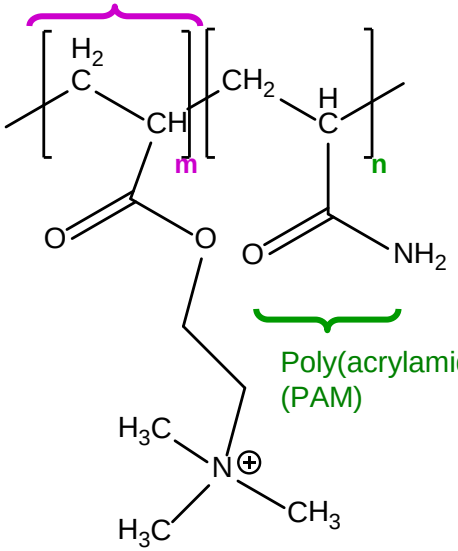

Poly(acrylamide) (PAM)

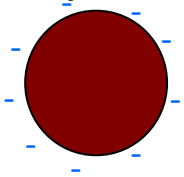

Citrate, PAA_{2k}, PAA_{5k}…

Guinier's radii (giration):

R_G=165 Å with $PTEA_{5k}$-*b*-PAM_{30k}

R_G=188 Å with $PTEA_{11k}$-*b*-PAM_{30k}

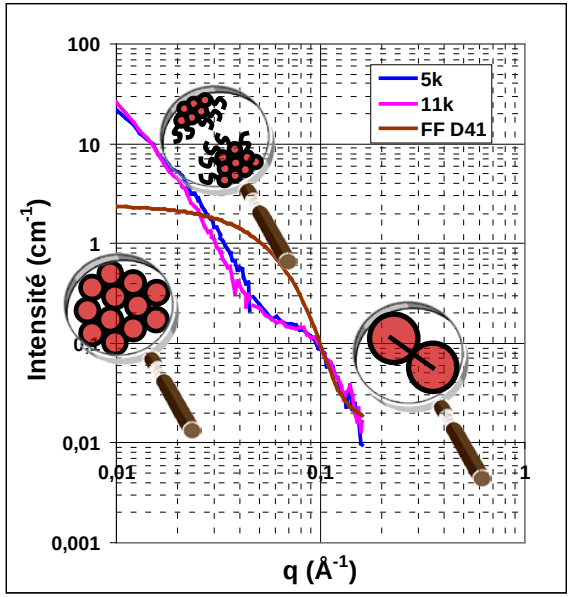

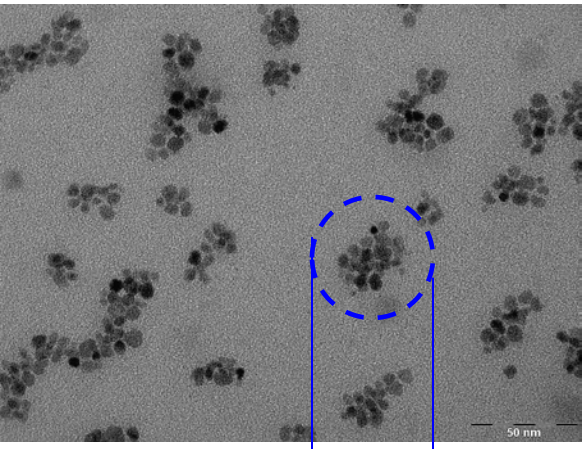

d_H=60 nm

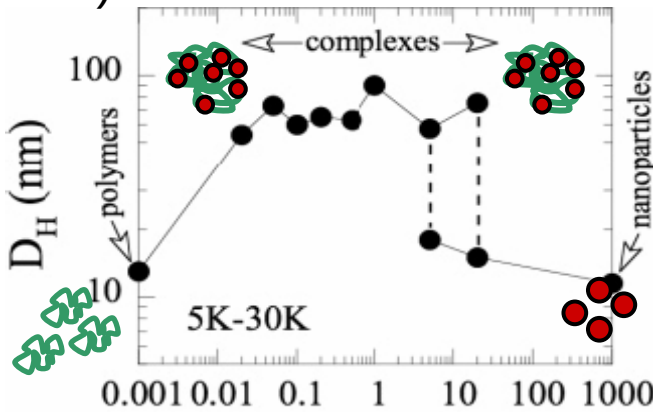

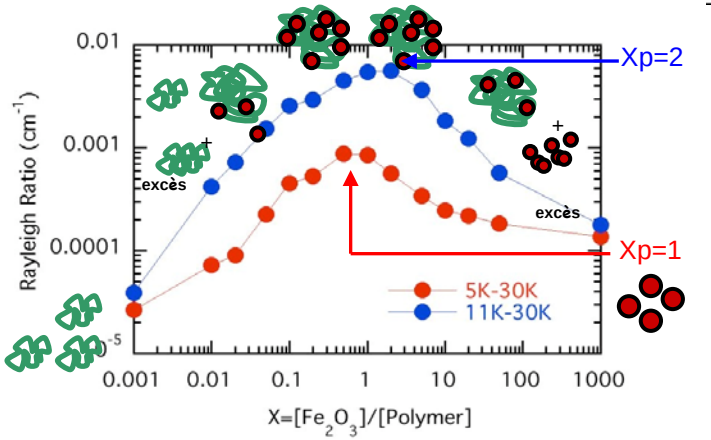

"one-shot" mixing

Berret J-F, Schonbeck N, Gazeau F, El Kharrat D, Sandre O, Airiau M, Vacher A, *JACS*. (2006) **128** 5 1755;
Berret J-F, Sehgal A, Morvan M, Sandre O, Vacher A, Airiau M, *J. Coll. and Inter. Sci.* (2006) **303** 315;
Berret J-F, Sandre O, Mauger A, *Langmuir* (2007) **23**(6) 2993

Clustering of USPIOs: strong impact T_2 Relaxometry

Longitudinal

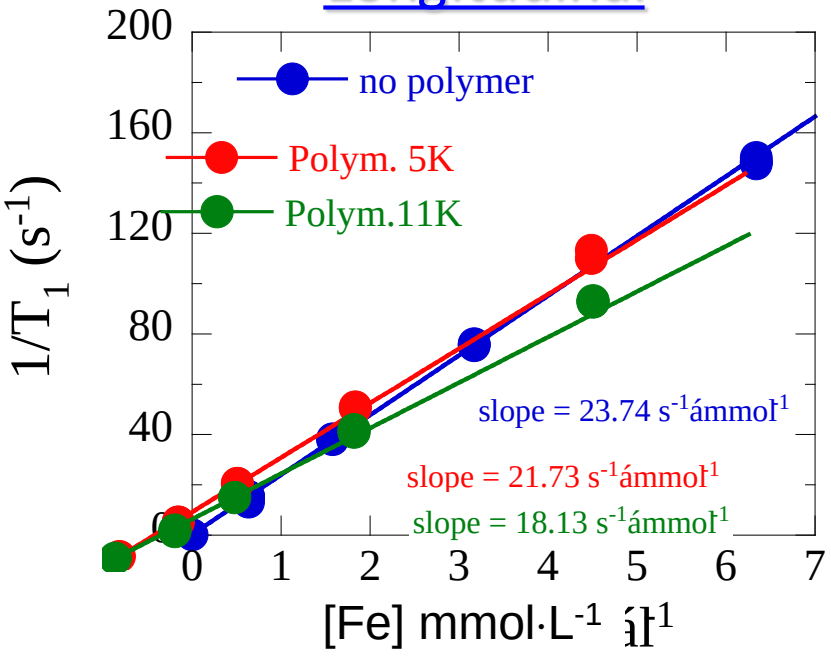

Transverse

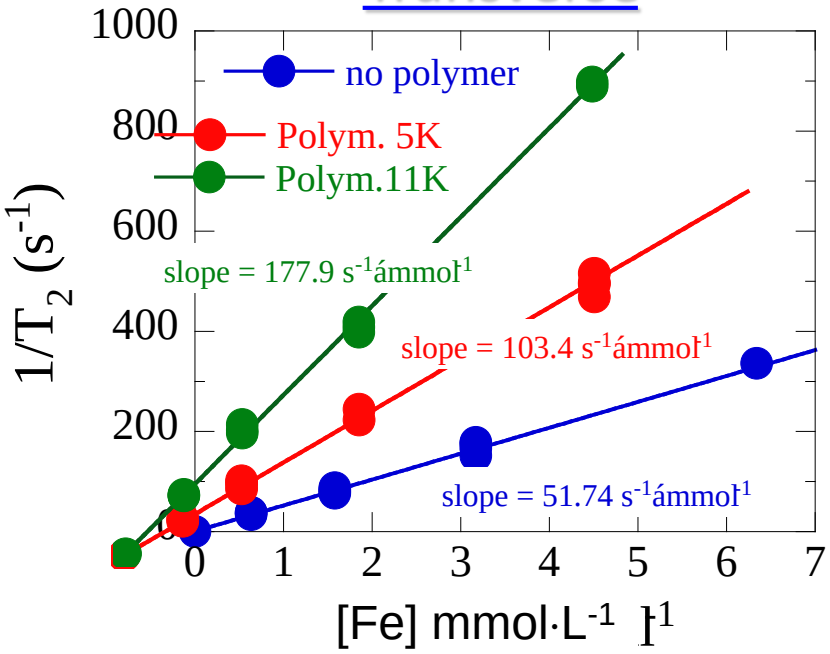

N = 1

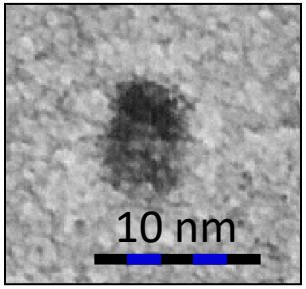

single nanoparticle

<N> ~ 20

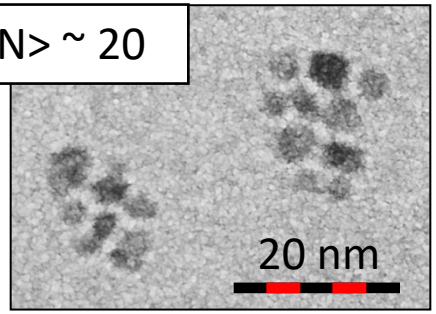

« small » aggregate

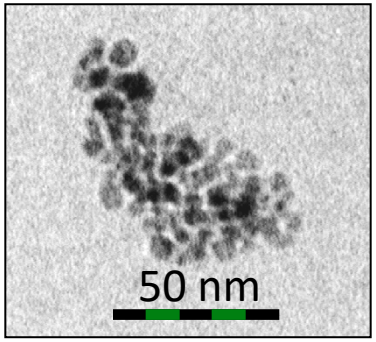

<N> ~ 100

« large » aggregate

J-F.Berret, N. Schonbeck, F. Gazeau, D. El Kharrat, O. Sandre, A. Vacher, M. Airiau, *Controlled clustering of superparamagnetic nanoparticles using block copolymers: Design of new contrast agents for magnetic resonance imaging.* **JACS 2006**. 128 1755

Perfectly spherical SPIO electrostatic clusters (coavervates) by controlling the desalting kinetics

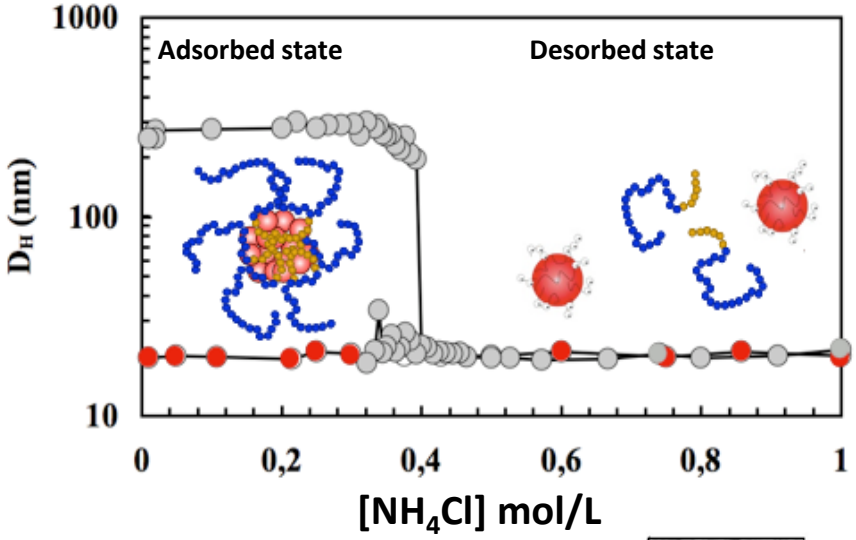

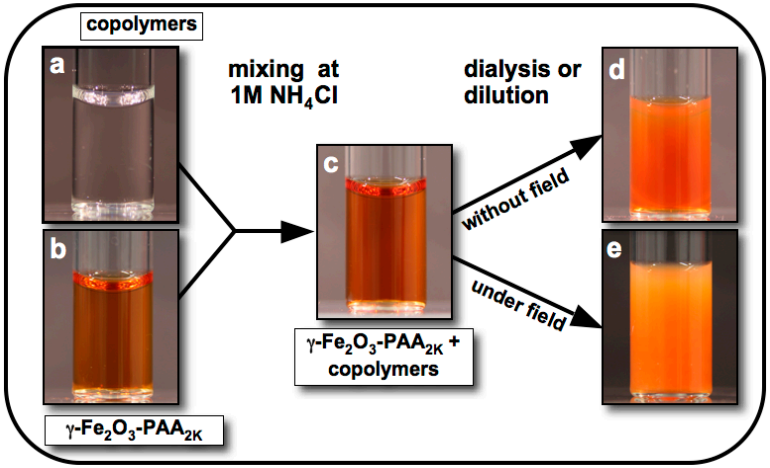

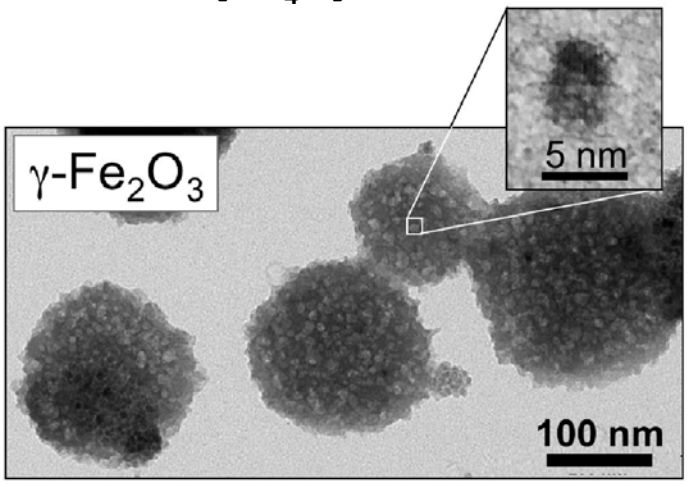

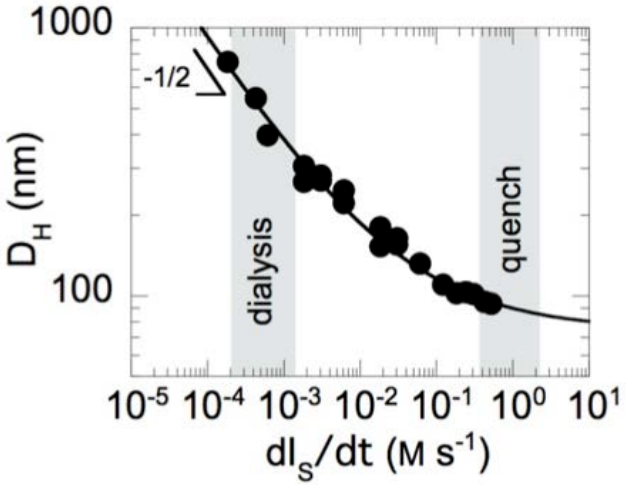

Fresnais J., Berret J.-F., Qui L., Chapel J.-P., Castaing J.-C., Sandre O., Frka-Petesic B., Perzynski R., Oberdisse J., Cousin F., *Phys. Rev.* E, **78** 040401R (2008)

T_2 contrast: *One master curve for all published (U)SPIOs…*

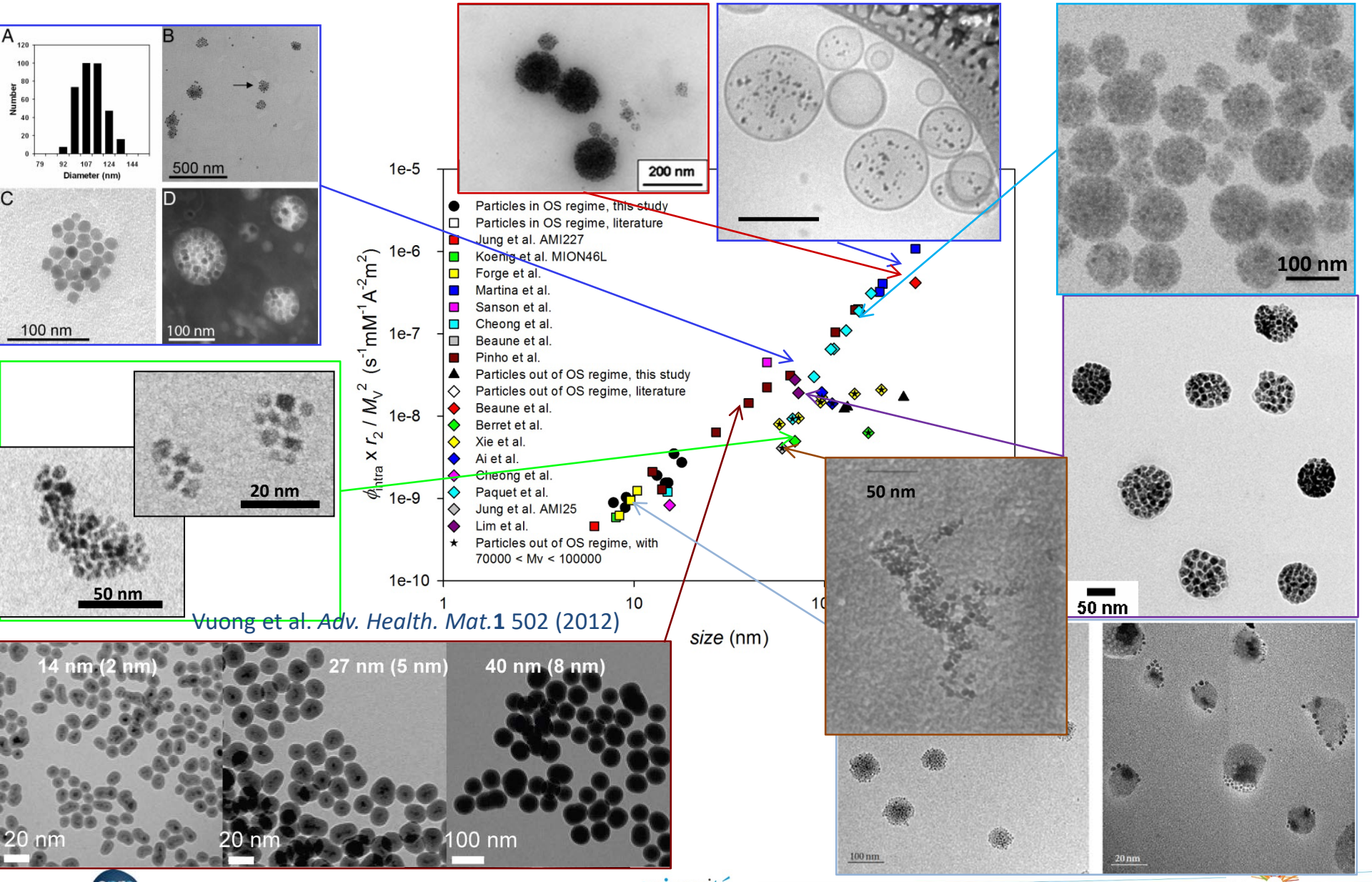

Vuong et al. *Adv. Health. Mat.***1** 502 (2012)

Relaxivity dependence upon USPIOs' size

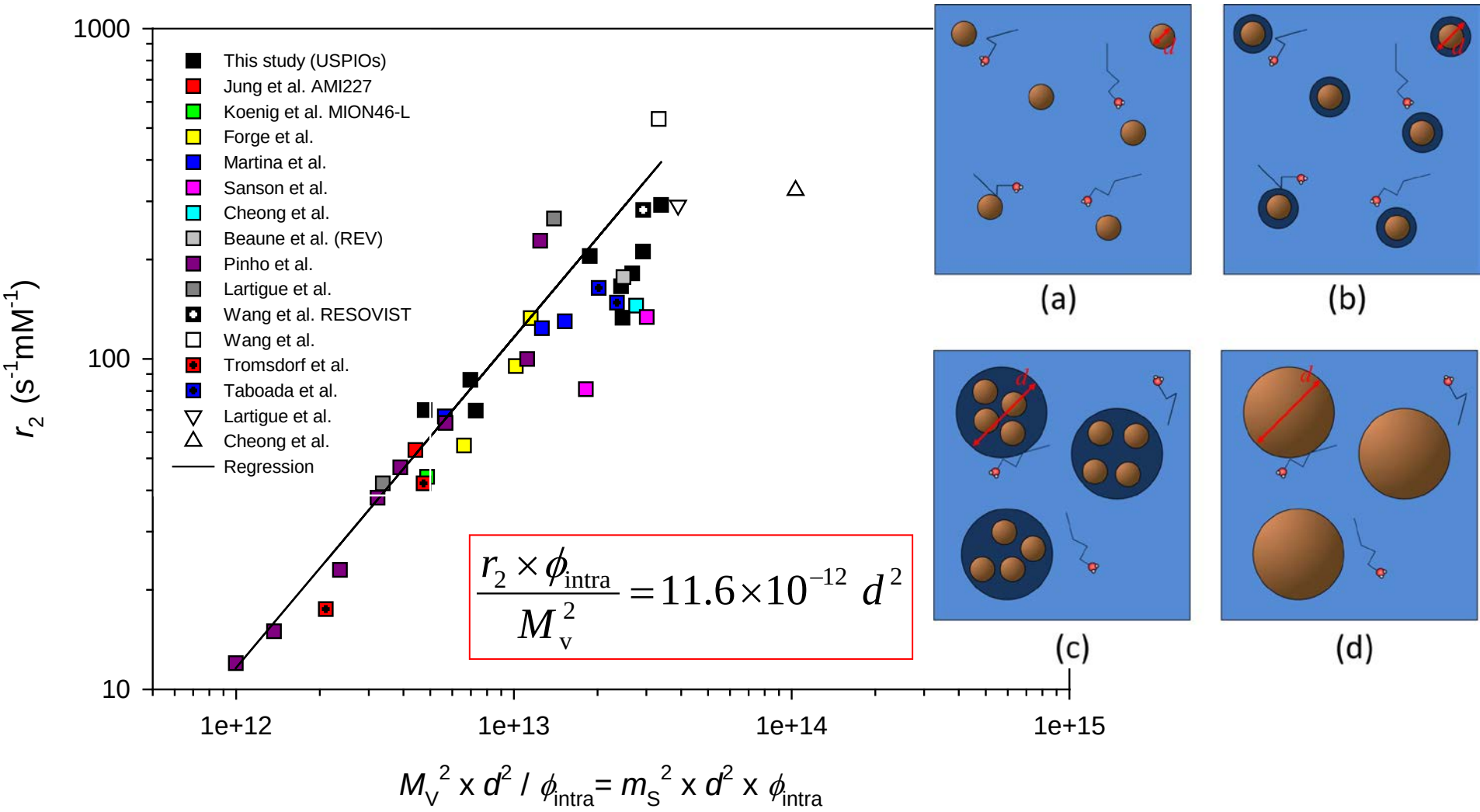

Vuong, Berret, Fresnais, Gossuin, Sandre, *Adv. Health. Mat.***1**(4) 502-512 (2012)

Optimization of MRI negative T_2 contrast agents:

Two curves for all published (U)SPIO(N)s !

Static Dephasing Regime (SDR)

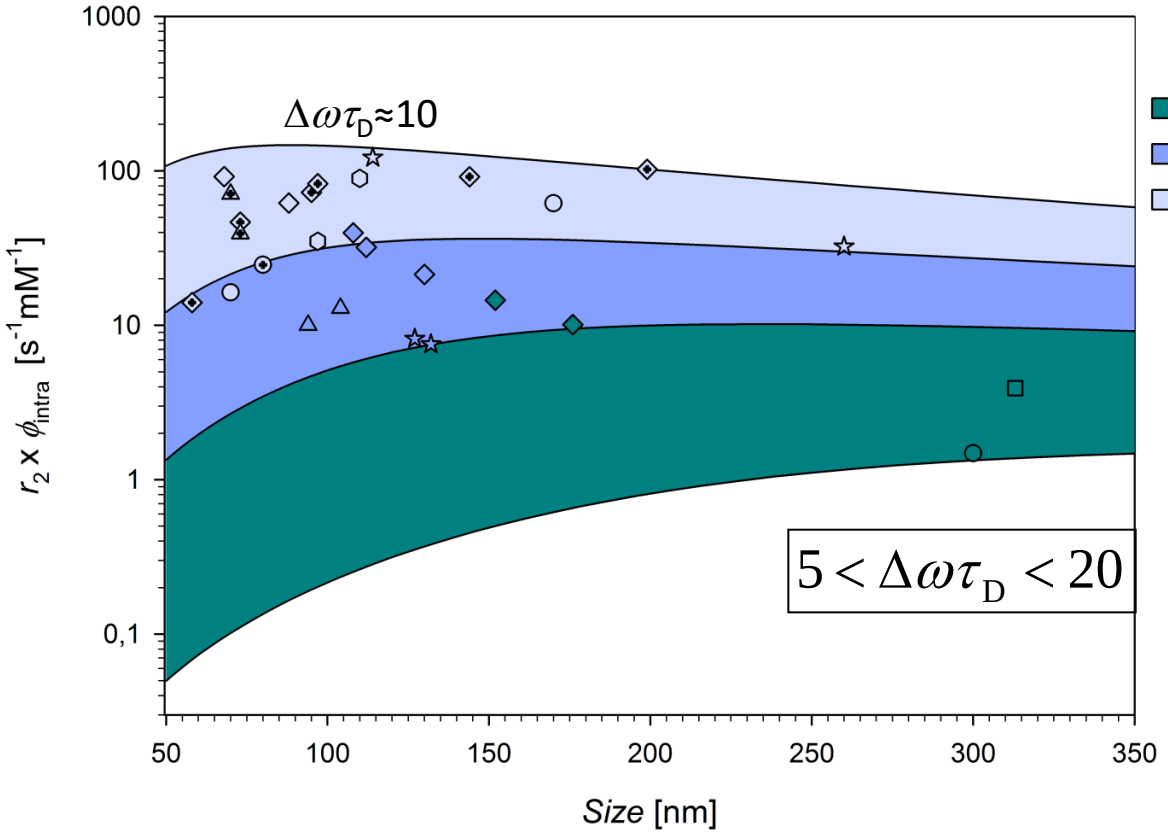

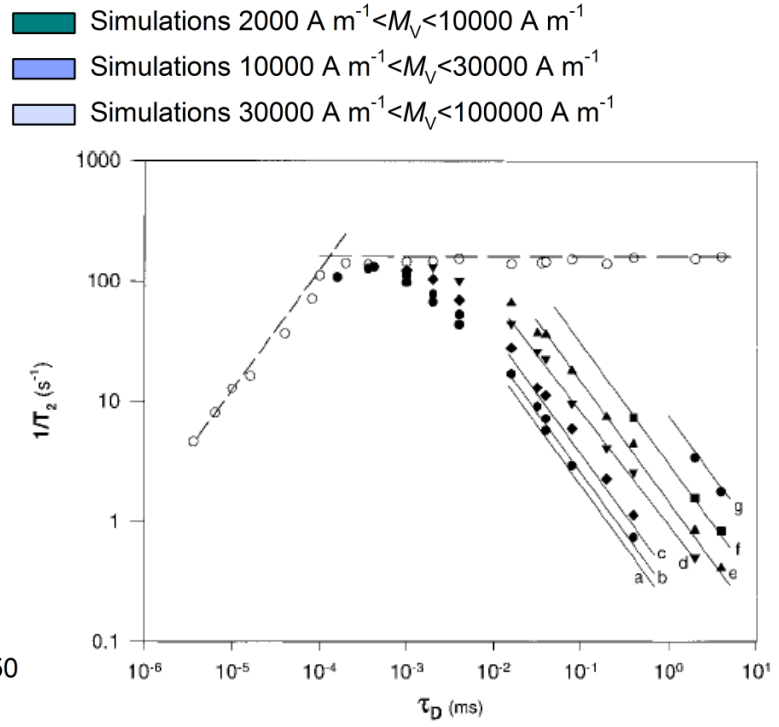

Vuong, Berret, Fresnais, Gossuin*, Sandre*, *Adv. Health. Mat.***1**(4) 502-512 (2012)

P. Gillis, R. Brooks, *Mag. Res. Med* 47 (2002) 257

$$r_2^* = \frac{R_2^*}{[Fe]} = \frac{2\pi\gamma\mu_0 v_{mat} M_v}{9\sqrt{3}} \approx r_2$$

Maximum T_2 relaxivities for different types of MNPs

$$\Delta\omega = \frac{\gamma \mu_0 M_v}{3}$$

$$\tau_D = \frac{d^2}{4D}$$

$\Delta\omega \cdot \tau_D \approx 10$

Type of contrast agent	M_v $A \cdot m^{-1}$	$d_{optimal}$ nm	r_2^{max} $s^{-1} \cdot mM^{-1}$
Maghemite nanoparticles	3.5×10^5	55	750
Clusters of maghemite nanoparticles at a volume dilution of 5 (ϕ_{intra}=20% v/v)	7×10^4	120	750
Iron/iron oxide core-shell particles	6.6×10^5	38	1200
$(Zn_{0.4}Mn_{0.6})Fe_2O_4$ nanoparticles	8.75×10^5	35	1860

Vuong, Berret, Fresnais, Gossuin*, Sandre*, *Adv. Health. Mat.***1**(4) 502-512 (2012)

The scaling law fits perfectly data for γFe_2O_3@SiO_2 particles

"Relaxometric Studies of γ-Fe2O3@SiO2 Core Shell Nanoparticles: When the Coating Matters" Sonia L. C. Pinho, Sophie Laurent, Joao Rocha, Alain Roch, Marie-Helene Delville, Stéphane Mornet, Luis D. Carlos, Luce Vander Elst, Robert N. Muller, Carlos F. G. C. Geraldes, *J. Chem. Phys.* C 116 (2012) 2285

	r_2 (20 MHz, s^{-1} mM^{-1})	TEM diameter (nm)	magneto metric diameter (nm)	NMRD diameter (nm)	calculated M_{sat} NMRD (A m^2/kg of particle)[a]	calculated M_{sat} TEM (A m^2/kg of particle)[b]
FF	129.25 ± 3.88	9.6 ± 1.3	10.9 ± 0.12	13.6 ± 0.1	51.1	51.1
FF@SiO_2_1	114.18 ± 3.43	11.2 ± 1.7	11.3 ± 0.12	16.1 ± 0.1	39.4	40.4
FF@SiO_2_2	96.16 ± 2.89	24.7 ± 3.2	11.0 ± 0.12	21.8 ± 0.1	21.3	6.2
FF@SiO_2_3	85.89 ± 2.58	46.4 ± 8.0	11.1 ± 0.12	27.6 ± 0.2	11.9	1.00
FF@SiO_2_4	50.25 ± 1.51	73.8 ± 8.1	11.2 ± 0.12	38 ± 0.3	4.94	0.25
FF@SiO_2_5	39.78 ± 1.19	94.9 ± 7.0	11.2 ± 0.14	40 ± 0.8	4.27	0.12
FF@SiO_2_6	40.57 ± 1.22	114.2 ± 12.7	11.2 ± 0.12	36 ± 0.6	5.76	0.07
FF@SiO_2_7	39.18 ± 1.18	152.9 ± 13.1	11.1 ± 0.12	43.8 ± 0.9	3.29	0.03

$$\varphi_{intra} = \left(\frac{d_{bare\ particle}}{d_{coated\ particle}} \right)^3$$

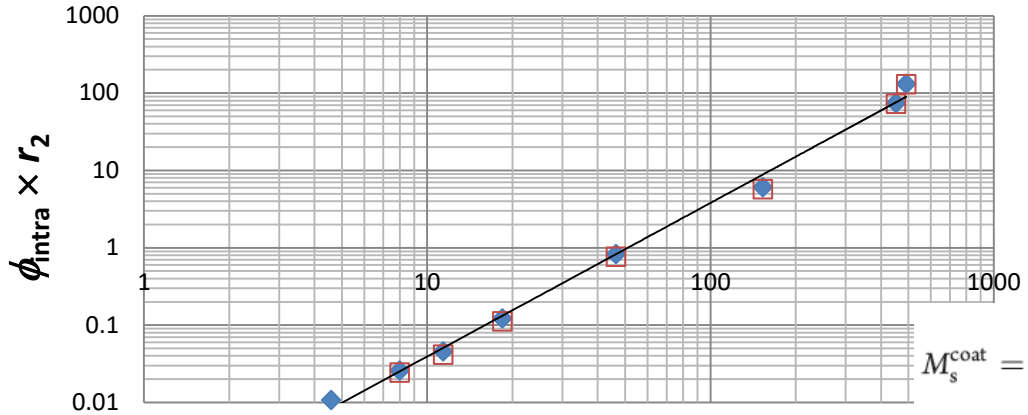

$$M_s^{coat} = M_s^{bp} \frac{4.90 \times {d_{bp}}^3}{4.90 \times {d_{bp}}^3 + 2.2 \times ({d_{coat}}^3 - {d_{bp}}^3)}$$

Fitting of T1 NMRD profiles with the Outer Sphere model

By P. Arosio, T. Orlando, F. Orsini, and A. Lascialfari (INSTM, Milano)
using the "Outer-Sphere" model Arosio et al, ***J. Mater. Chem. B***, 2013,**1**, 5317-5328

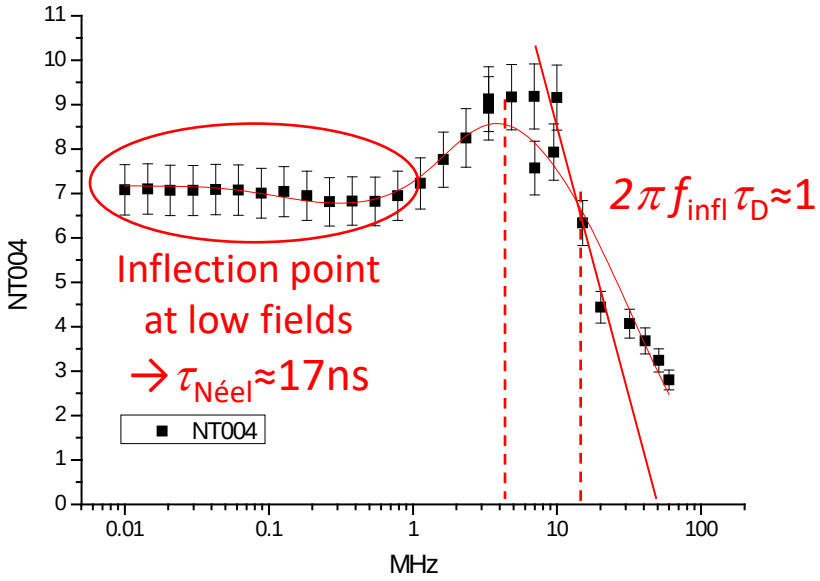

M6-5 micelles

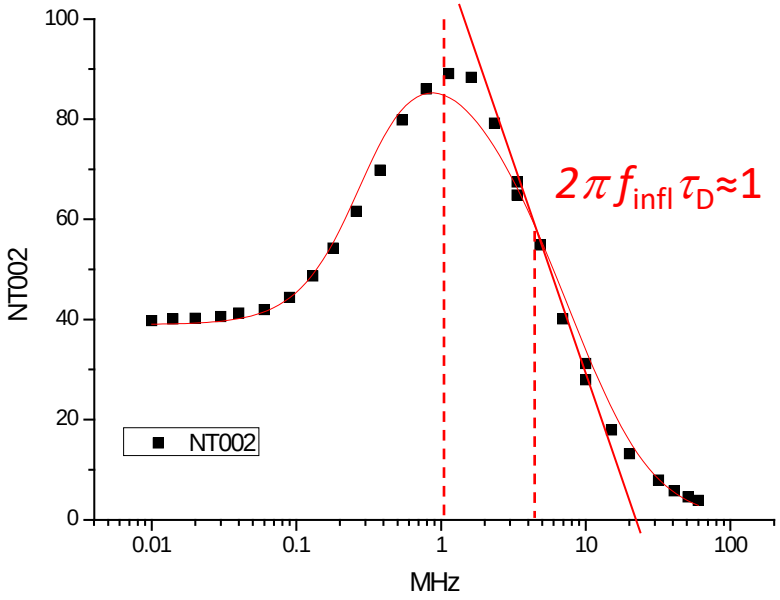

M10-20 micelles

NMRD T1: f_{max}≈4 MHz, f_{infl}≈15 MHz
$t_D=R^2/D=3.2\cdot10^{-9}$ s → $\boldsymbol{R_{NMR}}$**=5.57** nm
$D_{H2O}=2\cdot10^{-9}$ m^2/s
r_1^{max}≈ 9 s^{-1}·mM^{-1} → $\boldsymbol{m_S}$**=54.1 emu/g**

NMRD T1 : f_{max}≈1 MHz, f_{infl}≈4 MHz
$t_D=R^2/D$ =1.6·10^{-8} s → $\boldsymbol{R_{NMR}}$**=10.1 nm**
$D_{H2O}=1.5\cdot10^{-9}$ m^2/s
r_1^{max}≈ 90 s^{-1}·mM^{-1} → $\boldsymbol{m_S}$**=67 emu/g**

perfect agreement with magnetometry

Use of MRI contrast to map temperature?

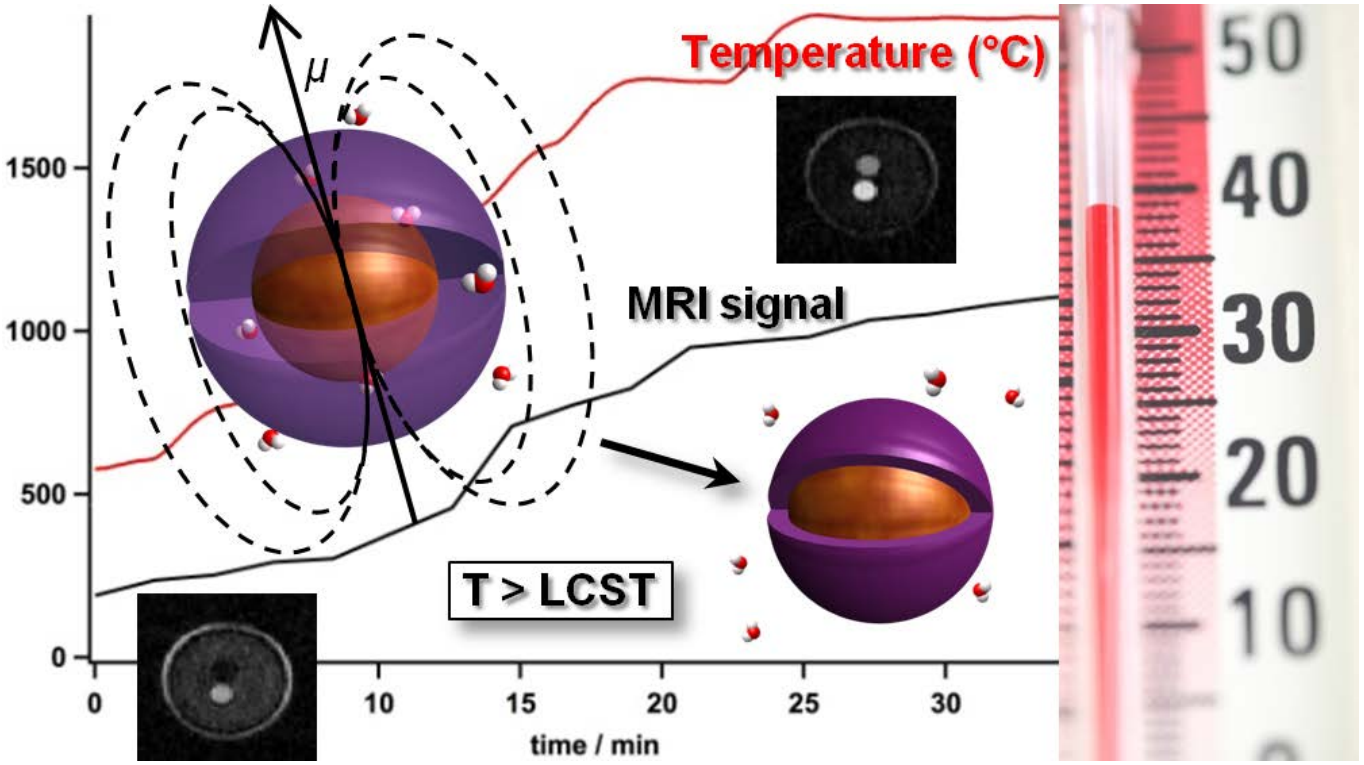

A. Hannecart, D. Stanicki, L. Vander Elst, R. N. Muller, S. Lecommandoux, J. Thévenot, C. Bonduelle, A. Trotier, P. Massot, S. Miraux, O. Sandre, and S. Laurent, *Nano-thermometers with thermo-sensitive polymer grafted USPIOs behaving as positive contrast agents in low-field MRI*, **Nanoscale**, 2015. **7**: 3754-3767

Use of (U)USPIOs for T_1-contrast: known by radiologists

C. Corot et al. (Guerbet)
Advanced Drug Delivery Reviews 58 (2006) 1471–1504

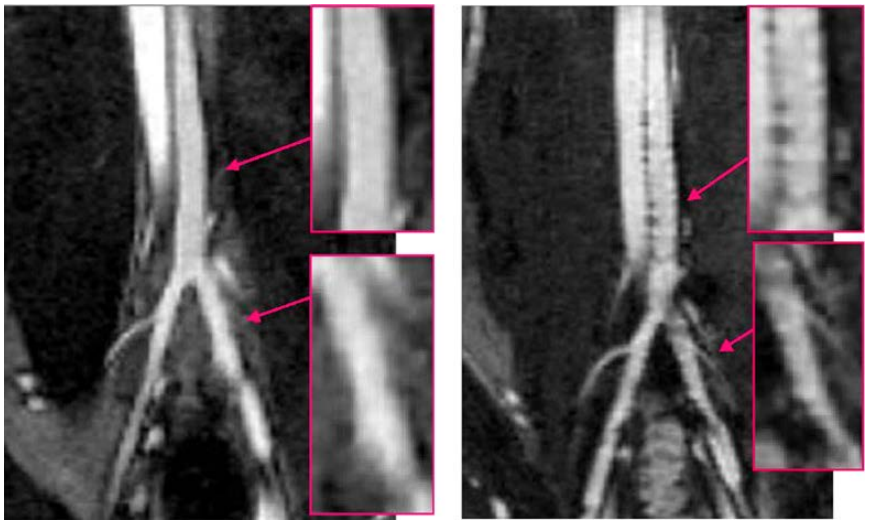

Atherosclerotic MR-imaging in rabbits 5 days after the injection of 1000 µmol. Fe/kg of Ferumoxtran-10
Left: Normal rabbit: bright blood due to the T1 effect of ferumoxtran-10 (AMI-227, T-10 Dextran coating)*
Right: Atheroscleoric rabbit: note the dark signal in the vessel wall due to the macrophage uptake of ferumoxtran-10 in atherosclerotic lesions.

* 4-5 nm core, D_H=28 nm, r_2/r_1=2.1 at 20MHz (Forge et al, *Contrast Media Mol. Imaging* 2010, 5 126–132)

Angio-MR in rabbit after the injection of 45 µmol Fe/kg of ferumoxtran-10 (AMI-227). Due to the blood pool effect, even small arteries and veins are visible

Use of (U)USPIOs for T_1-contrast: chemists who know…

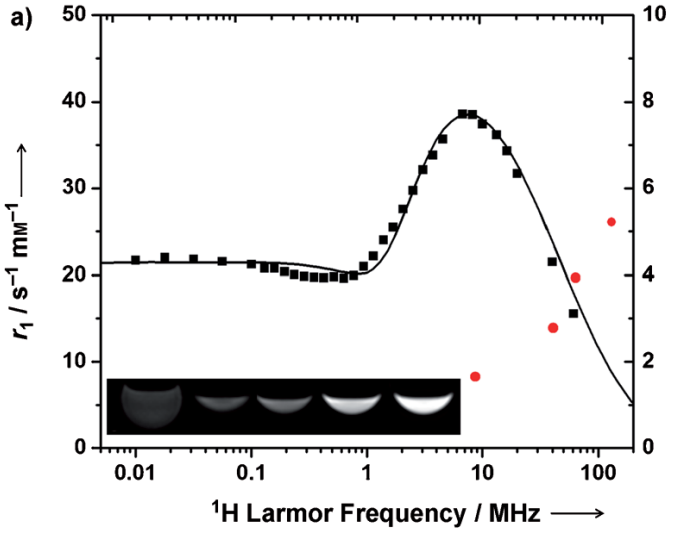

4 nm core size

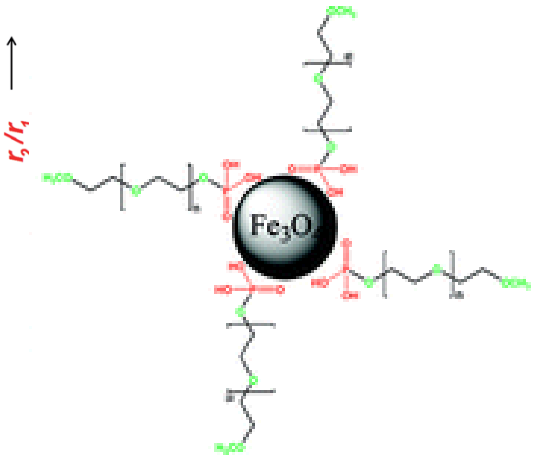

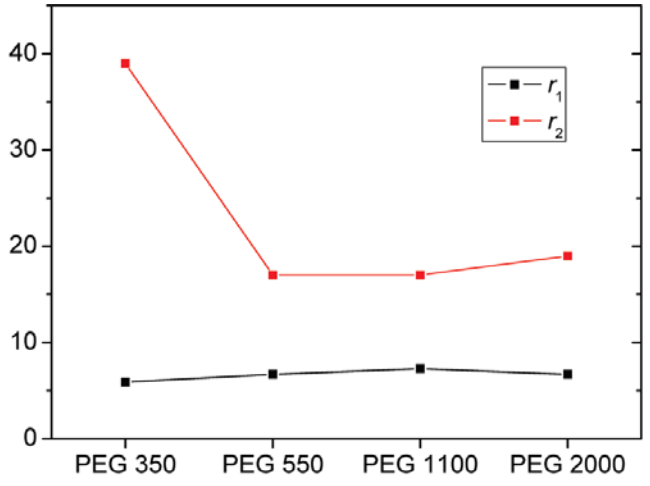

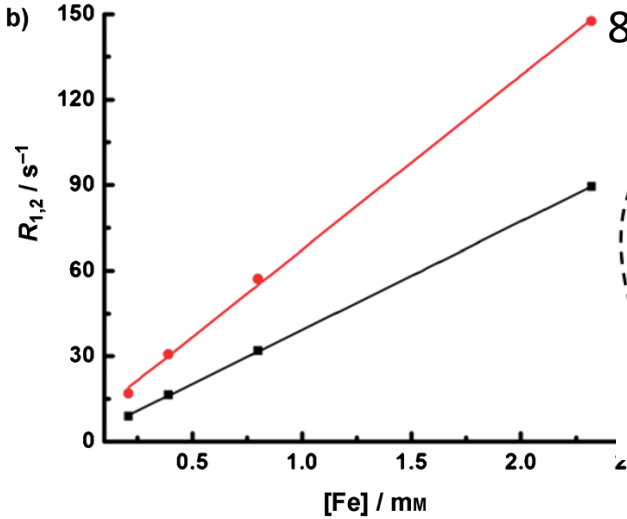

8.3±2 nm core size

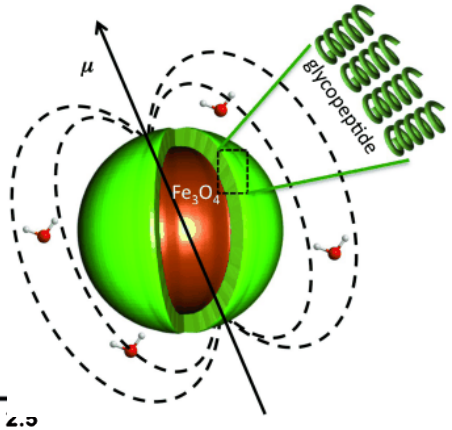

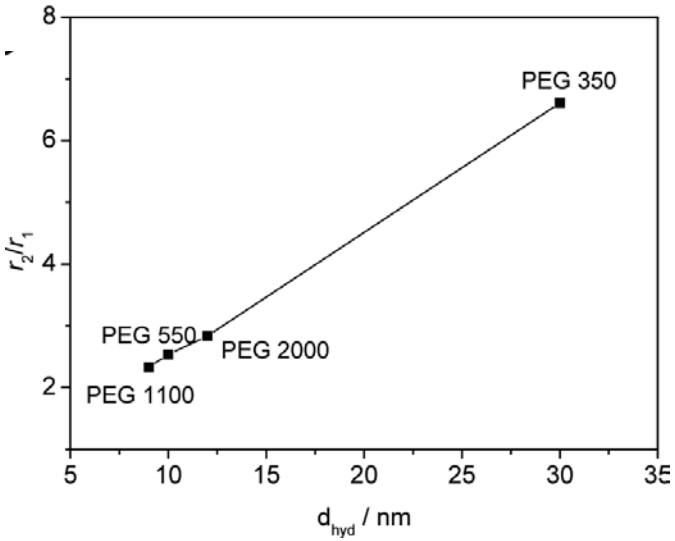

T. Borase, T. Ninjbadgar, A. Kapetanakis, S. Roche, R. O'Connor, C. Kerskens, A. Heise, D. F. Brougham, *Angew. Chem. Int.-Ed.* 2013 52, 164

U. I. Tromsdorf, O. T. Bruns, S. C. Salmen, U. Beisiegel, H. Weller, *Nano Lett.* 2009 9, 4434

Grafting of thermo-sensitive chains onto USPIOs' surface

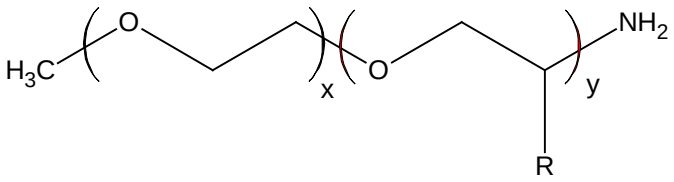

R = H for (EO) of CH_3 for (PO)

Jeffamine® M-2005 : PEO_5-st-PPO_{36}
Jeffamine® M-2070 : PEO_{46}-st-PPO_{13}

LCST values:
Jeffamine® M-2005 :
22±1°C (DLS / NMR)
Jeffamine® M-2070 :
52±1°C (DLS / NMR)

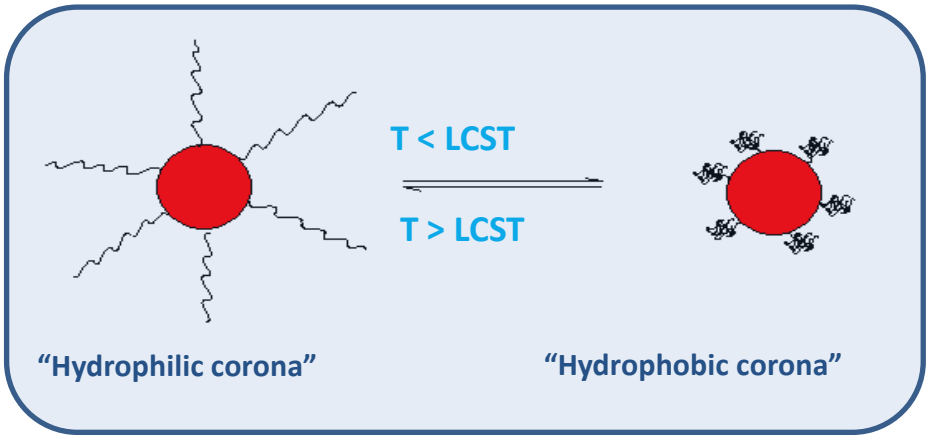

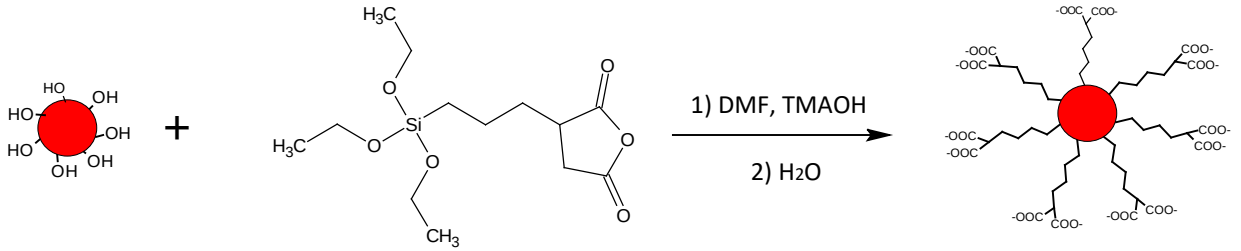

3-triethoxysilylpropyl succinic anhydride (TEPSA)

Chemical route:
-1/silanization
-2/amide bond formation

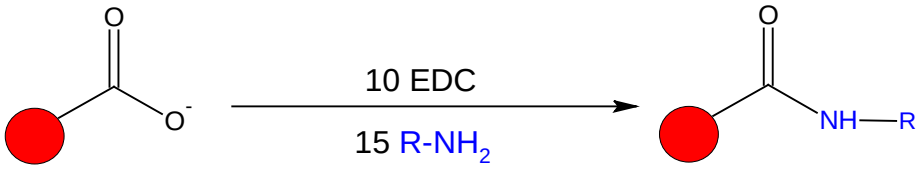

A. Hannecart, M.Sc. Thesis (UMONS, 2012)

Size distribution of magnetic cores

$$Fe^{2+}_{(2Cl^-)} + 2Fe^{3+}_{(6Cl^-)} + 8OH^-_{(8Na^+)} \rightarrow Fe_3O_{4(s)} + 4H_2O$$

in diethyleneglycol (170°C)

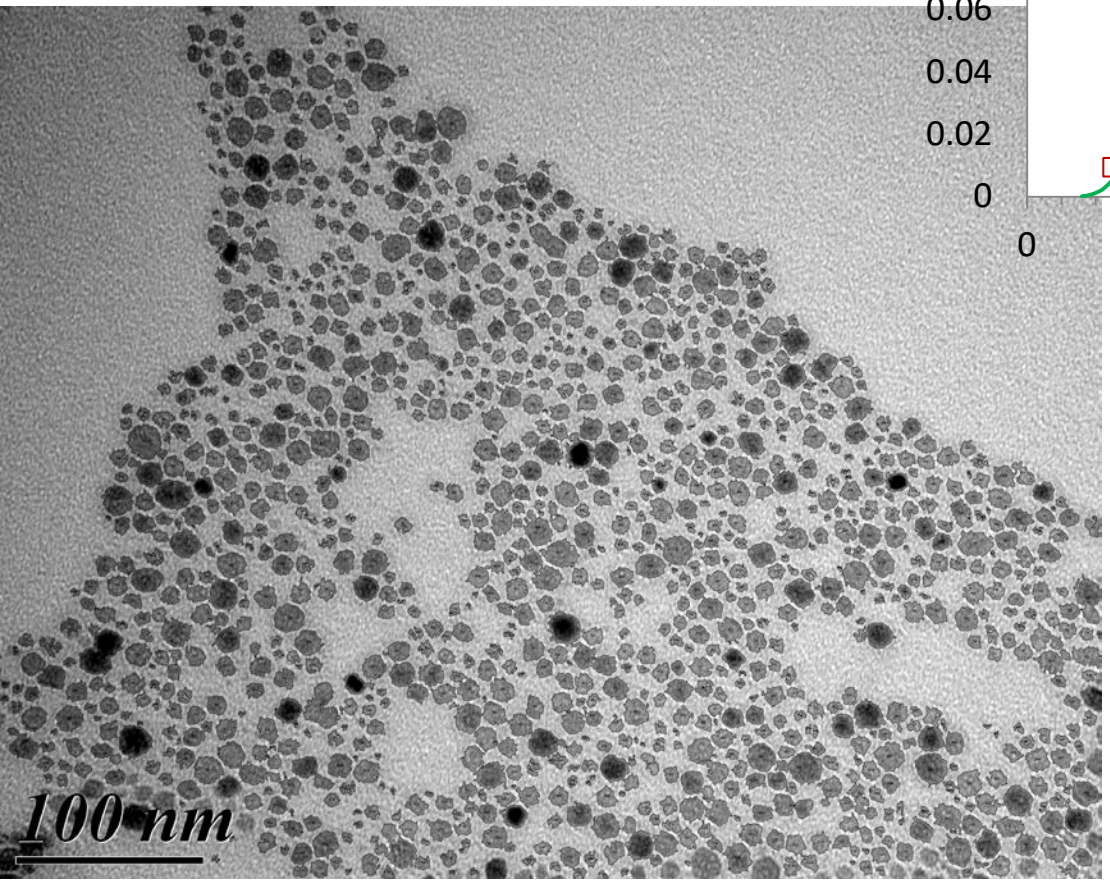

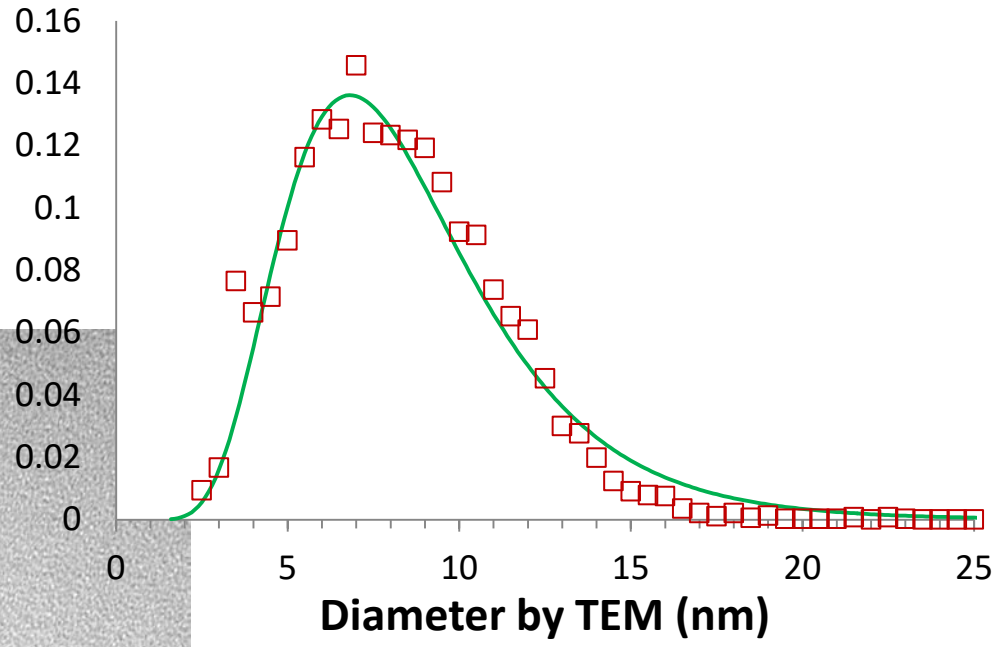

-median: d_0=8 nm
-standard width (Ln d): σ=0.4
-number-average: d_n=8.6 nm
-weight-average: d_w=13.9 nm
-polydispersity index: $Đ$=1.6

Forge, D.; Roch, A.; Laurent, S.; Tellez, H.; Gossuin, Y.; Renaux, F.; Vander Elst, L.; Muller, R. N. *J. Phys. Chem. C* **2008**, *112*, 19178-19185

Solution properties of the poly(ether)amine chains

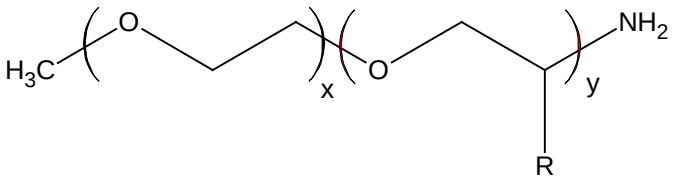

R = H for (EO) of CH_3 for (PO)

Jeffamine® M-2005 : PEO_5-st-PPO_{36}
Jeffamine® M-2070 : PEO_{46}-st-PPO_{13}

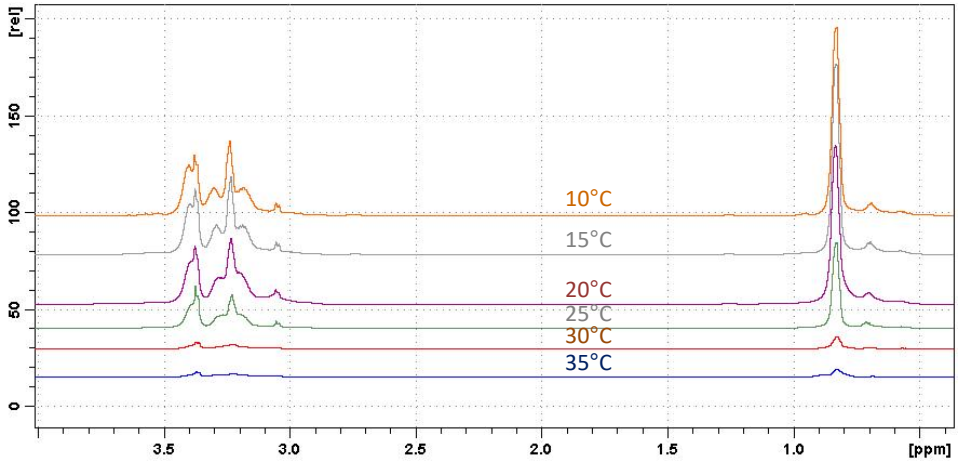

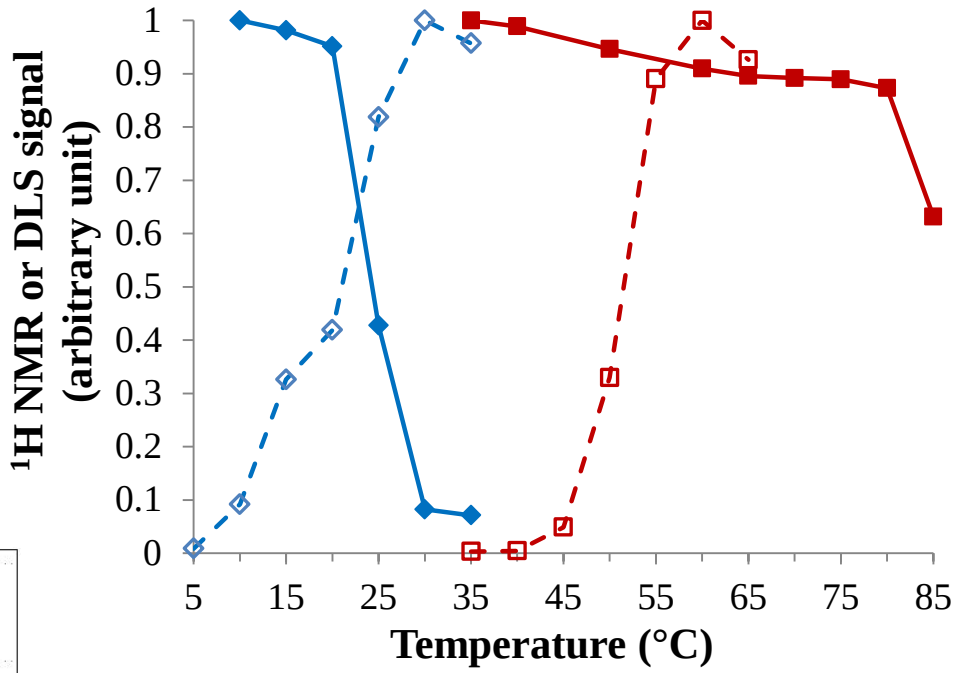

LCST values:
Jeffamine® M-2005 :
22±1°C (DLS / NMR)
Jeffamine® M-2070 :
52±1°C (DLS / NMR)

↗ PO → ↘ LCST

Colloidal behavior of the grafted USPIO nanoparticles

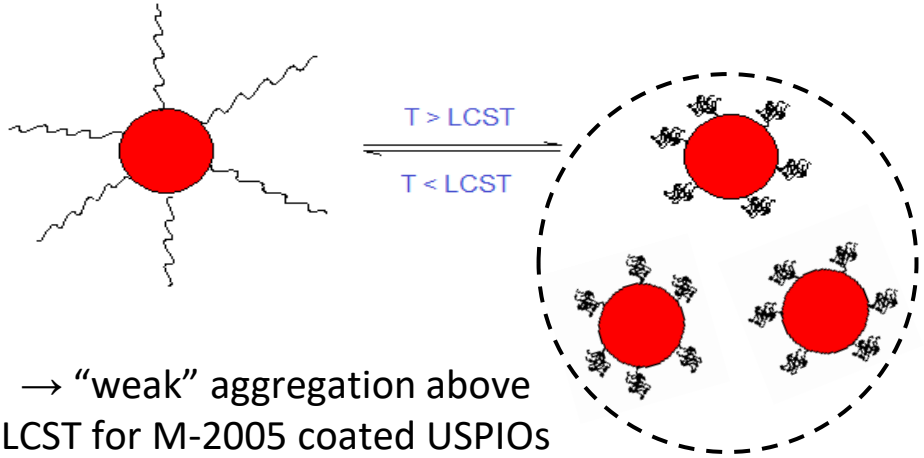

→ "weak" aggregation above LCST for M-2005 coated USPIOs

$D_H \sim N_{agg}$

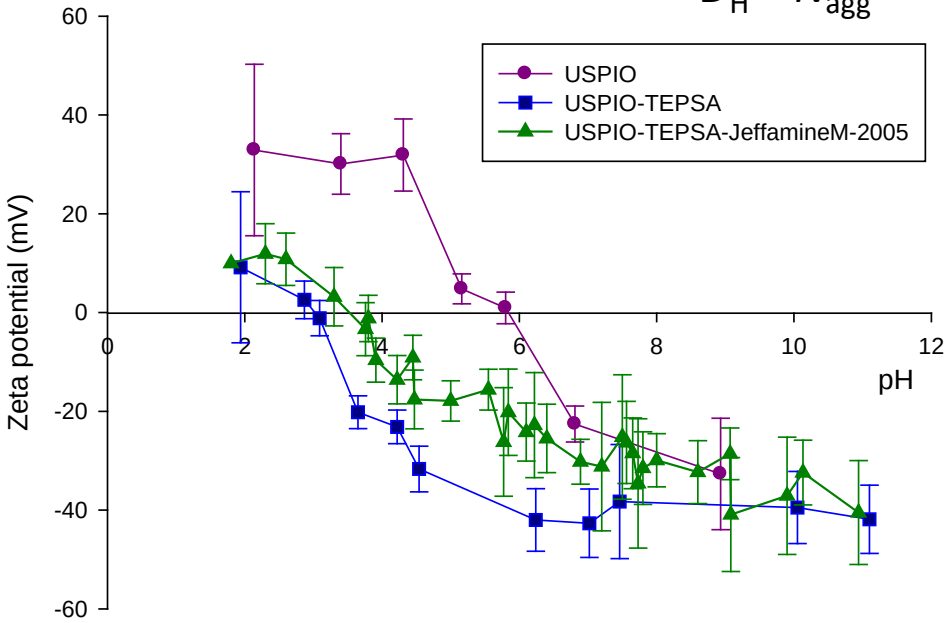

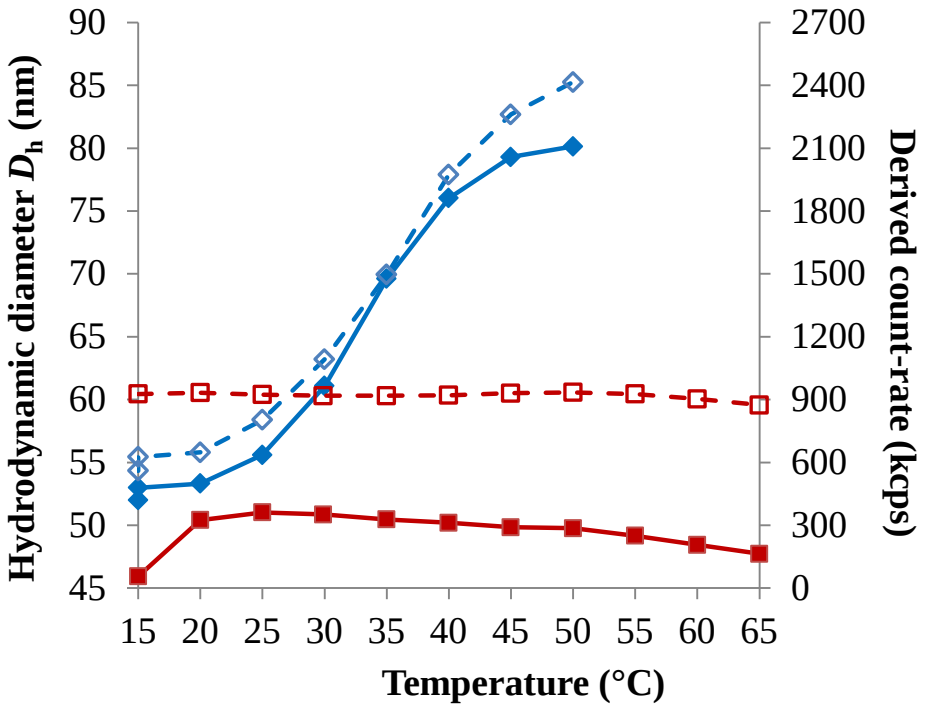

Jeffamine® M-2005 : PEO_5-st-PPO_{36}
Jeffamine® M-2070 : PEO_{46}-st-PPO_{13}

→ electro-steric stabilization (TEPSA charges not totally screened by poly(ether) chains)

Thermo-gravimetric study of the grafted USPIOs

Sample (coating)	Bound water (wt. %)	Inorganics =Iron oxide (wt. %)	Total organics = (wt. %)	TEPSA + (wt. %)	Polymer (wt. %)
TEPSA coated	2.7[a]	87.5 [a]	12.5 [a]	12.5 [a]	0
		100 [b]	14.3 [b]	14.3[b]	
M-2005 coated	1.4[a]	60.1 [a]	39.9 [a]	8.6 [a]	31.3 [a]
		100 [b]	66.4 [b]	14.3[b]	52.1 [b]
M-2070 coated	1.6[a]	77.8 [a]	22.2 [a]	11.1 [a]	11.1 [a]
		100 [b]	28.5 [b]	14.3 [b]	14.2 [b]

[a] relatively to dry matter at 120°C; [b] ratio to burnt matter at 600°C.

$$\frac{\text{organic wt.\%}}{\text{inorganic wt.\%}} = \frac{n_{\text{TEPSA}} \times M_{\text{w}}^{\text{TEPSA}}}{M_{\text{w}}^{\text{USPIO}}} + \frac{n_{\text{polymer}} \times M_{\text{w}}^{\text{polymer}}}{M_{\text{w}}^{\text{USPIO}}}$$

$$M_{\text{w}}^{\text{USPIO}} = \rho \times N_{\text{A}} \times \frac{4}{3} \pi \, r_{\text{USPIO}}^{3}$$

$n_{polymer}$≈430 chains per USPIO for Jeffamine® M-2005 ($M_w^{polymer}$=2400 g·mol^{-1})

$n_{polymer}$≈100 chains for M-2070 ($M_w^{polymer}$=2800 g·mol^{-1})

molecules per nm^2 :	grafting yield:
-TEPSA : 2.6	
- M-2005 : 1.1	43%
- M-2070 : 0.26	10%

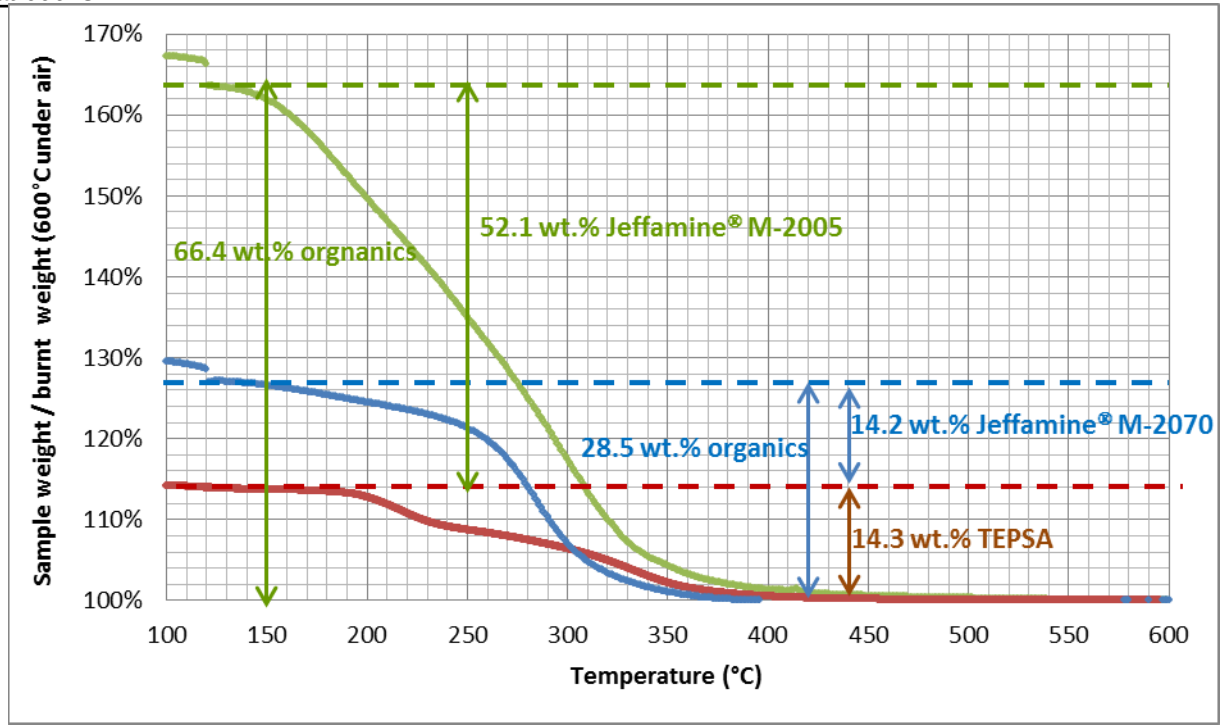

Fitting of the NMRD profiles by the Outer Sphere model

TEPSA control

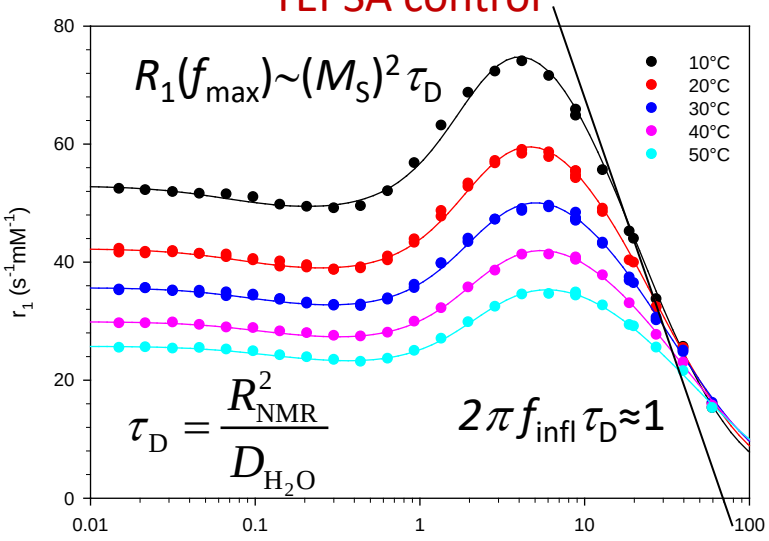

Jeffamine® M-2005 coated USPIOs

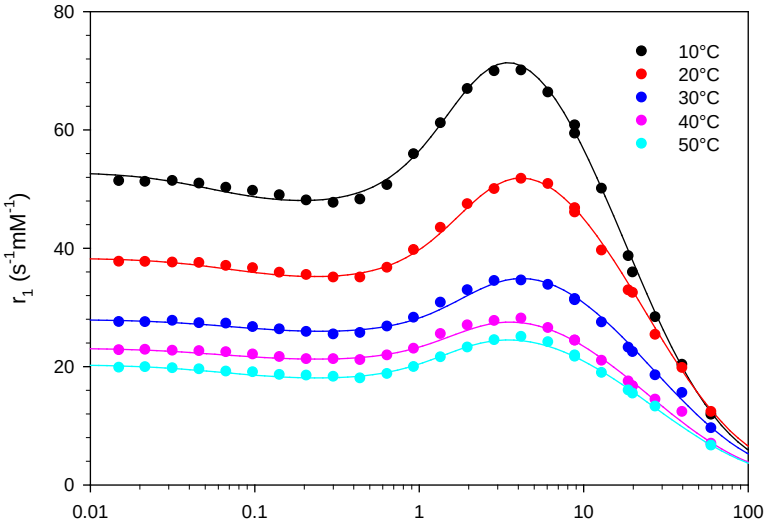

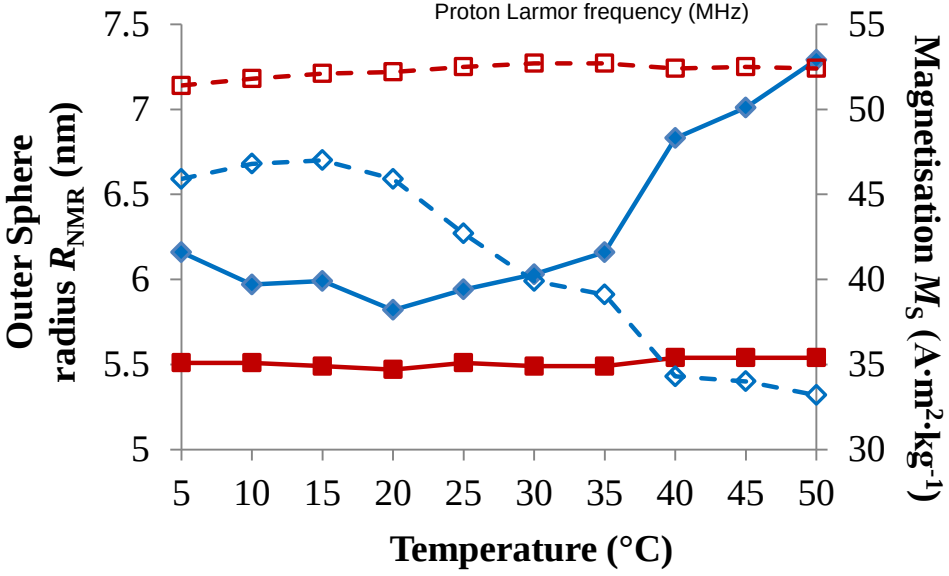

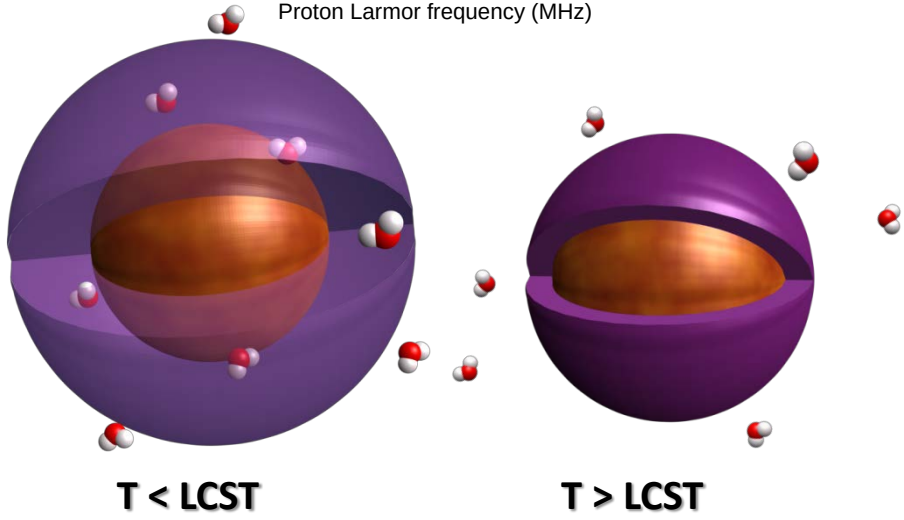

Relaxivities vs. temperature: at low magnetic field/freq.

r_1

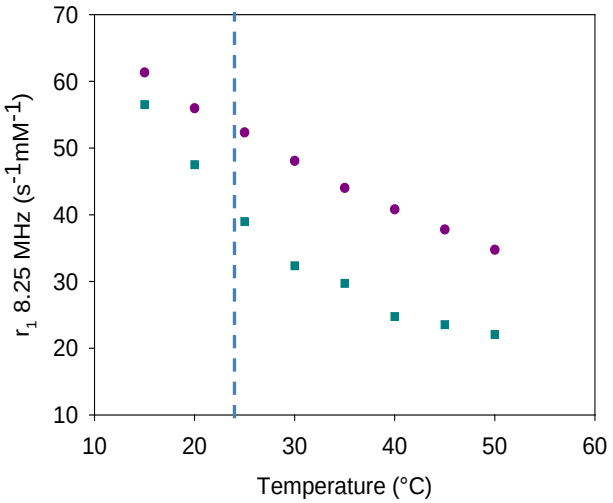

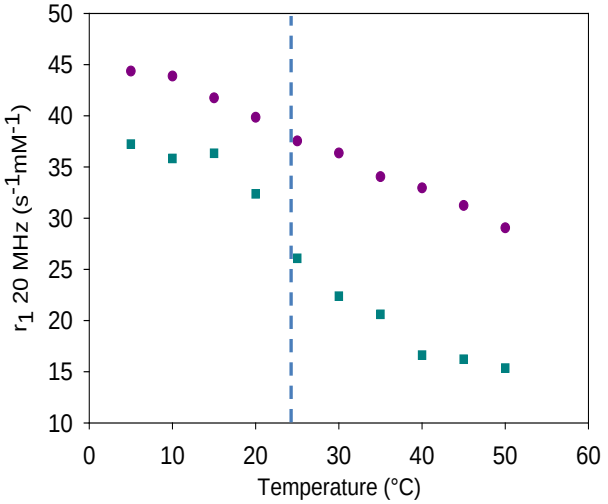

8.25 MHz (0.2 T)

NP-JeffamineM2005

NP

20 MHz (0.47T)

r_2

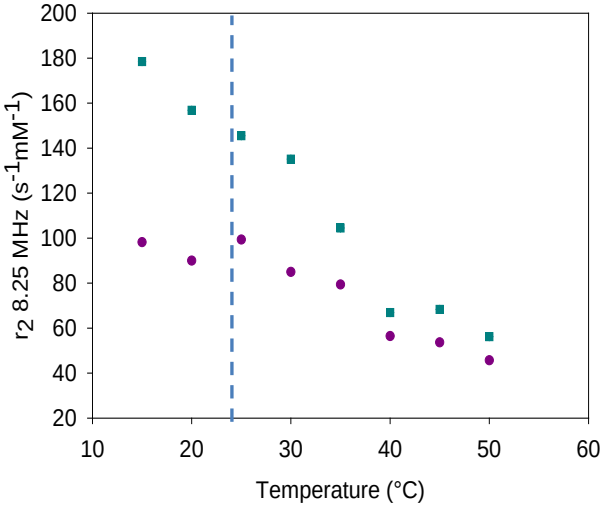

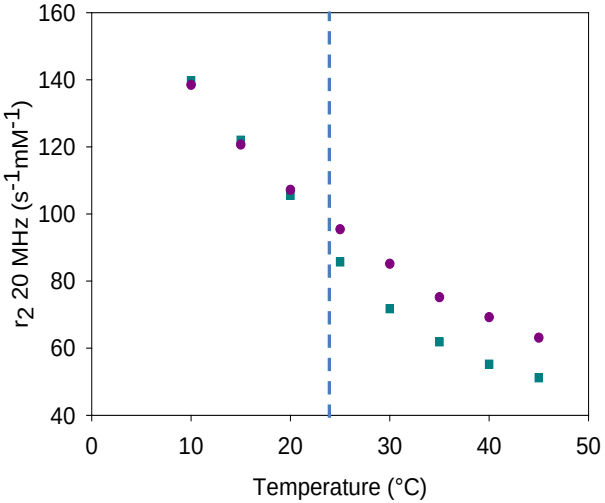

Relaxivities vs. temperature: at high magnetic field/freq.

r_1

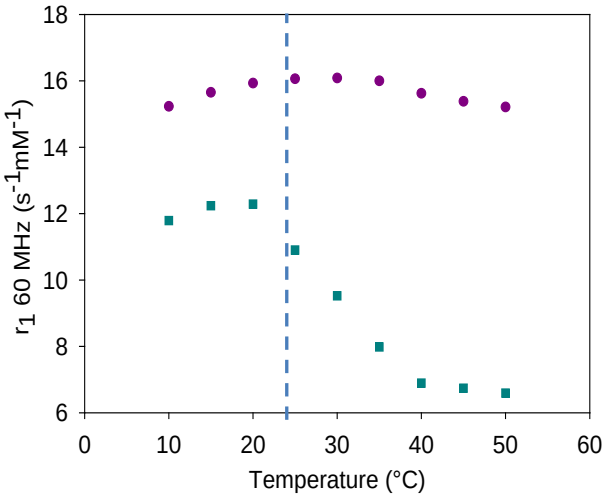

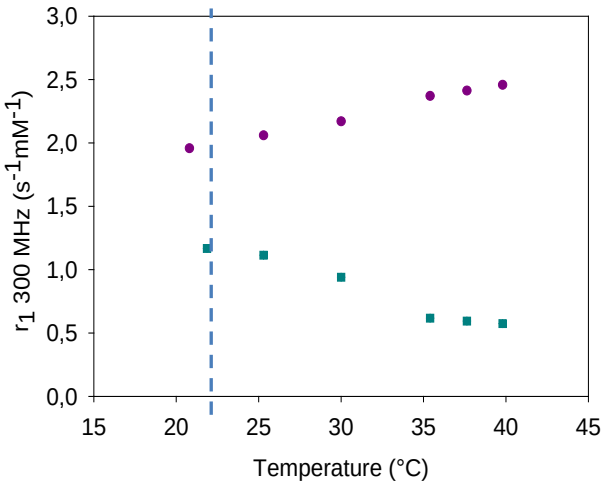

60 MHz (1.4T)

NP-JeffamineM2005

NP

300 MHz (7T)

r_2

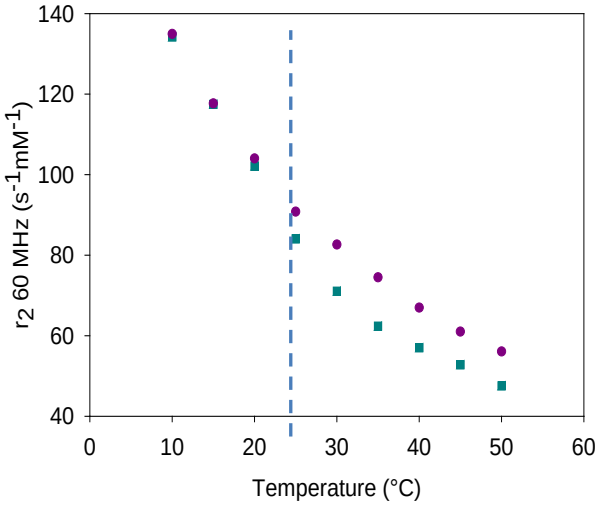

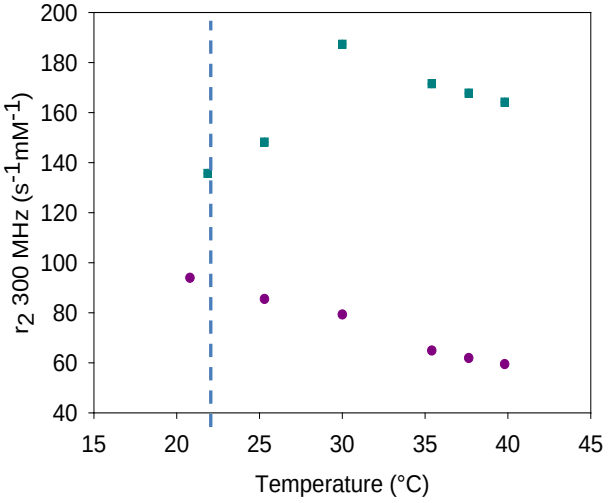

From thermo-sensitive relaxivities to positive MR contrast

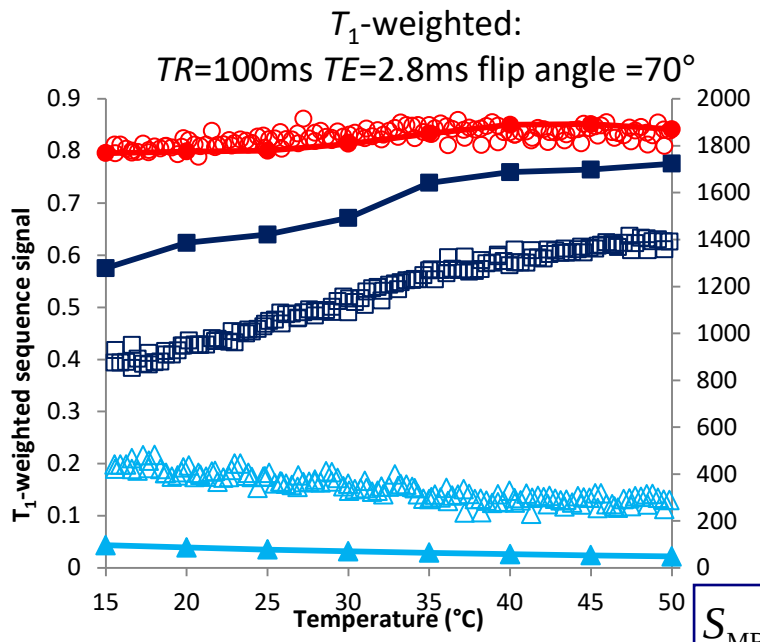

Low-field MRI
(8.25 MHz)

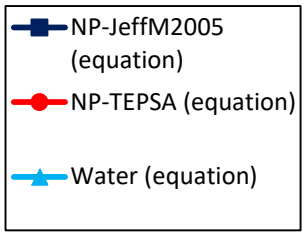

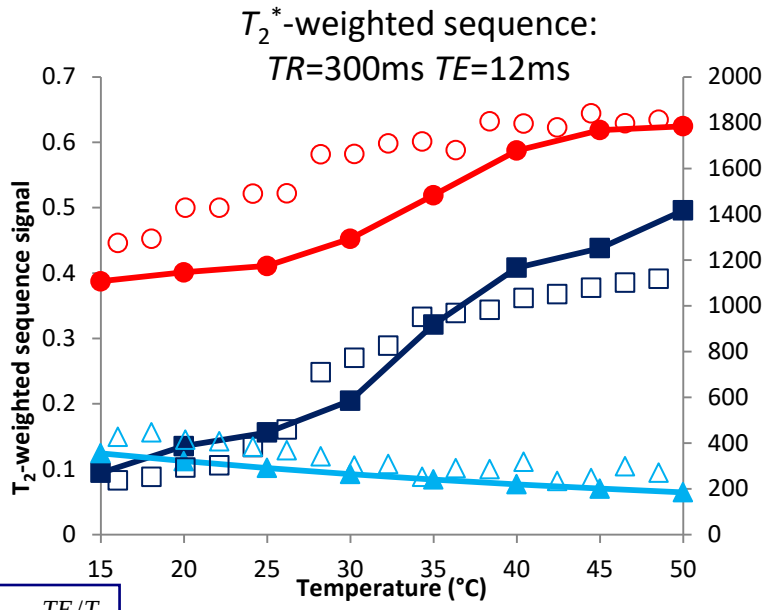

$$S_{\mathrm{MRI}} \propto \rho_{\mathrm{H}} \left(1 - e^{-TR/T_1}\right) \cdot e^{-TE/T_2}$$

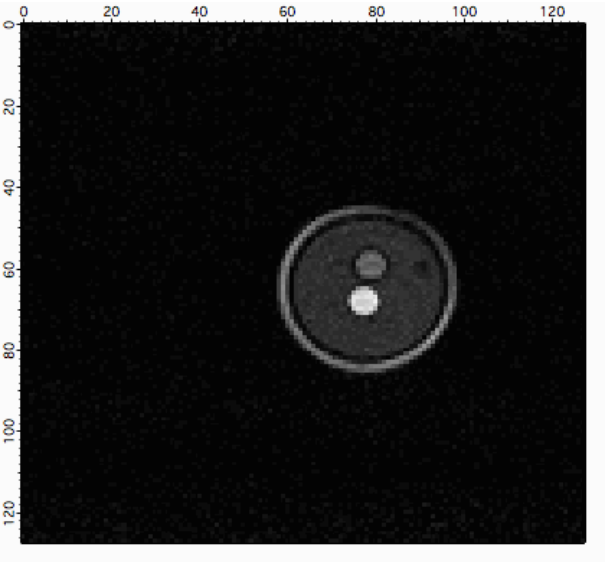

High-field MRI: negative contrast due to aggregation

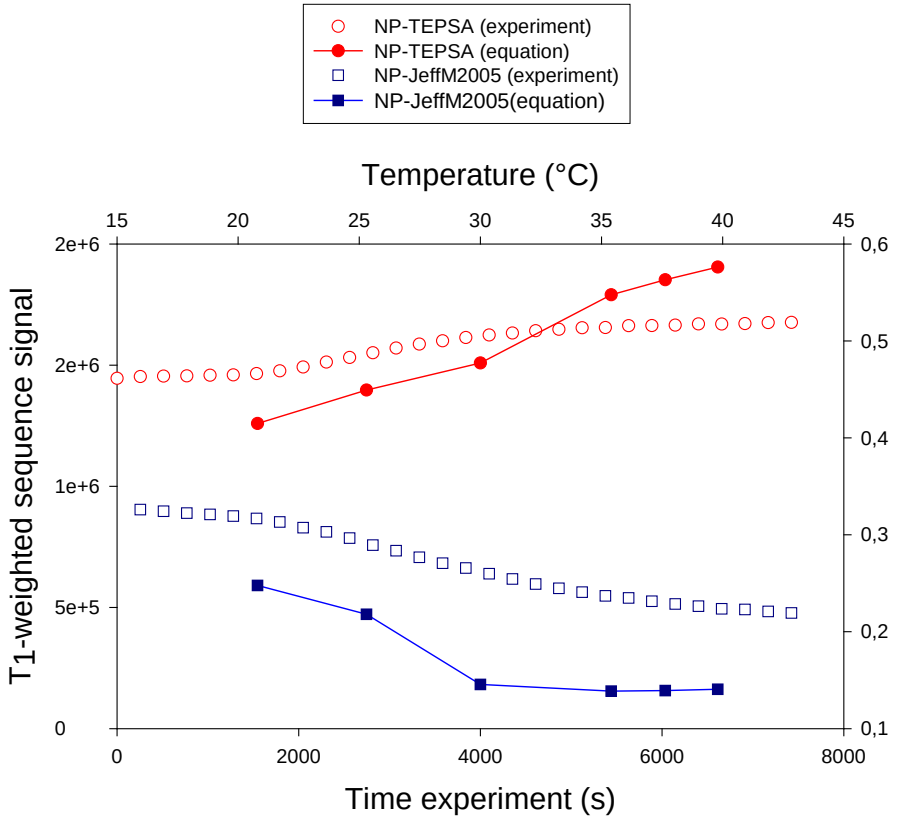

High-field MRI (300 MHz, B_0=7.05T)

T < LCST

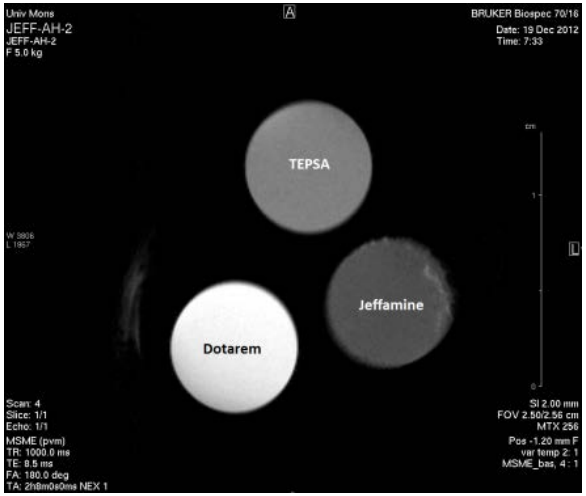

T > LCST

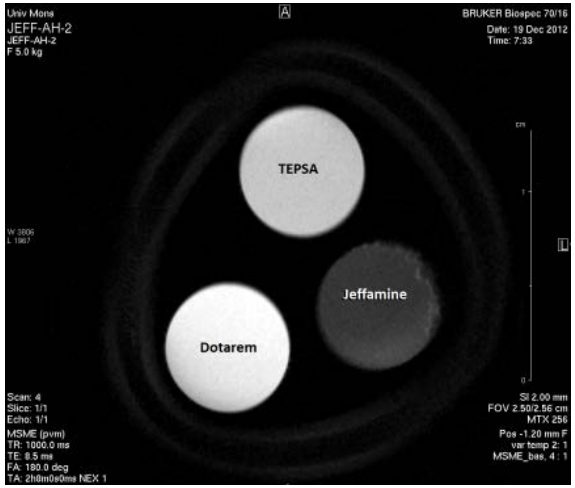

→ the TEPSA control USPIOs remains dispersed even under strong B_0 and induces positive contrast

→ the aggregation effect above LCST is enhanced by dipolar interaction for M-2005 coated-USPIOs

Use of MRI to map temperature during magnetic hyperthermia?

A. Hannecart, D. Stanicki, L. Vander Elst, R. N. Muller, S. Lecommandoux, J. Thévenot, C. Bonduelle, A. Trotier, P. Massot, S. Miraux, O. Sandre, and S. Laurent, *Nano-thermometers with thermo-sensitive polymer grafted USPIOs behaving as positive contrast agents in low-field MRI*, **Nanoscale**, 2015. **7**: 3754-3767

Future Developments 9

Low-field MRI is a fallow-lying field. For decades, the technical developments mainly addressed MRI with higher field strength. Very few attempts have been made, to transfer this progress to systems with a field strength below 0.5 T.

To activate our fantasy, let us have a look on possible developments specifically for low-field MRI systems.

9.1 Technical Improvements

9.1.1 Magnet Design

There have been a lot of innovative designs. Toshiba developed the OPART, a 0.35 T system with a high-temperature superconducting magnet.

The four poles of the magnet enabled wide open access at a high mechanic stability. This system is no longer available.

The C-arm concept is most frequently used for permanent magnet systems. Mainly Hitachi and Siemens pursue this design (Fig. 9.1).

A variation of the C-arm concept is a tiltable magnet, realized by Esaote. The G-scan magnet can be tilted, to enable weight-bearing examinations, which are of importance in musculoskeletal imaging (Fig. 9.2).

Another innovative approach has been proposed by FONAR, with one magnet on the ceiling and one on the ground, resulting in a 360° open magnet. The MRI is installed as work in progress in Oxford/GB (Fig. 9.3).

The FONAR Upright MRI is an open 0.6 T system with a resistive electromagnet for functional imaging. It fills a small, but important market segment (Fig. 9.4). PARAMED Inc./Italy has combined an upright imaging concept with tiltable table/seat, providing new application options.

A very innovative approach is the development of single-sided MRI. It is used for the so-called magnetic particle imaging (MPI). In MRI, the influence of tissue substance on the relaxation properties of protons is measured. In MPI, the

© Springer International Publishing Switzerland 2016

H.-M. Klein, *Clinical Low Field Strength Magnetic Resonance Imaging: A Practical Guide to Accessible MRI*, DOI 10.1007/978-3-319-16516-5_9

Fig. 9.1 Open C-arm Magnets: *Left* Siemens Magnetom C! 0.35 T. *Right*: Hitachi Aperto 0.4 T

Fig. 9.2 Esaote G-scan Brio with a field strength of 0.25 T

magnetization of the magnetic particles (magnetites, ultrasmall particles of iron oxide USPIO) is measured directly.

This method can produce extremely high-resoluted images in low magnetic fields (0.164 T) using the T1 relaxation time shortening. A vertical resolution of up to 20 µm is possible (Rössler et al. 2014). The magnetite particles are thermosensitive and can be used as nanothermometers, behaving as positive contrast agents in low-field MRI (Hannecart et al. 2015) (Fig. 9.5).

These different magnet designs give an impression of the variability of applications. Innovative magnet design is facilitated by low-field concepts.

High-field MRI: prevent aggregation in Matrigel™

SEM image of Matrigel™ (10 mg/mL BD Sci.) from R. Poincloux et al, *Journal of Cell Science* 122, 3015-3024

- dense protein network of meshsize 50-500 nm
- Viscous liquid at 4°C
- Gel at 37°C

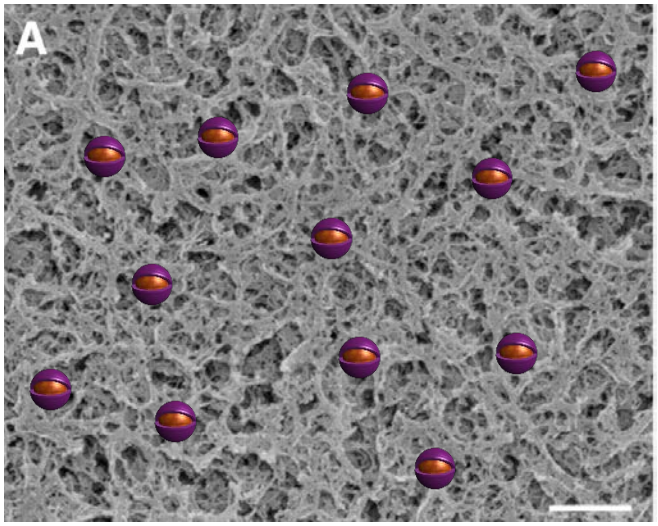

High-field MRI
(200 MHz, B_0=4.7T)

Ferro@Jeffamine B_0=4.7T (200MHz)

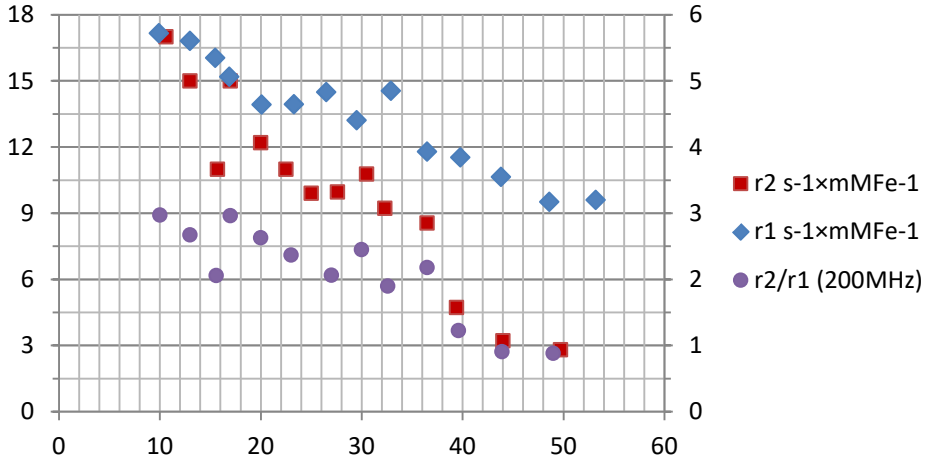

⟶ r_2/r_1 remains limited (aggregation prevented) but both relaxivities are significantly decreased, maybe due to water confinement effect like in USPIO up-taken by cells
Cf. Ribot et al, *Contrast Media Mol. Imaging* 2009, 4 109–117

Magnetic Responsive Polymer Composite Materials

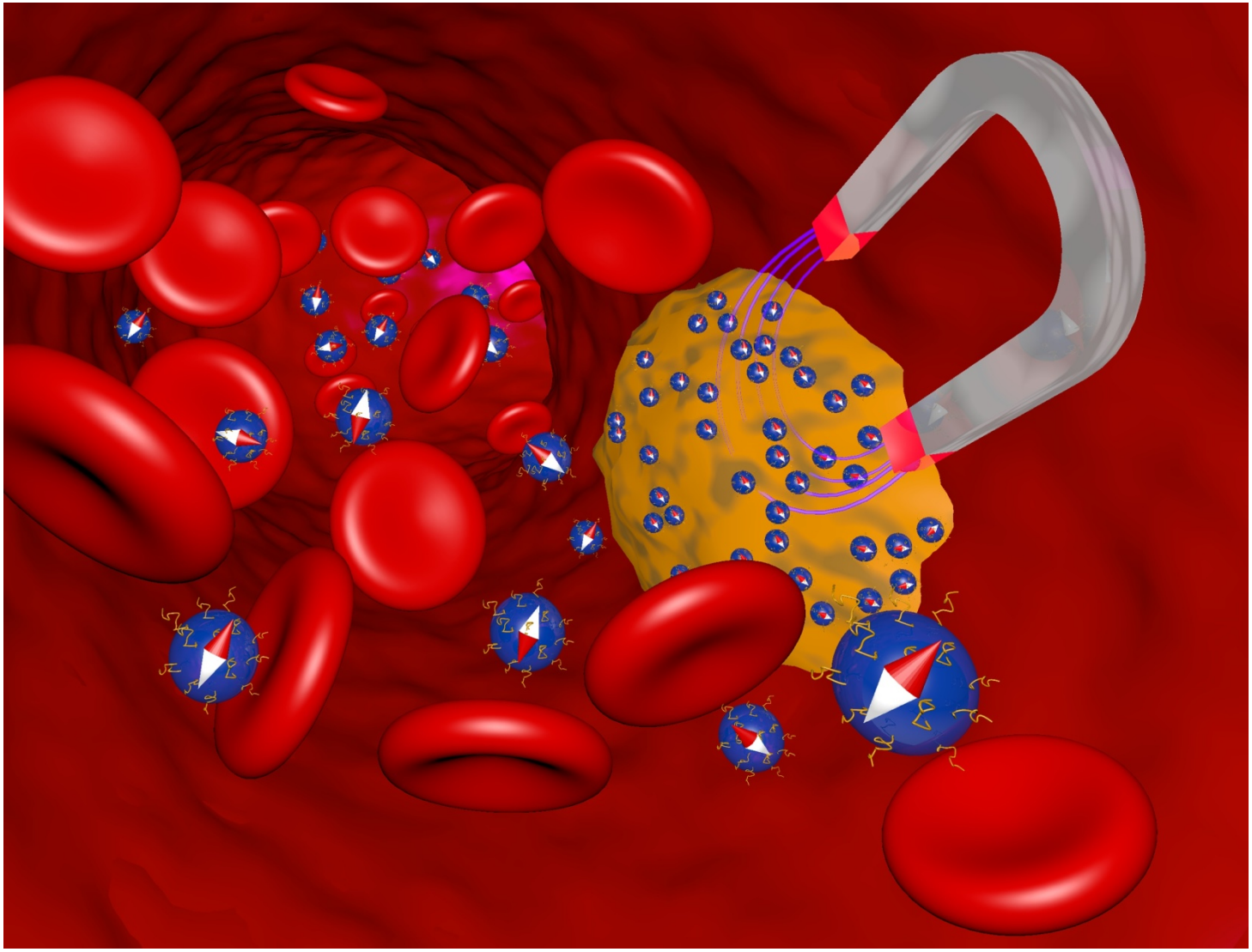

J. Thévenot, H. Oliveira, O. Sandre, S. Lecomandoux, **Chem. Soc. Rev.** **2013**, 42, 7099-7116

Magnetic Responsive Polymer Composite Materials

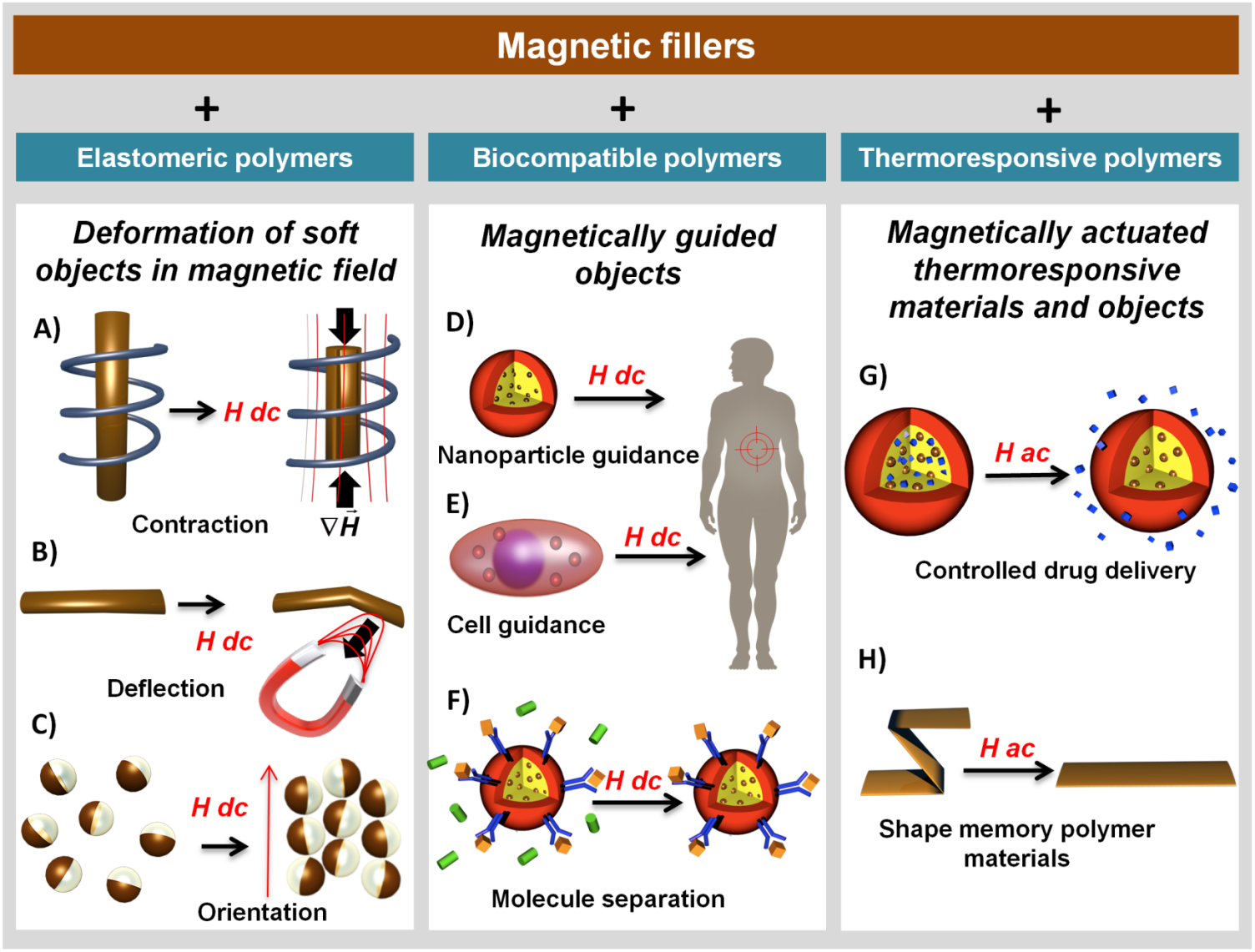

J. Thévenot, H. Oliveira, O. Sandre, S. Lecomandoux, **Chem. Soc. Rev.** **2013**, 42, 7099-7116

Thermotherapies as old as Hippocrates !

which dates back to about 3000 B.C. (BREASTED 1930). Therein a clinical report is presented of a woman suffering from a (malignant?) breast tumor. In this case it was recommended that the tumor be treated by means of the so-called fire drill, which was clearly meant to be a local caustic therapy. Subsequently, such local heat treatments were described in numerous other reports by Greek and Roman physicians. This ancient confidence in the application of local heat is underscored by one of the famous aphorisms of the Greek physician Hippocrates, who stated (translated in Latin words, according to OVERGAARD 1985):

Quae medicamenta non sanant, ferum sanat.
Quae ferum non sanat, ignis sanat.
Quae vero ignis non sanat, insanobilia reportari oportet.

which means:

Those who cannot be cured by medicine can be cured by surgery.
Those who cannot be cured by surgery can be cured by heat.
Those who cannot be cured by heat are to be considered incurable.

1st attempt of magnetic hyperthermia by physicians (not physicists!)

R. K. Gilchrist, R. Medal, W. D. Shorey, R. C. Hanselman, J. C. Parrot, 2386 and C. B. Taylor, *J. Ann. Surg.* 146, 596 (1957).

A broad variety range of MFH applicators

- Lab-made setups
- Commercial setups for other purposes than MFH research (dentistry, jewelry, soldering)
- Commercial setups dedicated to MFH research

- Applicators for SAR measurements
- Applicators for in vitro MFH (Petri dishes for cell culture)
- Applicators for in vivo MFH (pre-clinical assays on rodents, clinical assays on humans)

- Mono-frequency solid-state generators *vs.* multi-frequencies resonant circuits
- Open coils *vs.* ferrite circuits: control of field lines
- Hollow pipe *vs.* multi-strand conductor (Liz wire), water-circulation *vs.* air-cooling…

- Adiabatic conditions or not (need thermal loss correction)
- Thermometry: localized T-measurement (fiber probe) *vs.* infrared thermometry
- H field intensity and frequency assessment: redaction of a technical note by WG4

LCPO
Laboratoire de Chimie des Polymères Organiques

General concepts

a) Coil vs. b) Ferrite core

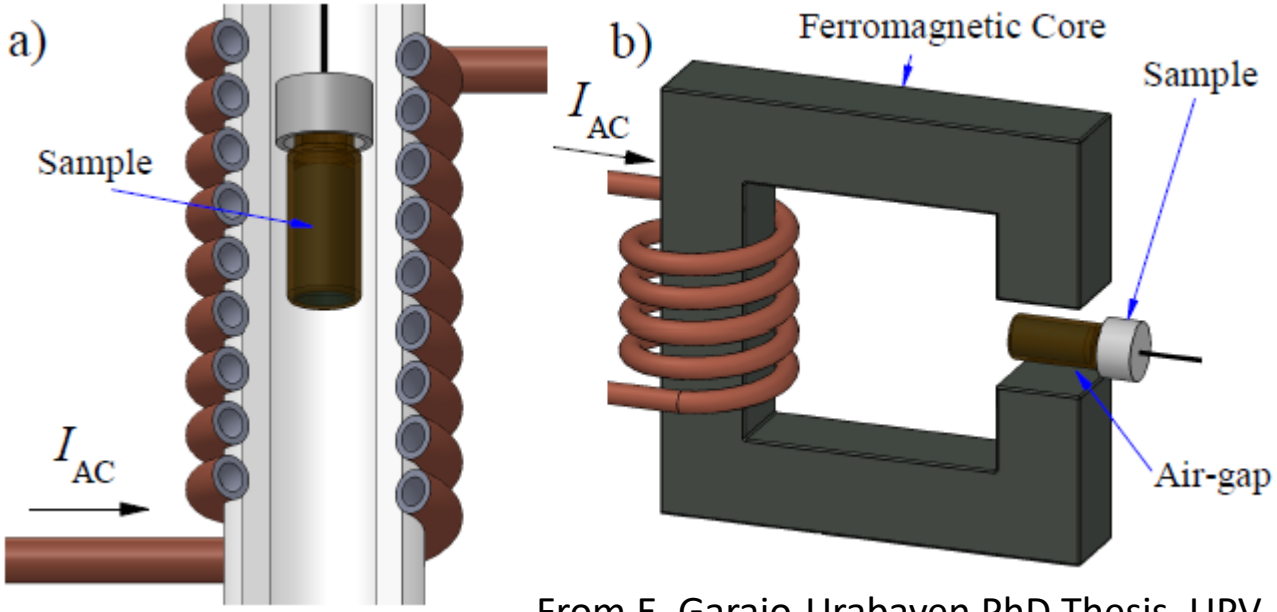

From E. Garaio-Urabayen PhD Thesis, UPV-EHU, March 2015

$$B(\text{Tesla}) \approx \frac{\mu_0 N \times I}{L}$$

a) Air-coils sample located in the center where the H field is more homogeneous and intense
b) Ferrite cores to concentrate the magnetic flux B inside sample, more homogeneous field

When large usable-gaps or usable volumes are required (whole human body applicators), electromagnetic applicator based on ferromagnetic cores are preferred). However, ferrite cores implies additional power consumption, especially at high frequencies.

In vivo applicator: clinical (human)

Clinical human applicator

Pr Andreas Jordan, Charité hosp. Berlin

MagForce AG, www.magforce.de

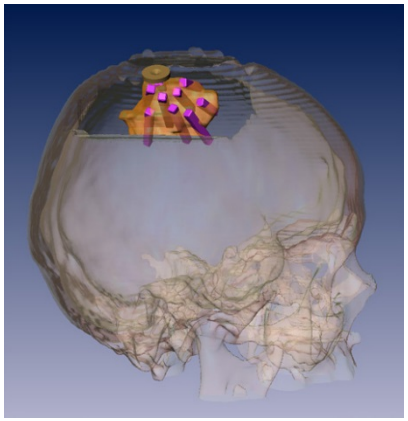

NanoPlan®: Computer-assisted Injection of magnetic NPs in glioblastoma

NanoTherm®: 15nm cores, -NH_2 coated

$$C_{\gamma\text{-}Fe_2O_3}^{tumor} \approx 160\,g/L$$

2003: Beginning of phase 1 clinical trial
2007: End of phase 1 clinical trial
2011: End of phase 2 clinical trial (68 patients)
Nowadays: Authorized on market in Europe

NanoActivator® T_{tumor}=43-50°C

f_{RF}=100 kHz, H_{max}=2 – 18 kA/m, B_{max}=2.5 – 23 mT

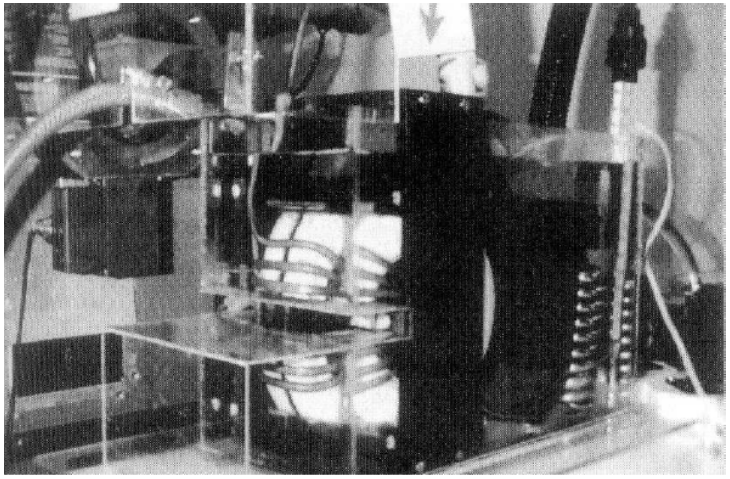

Picture of prototype (courtesy L. Vekas)

Components Of The NanoTherm® Therapy:

Novel method for local treatment of tumors

THERAPY PLAN

1. INJECTION

Iron oxide nanoparticles are injected directly into the tumor using conventional methods following therapy planning

NanoTherm® is a colloidal dispersion of superparamagnetic iron oxide nanoparticles with a diameter of approx. 15 nm and a coating of aminosilane. The iron concentration of the dispersion is 112 mg/ml (or 335 mg/ml)

NanoTherm® is injected directly into the tumor in an intraoperative procedure

Due to their special coating, the nanoparticles remain at the injection site

2. TUMOR TEMPERATURE SIMULATION

Treatment temperatures and corresponding magnetic field strengths are defined by the physician before the start of therapy (Post Implantation Analysis, PIA)

The software NanoPlan® simulates temperature distribution in the treatment area and suggests magnetic field strength for NanoTherm® therapy

The basis of the treatment plan is the concentration and position of the nanoparticles in the tumor measured by postoperative CT and temperature maxima defined by the physician

Components Of The NanoTherm® Therapy:

- Magnetic field activates Neel and Brownian relaxation processes of iron oxide nanoparticles generating heat
- Magnetic field strengths of approx. 2-15 kA/m
- NanoActivator'" induces therapeutic treatment temperatures within the tumor of > 40 °. Thermotherapy effect enhances theefficacy of radio- and chemotherapy
- Innovation values of NanoActivator™
- Can be applied to solid tumors in all body regions
- First therapy device specifically for nanomedicine
- Dose adjustment during therapy by regulating the magnetic field strength
- Direct intratumoral temperature measurement during therapy for securing optimal therapeutic temperatures and patient safety

In vivo applicators: pre-clinical (rodents)

Example of lab-made in vivo setup

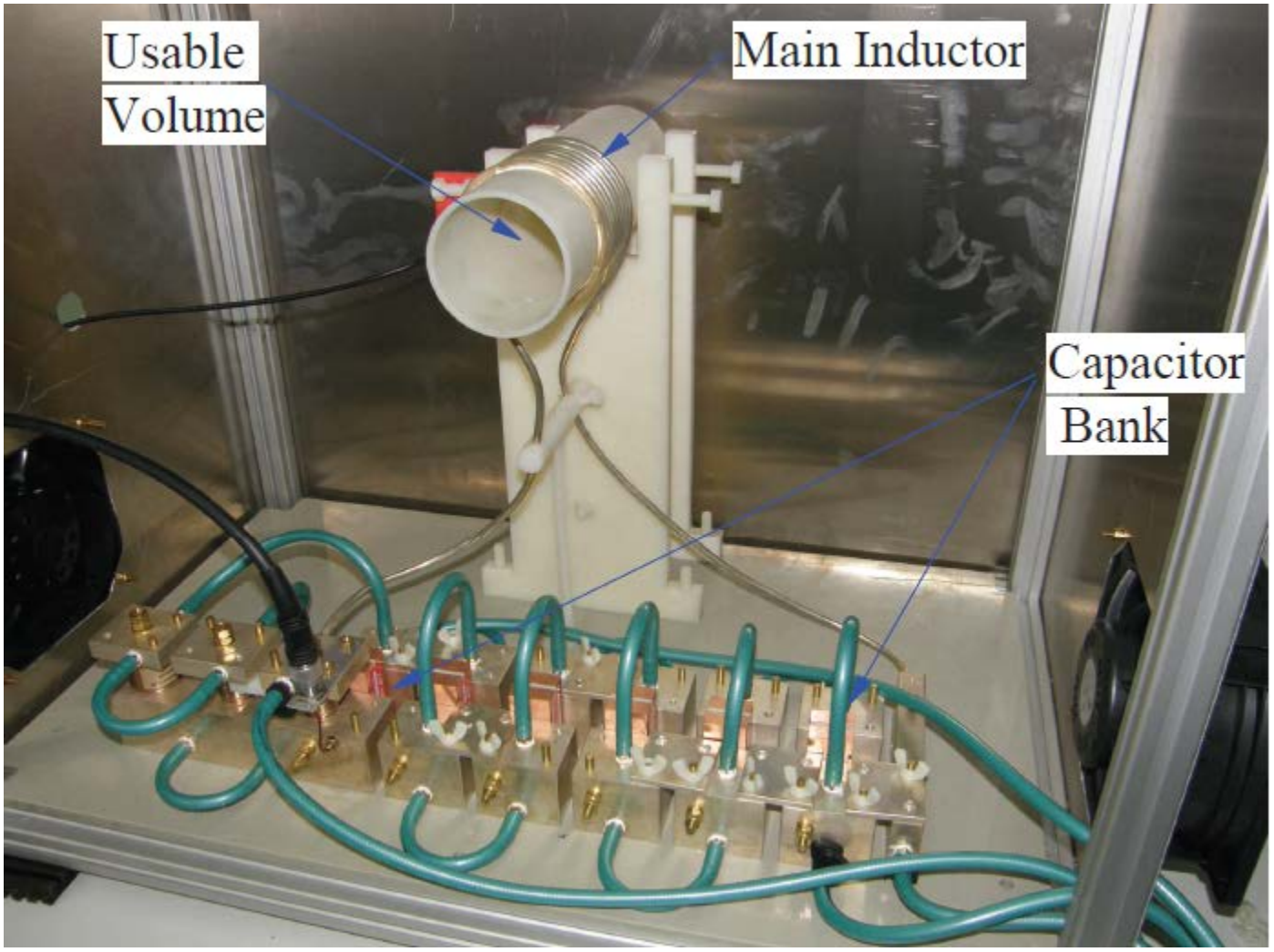

Nanotherics magneTherm™

Heat-Generating Iron Oxide Nanocubes: Subtle “Destructurators” of the Tumoral Microenvironment

Direct injection of nanocubes in the tumor (0.7 mg iron)

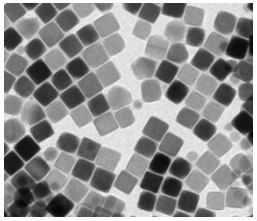

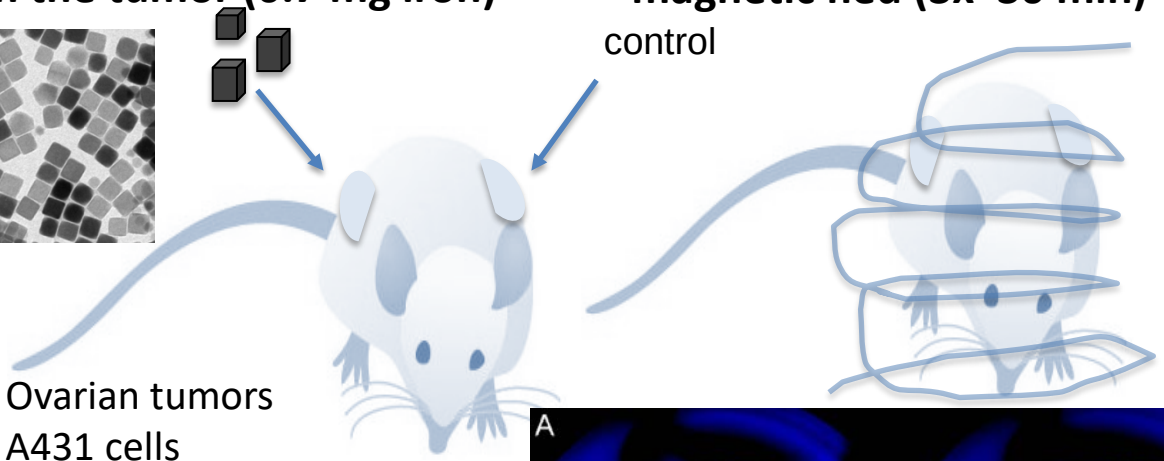

Ovarian tumors
A431 cells

Exposure to the alternating magnetic fied (3x 30 min)

110 kHz – 23,8 kA/m

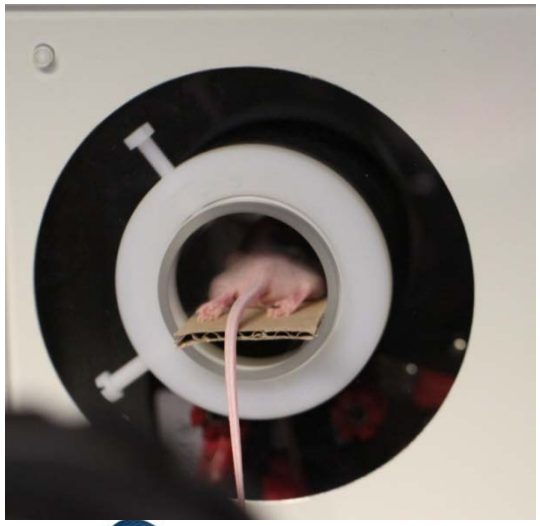

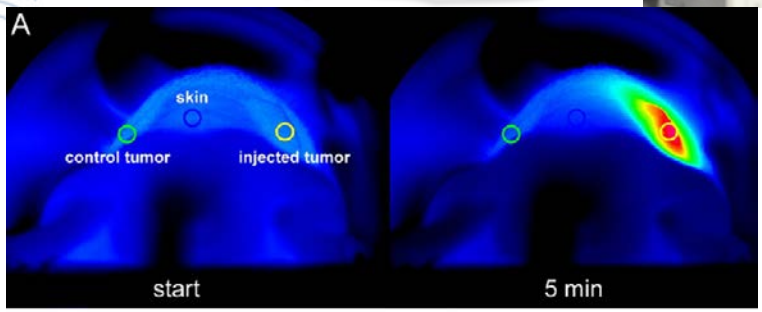

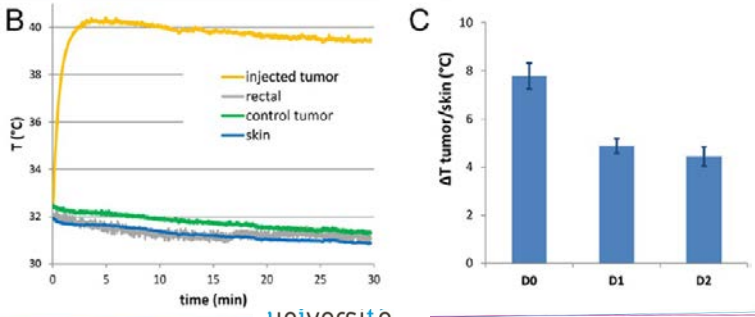

J. Kolosnjaj-Tabi et al
ACS Nano 8, 4268, 2014

Nanotherics magneTherm™

Recommended accessory for *in vivo* experiments:
Mouse restrainer / water-jacket (37°C)

2 coils Helmholtz-like configuration

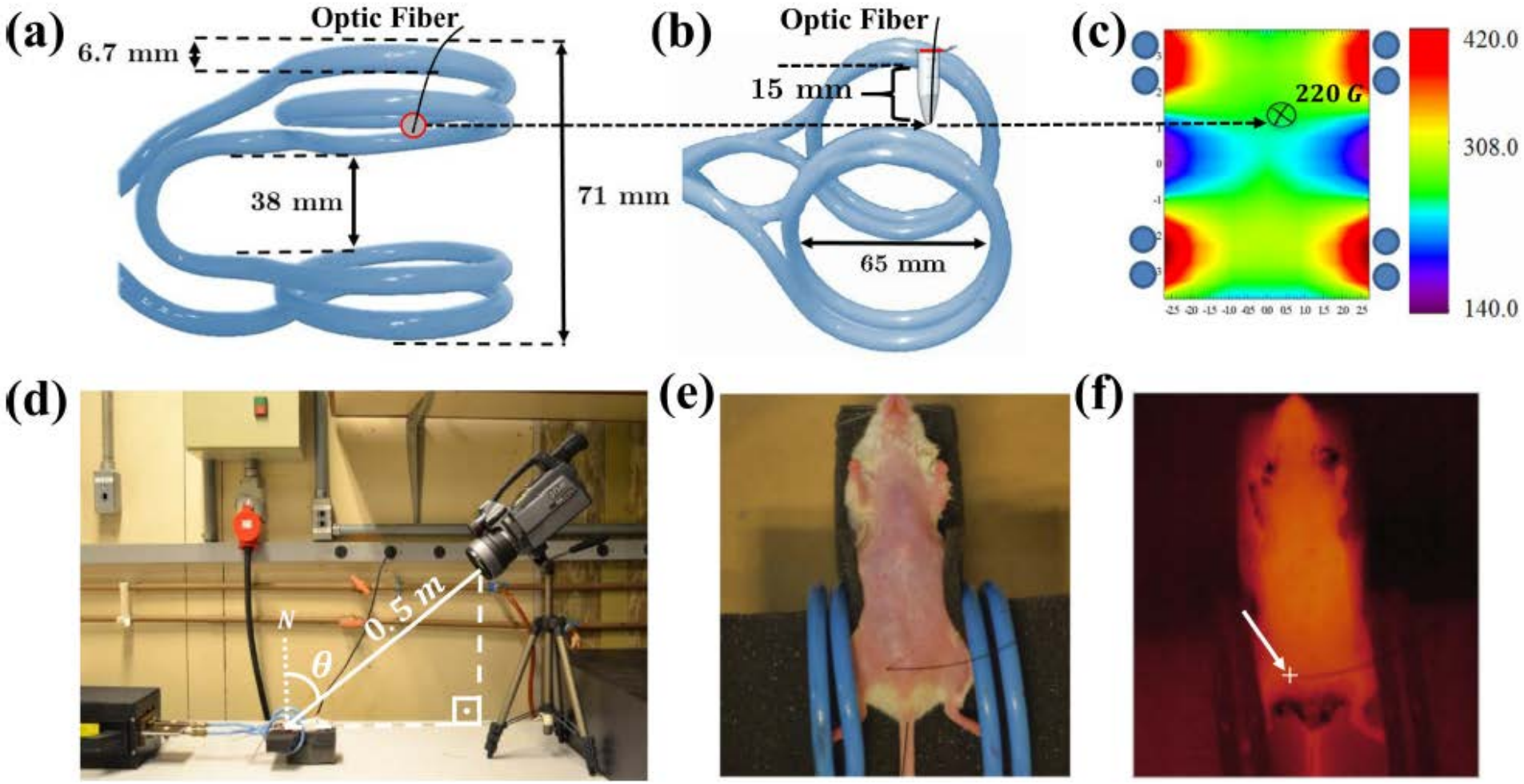

Rodrigues, Bakuzis, to appear in *Physics in Medicine and Biology* (IOP journal)

DM3 from nanoScale biomagnetics

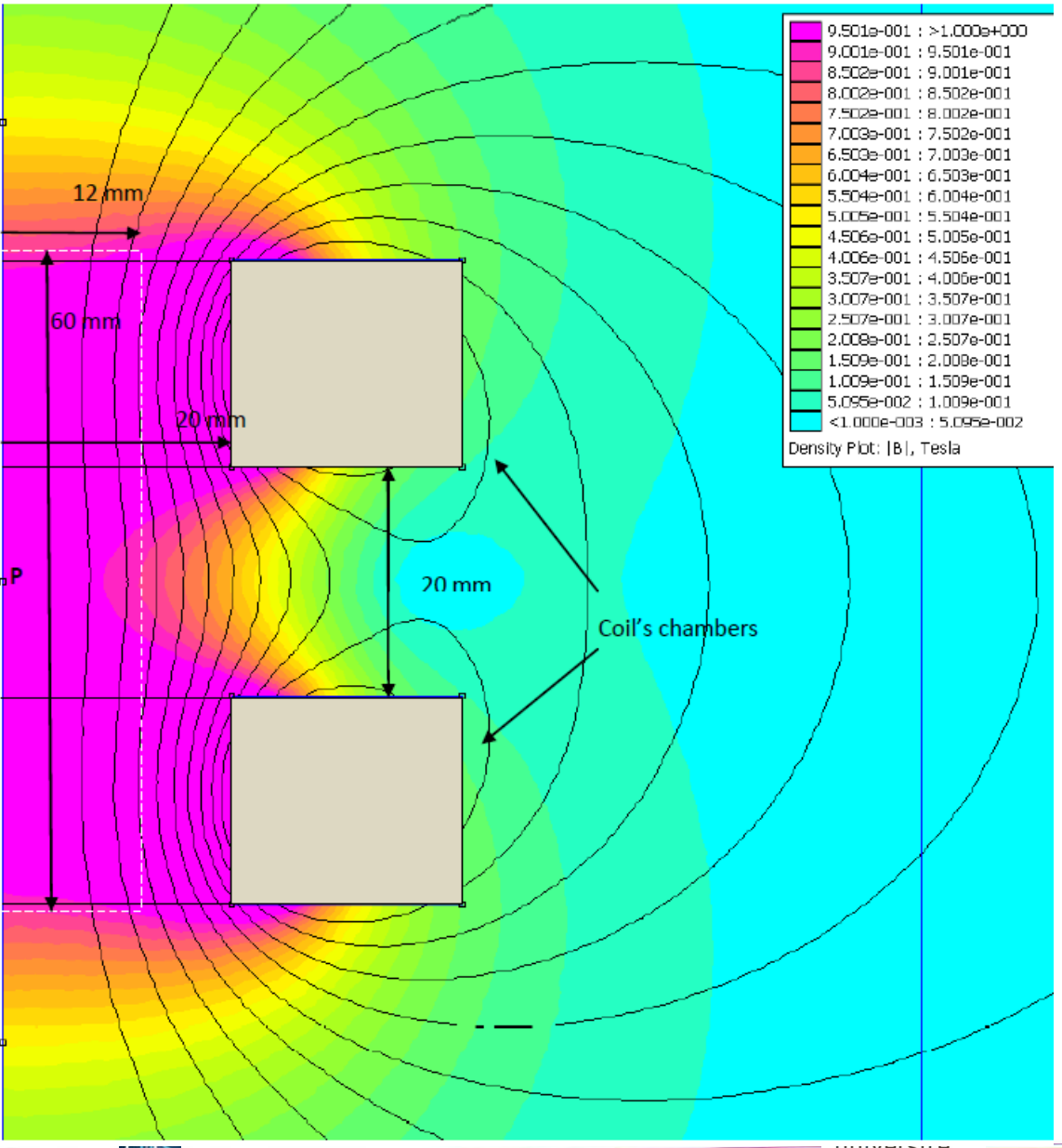

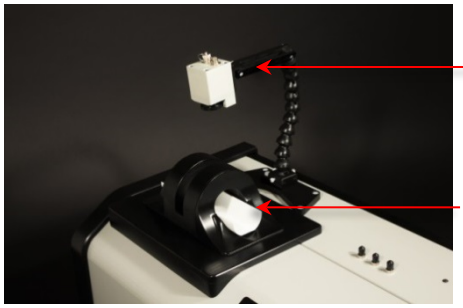

IR camera to measure T

Coil to generate the AMF

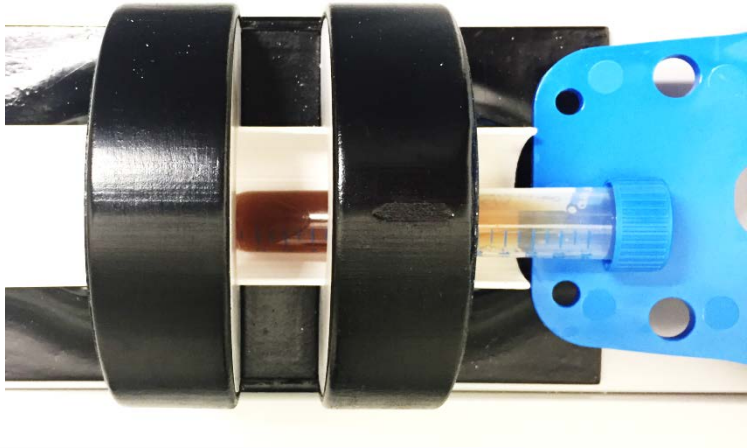

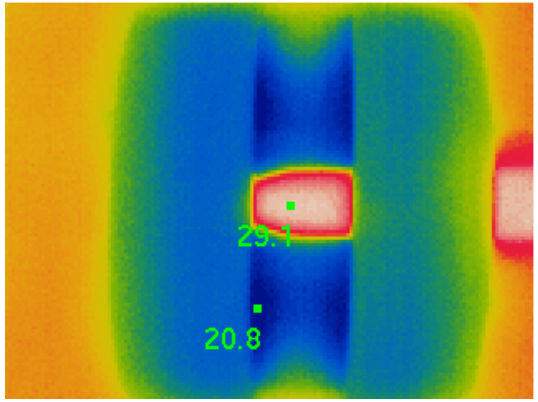

LCPO
Laboratoire de Chimie des Polymères Organiques

Applicators for SAR measurement

Example of lab-made SAR measurement setup (Paris 97')

Current generator : 300 kHz at f= 1.1 MHz / I_{max}= 12 A

J. Servais, MSC – Univ. Paris 7
J-P. Fortin et al
JACS 129, 9, 2628-2635, 2007

Fiber optic thermometer

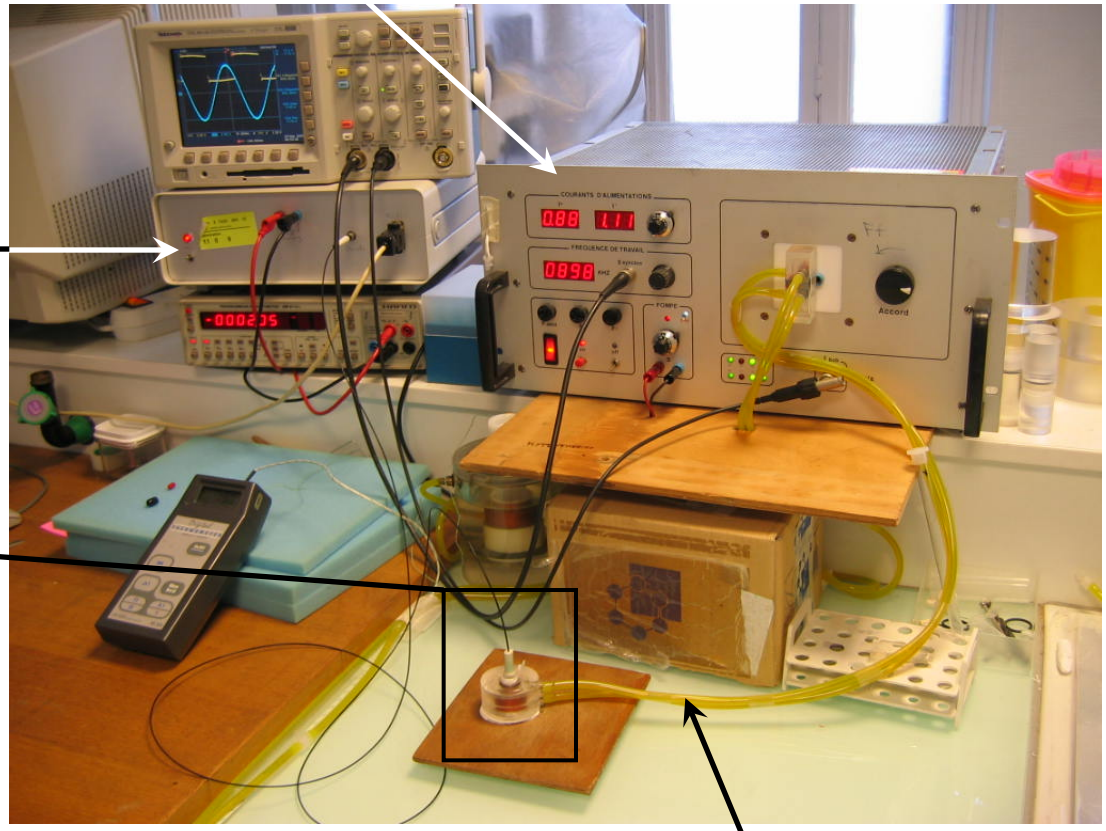

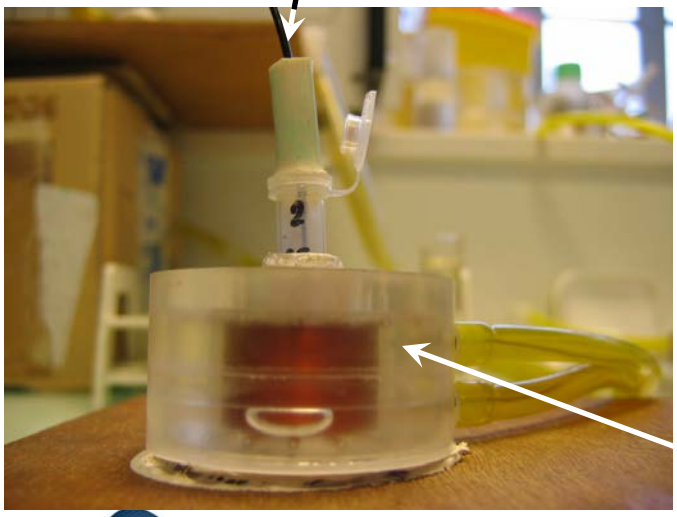

Thermal regulation (circulation of C_9H_{20} instead of water)

Coil: Ø 12 mm / H=1.8 (kA·m^{-1})/A (H_{max}=21.6 kA·m^{-1})

Measurement of magnetic hyperthermia efficiency

Measurements of the heat generation by ultra-small superparamagnetic iron oxide particles (USPIO) under AC magnetic field by calorimetry (here: non-adiabatic condition)
→ Specific Absorption Rate (SAR) or Specific Loss Power (SLP)

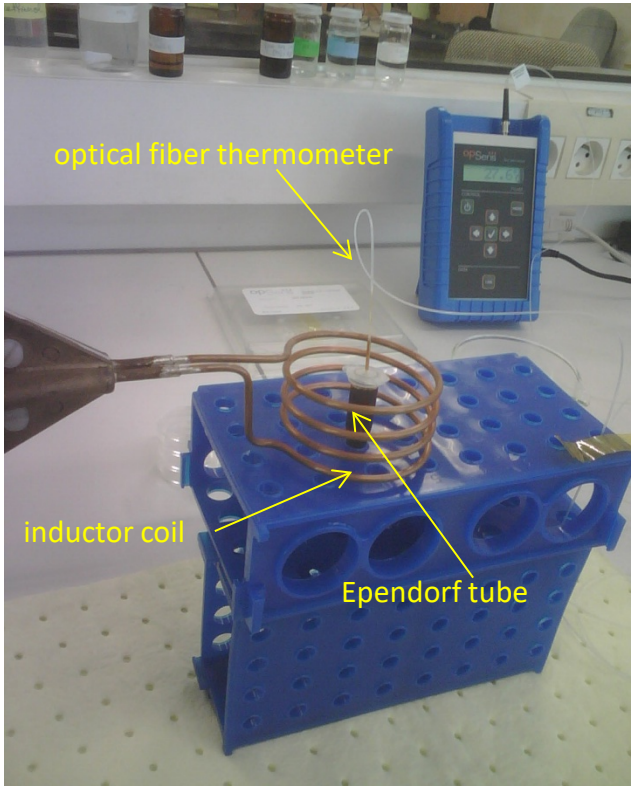

f_{RF}=755 kHz, H_{max}= 10.2 kA/m

RF heating of USPIOs' samples at 5mg/mL in H_2O at 755kHz magnetic field, H_{max}=10.2kA/m (I_{max}=233A)

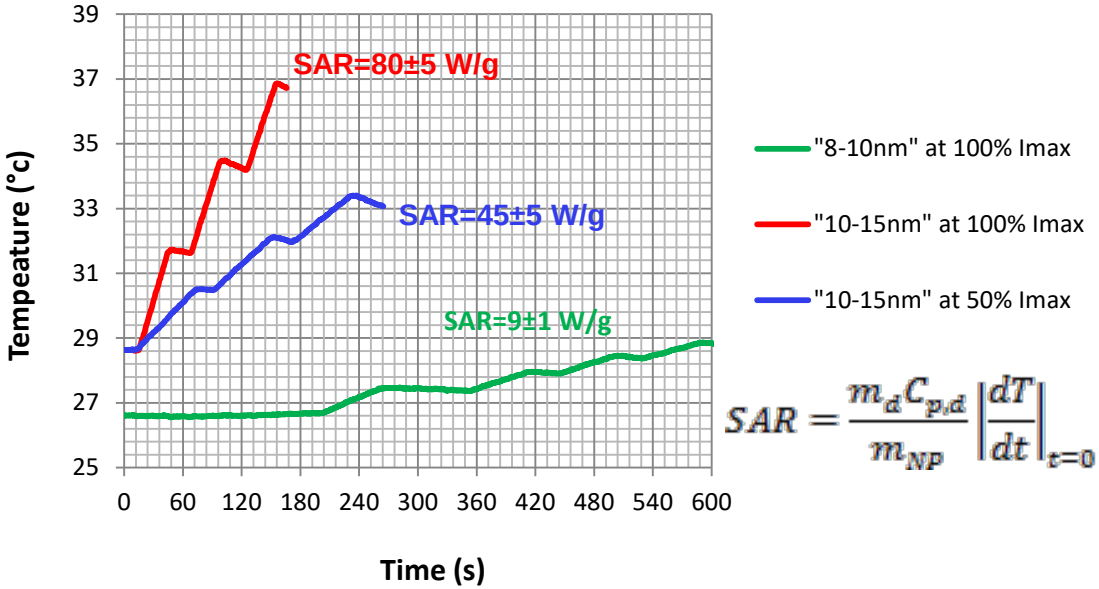

$$SAR = \frac{m_d C_{p,d}}{m_{NP}} \left|\frac{dT}{dt}\right|_{t=0}$$

'stepped heating' N. Iacob et al, *Eur. Phys. J.* E (2015) 38: 57

4.18J needed to heat 1g of water by 1°C
→ convert slopes $\Delta T/\Delta t$ into SAR values in W/g (of iron oxide)

Experimental conditions of 120 publications over 25 years compared to 'Brezovich criterion' $H_0 \cdot f < 4.8 \times 10^8$ A(ms)$^{-1}$

Scatter size proportional to $H_0 \cdot f$ product

SAR measurement

in vivo

in vitro

in vivo & in vivo

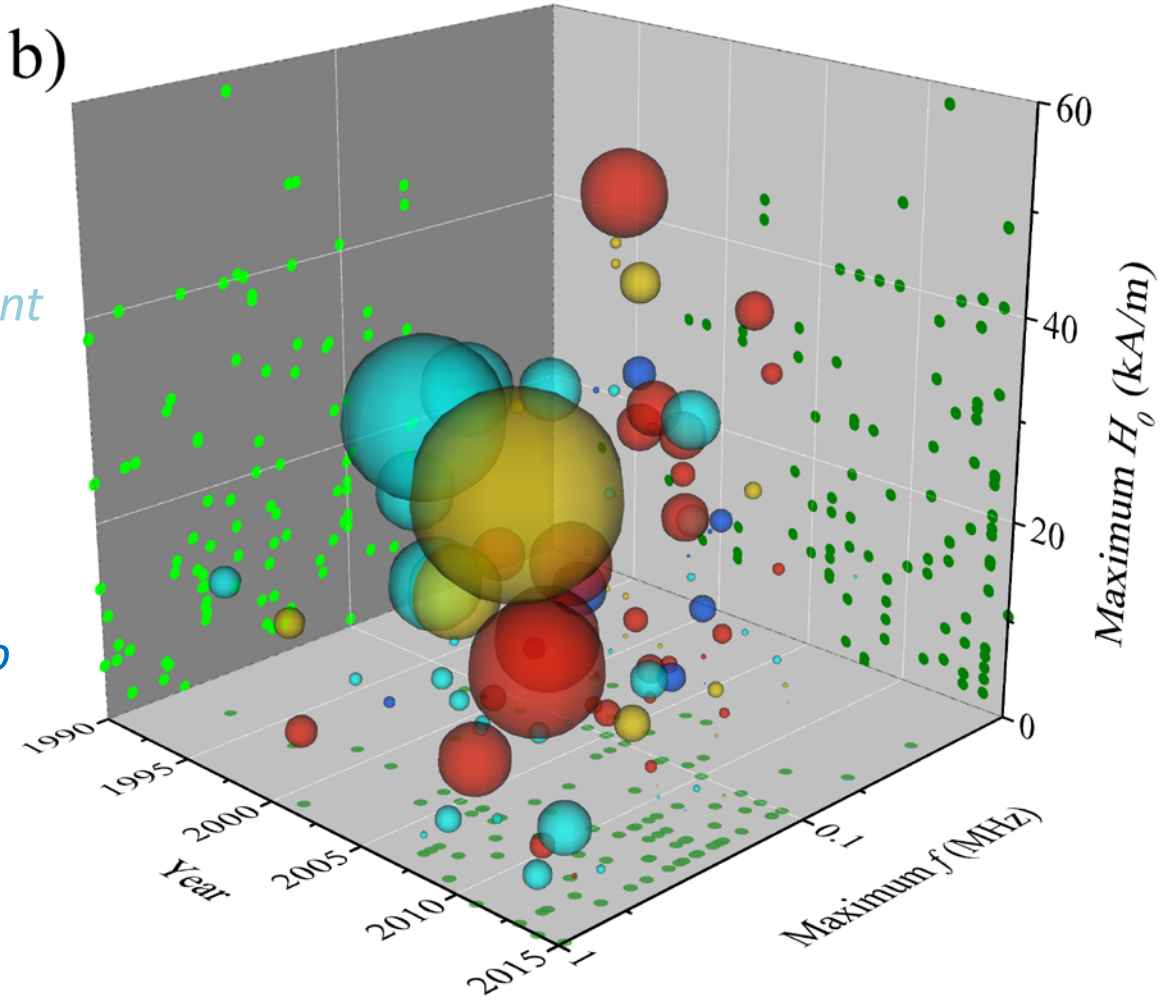

Fundamentals and advances in magnetic hyperthermia,
E. A. Périgo, G. Hemery, O. Sandre, D. Ortega, E. Garaio, F. Plazaola, F. J. Teran
Applied Physics Reviews **2**, 041302 (2015)

Bordeaux-Bilbao collaboration on magnetic hyperthermia

Aquitaine-Euskadi “Euro-region”

- **University of Basque Country (Bilbao, Spain)**

  Team of Fernando Plazaola (Vice-Rector), Eneko Garaio, Jose-Angel Garcia (Phys.), Juan-Mari Collantes (Electr. Eng.), MD Javier Echevarria

université de BORDEAUX

eman ta zabal zazu

UPV EHU

- **Université de Bordeaux / CNRS**

  Team of Sébastien Lecommandoux, Olivier Sandre (LCPO)

  Team of Etienne Duguet, Stéphane Mornet, Graziella Goglio (ICMCB)

  Team of Franck Couillaud (RMSB), MD Nicolas Grenier, MD Hugues Loiseau, MD Arnaud Hocquelet

Setups travelling between Bilbao and Bordeaux

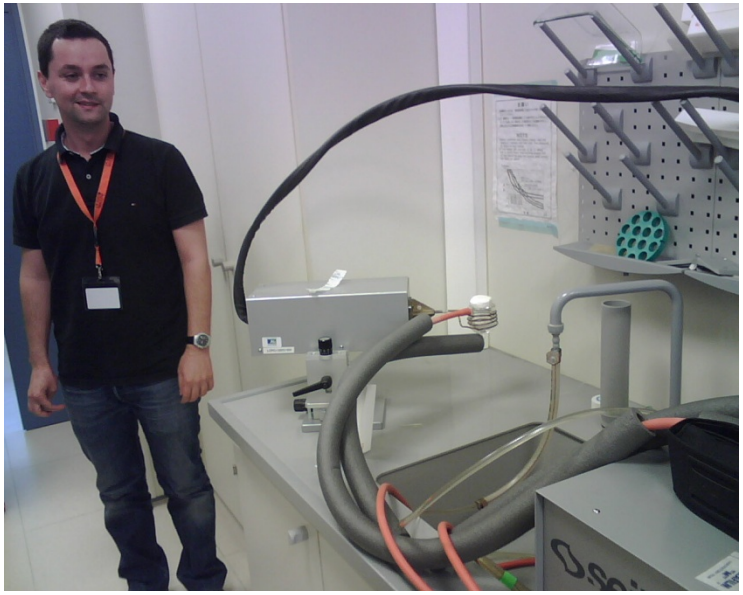

LCPO' "magnethermon" brought to Bilbao by Hugo Oliveira for *in vitro* expts at CIC biogune (Edurne Berra) in July 2012

European NMP-Health-FP7"
Leader: Gaiker (Bilbao) www.nanother.eu
dedicated to cancer nanotherapy (11 M€)
In Bordeaux: LCPO, RMSB, CBMN
In Bilbao and San Sebastian: CIC biogune, Gaiker, Vicomtech

Bilbao's setup (Eneko Garaio's prototype) brought to Bordeaux for SAR measurements in Spring 2014

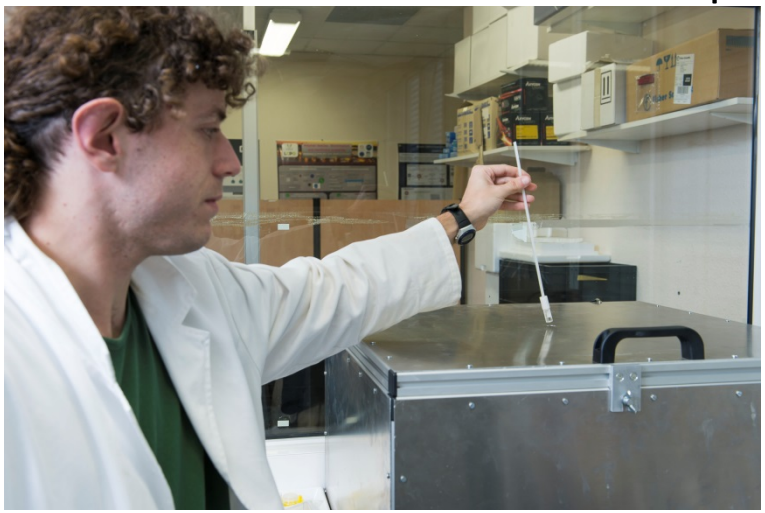

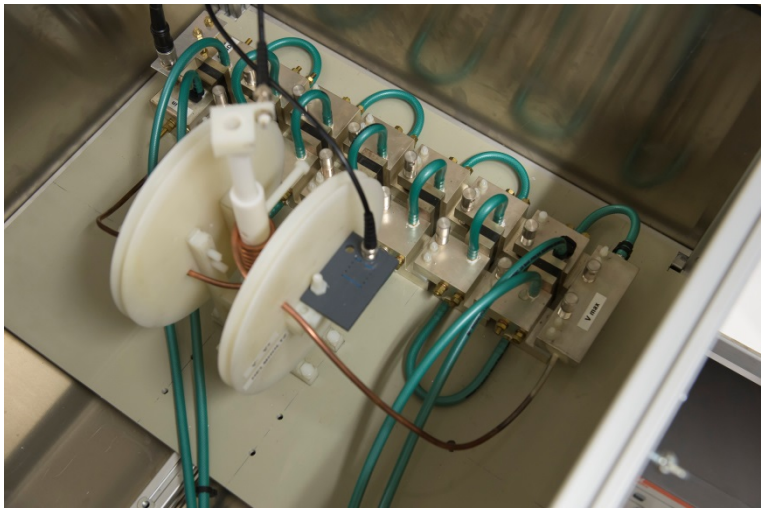

Example of lab-made setup: all Bilbao's setups

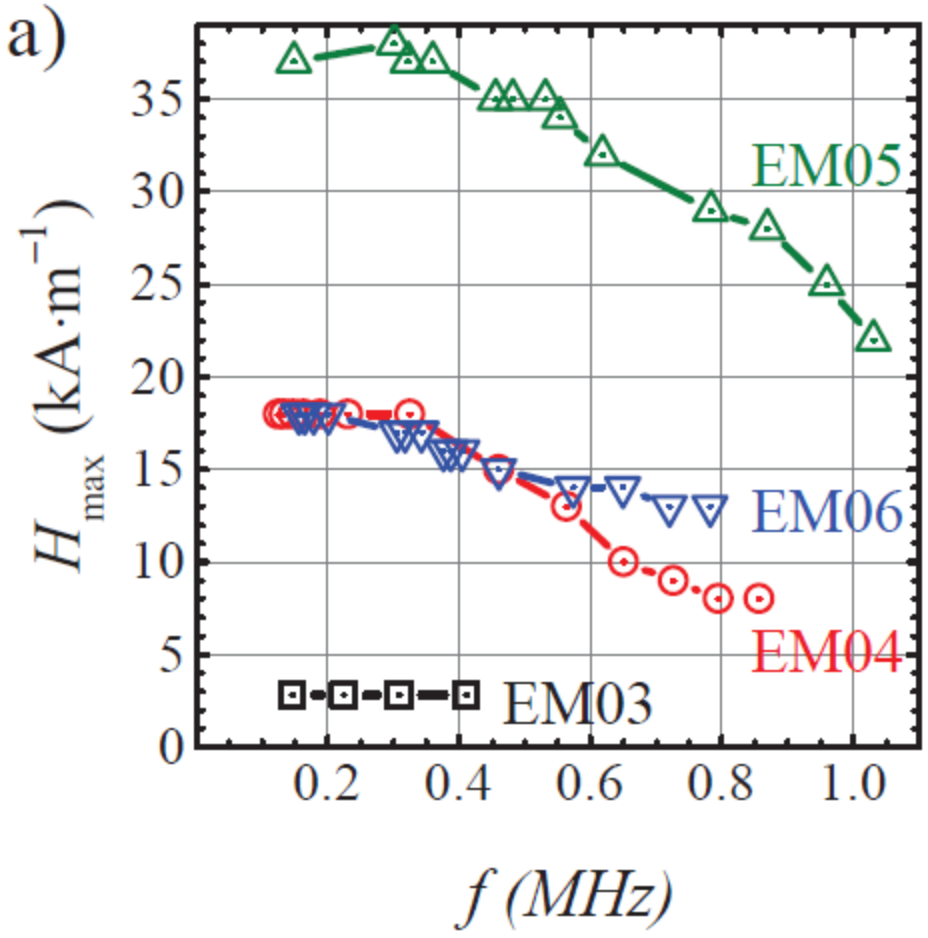

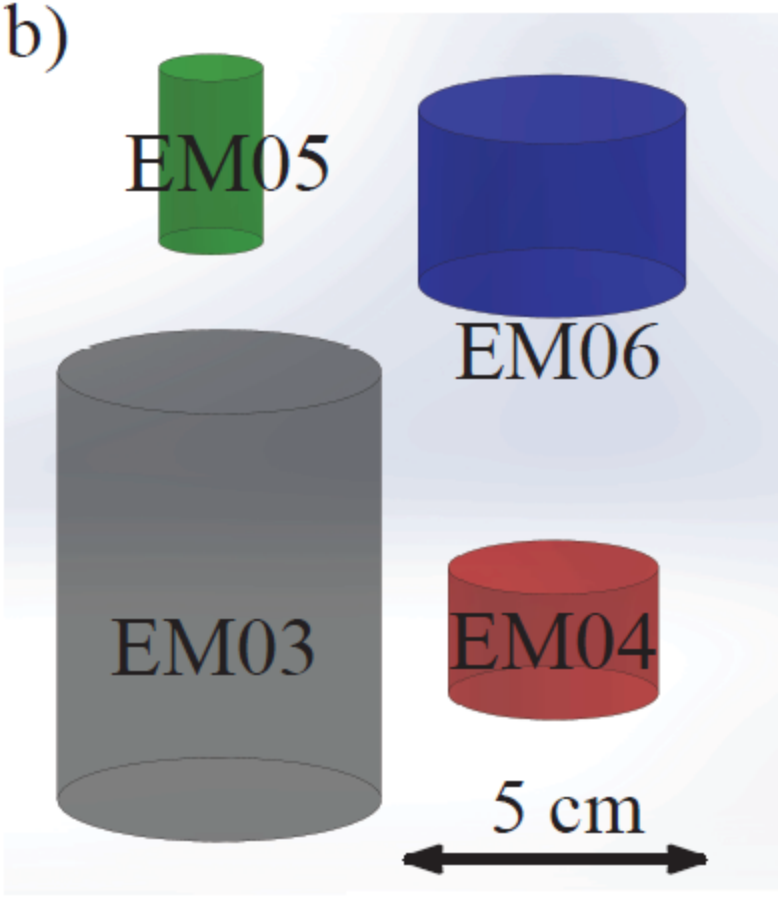

Bordeaux's setup improved with help of UPV-EHU

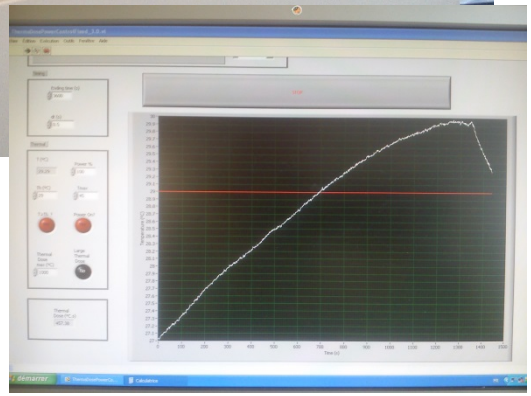

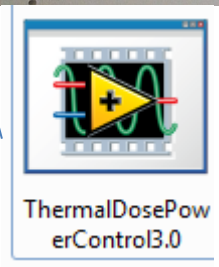

Thermal Dose & Power Control by Eneko Garaio

eman ta zabal zazu

UPV EHU

"VASCO Flex" by Cordouan Technologies (startup company nearby Bordeaux campus)

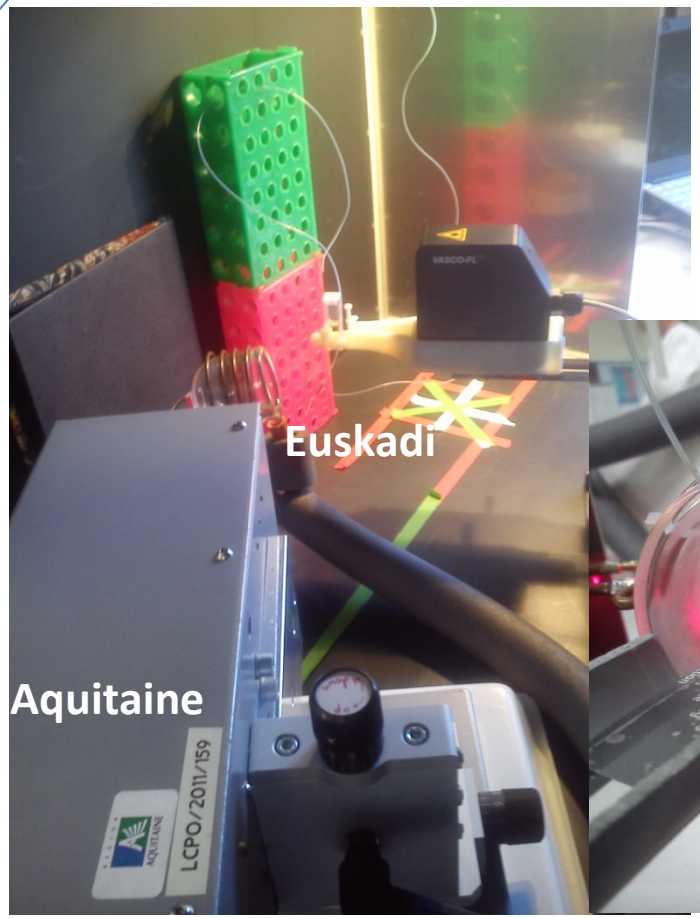

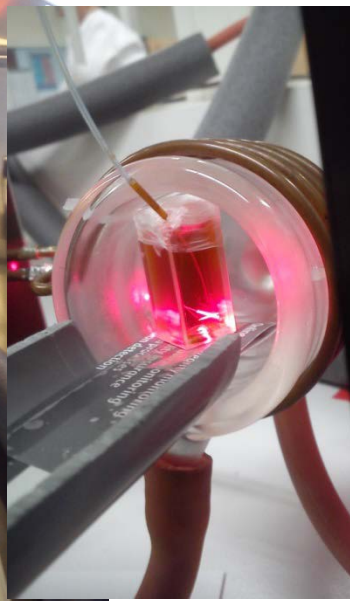

Calorimetry vs. magnetometry to measure SAR

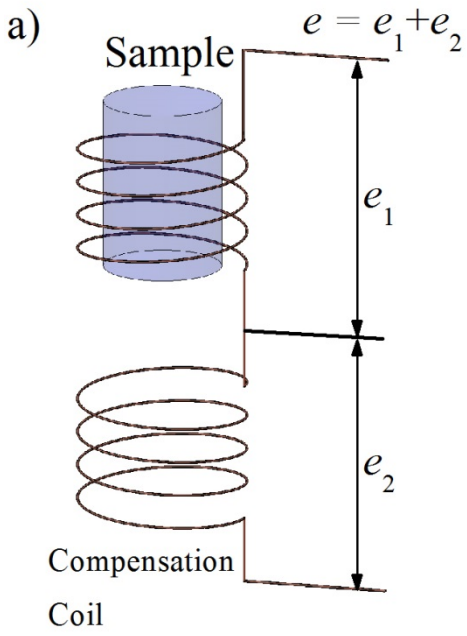

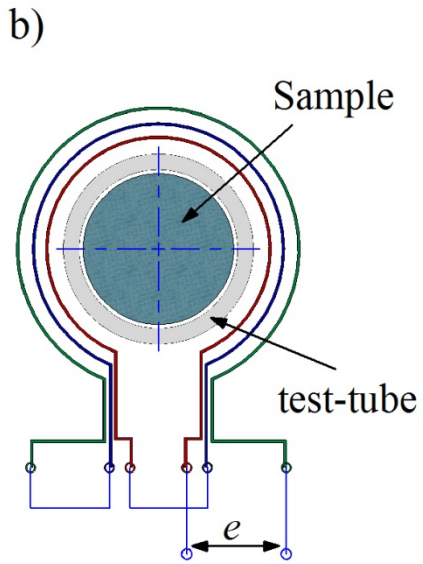

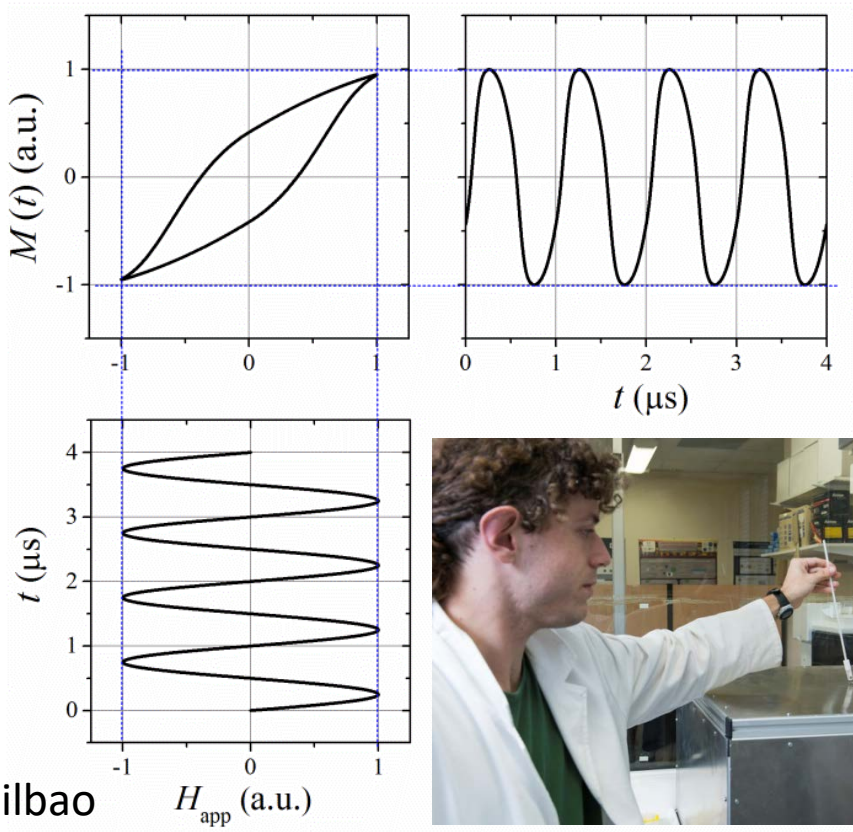

Eneko Garaio-Urabayen PhD Thesis 2015, UPV-EHU, Bilbao

- E. Garaio, J. M. Collantes, J. A. García, F. Plazaola; S. Mornet, F. Couillaud, and O. Sandre, *A wide-frequency range AC magnetometer to measure the specific absorption rate in nanoparticles for magnetic hyperthermia*. **J. Mag. Mag. Materials**, 2014. **368**: 432-437
- E. Garaio, O. Sandre, J-M. Collantes, J. A. Garcia, S. Mornet, and F. Plazaola, *Specific absorption rate dependence on temperature in magnetic field hyperthermia measured by dynamic hysteresis losses (AC Magnetometry)*, **Nanotechnology**, 2015. **26**: 015704
- E. Garaio, J-M. Collantes, J. A. Garcia, F. Plazaola, and O. Sandre, *Harmonic phases of the nanoparticle magnetization: an intrinsic temperature probe*, **Applied Physics Letters**, 2015. **107**: 123103
- E. A. Périgo, G. Hemery, O. Sandre, D. Ortega, E. Garaio, F. Plazaola, and F. J. Teran, *Fundamentals and advances in magnetic hyperthermia*, **Applied Physics Reviews**, accepted, arXiv:1510.06383

The heating efficiency (SAR) varies with temperature

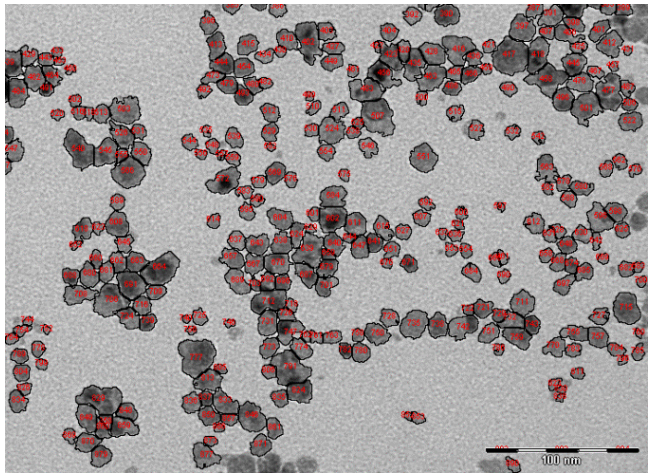

d_{TEM}=12.9 ± 4.6 nm for sample III

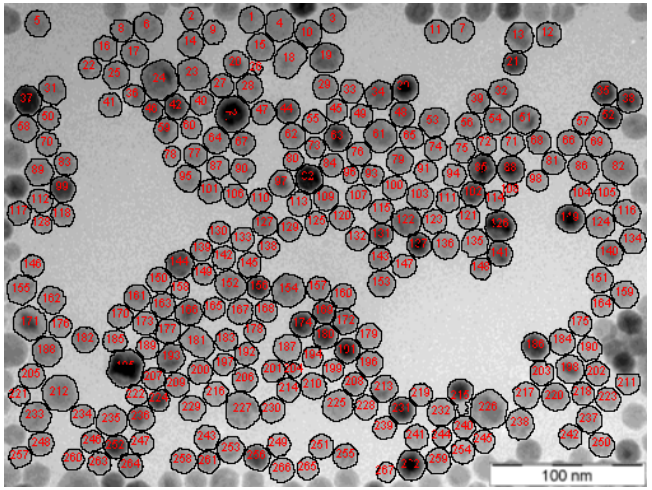

d_{TEM}=16.9 ± 1.7 nm for sample IV

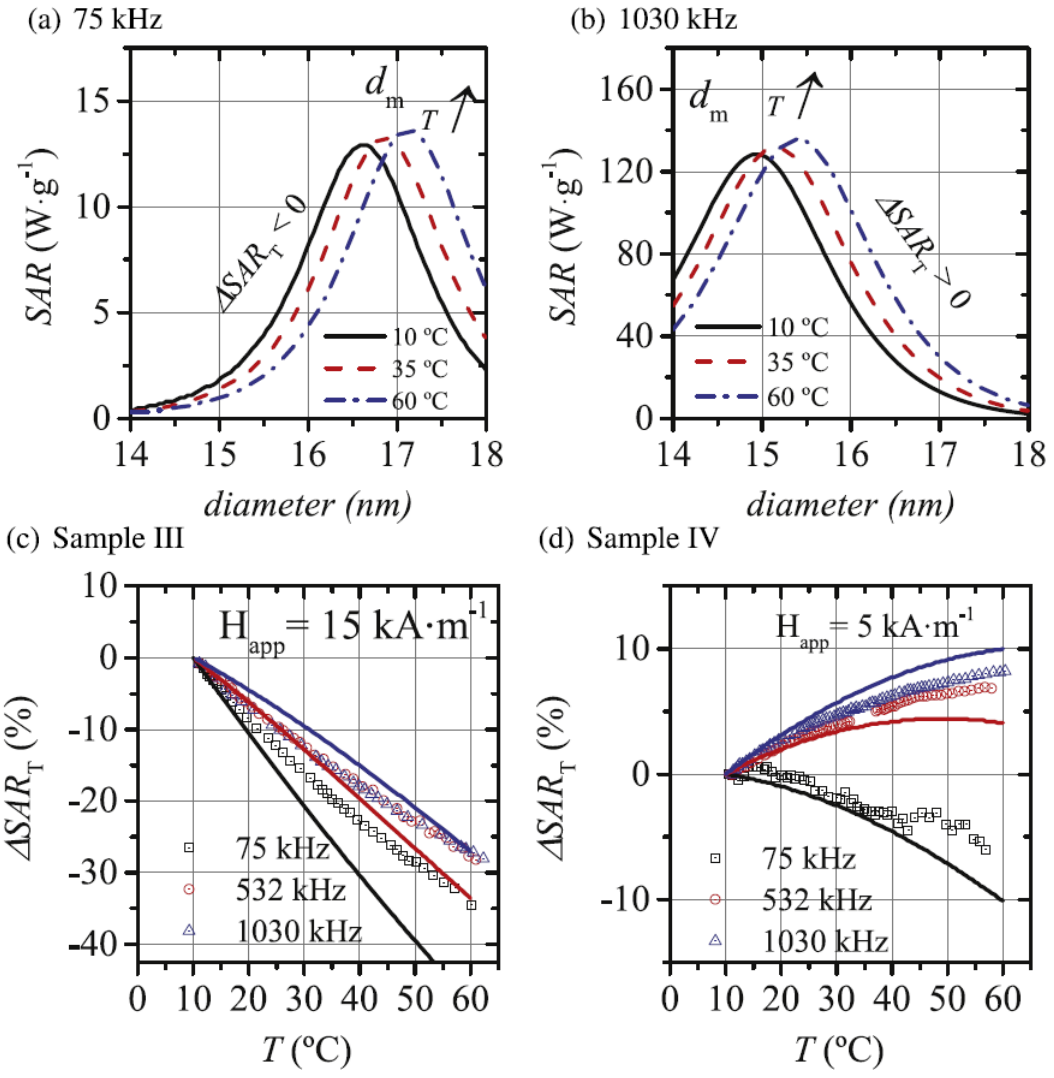

- E. Garaio, O. Sandre, J-M. Collantes, J. A. Garcia, S. Mornet, and F. Plazaola, *Specific absorption rate dependence on temperature in magnetic field hyperthermia measured by dynamic hysteresis losses (AC Magnetometry)*, **Nanotechnology**, 2015. **26**: 015704

The forced hydrolysis route or "New Orleans synthesis"

D. Caruntu, G. Caruntu, Y. Chen, C. J. O'Connor, G. Goloverda, V. L. Kolesnichenko, *Chem. Mater.* **2004,** *16,* 5527-5534

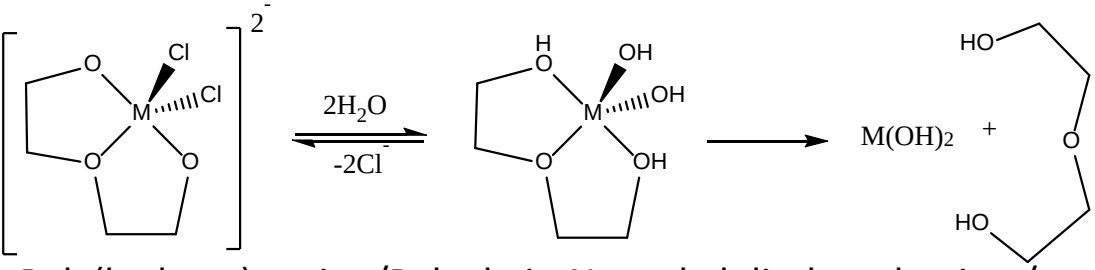

Poly(hydroxy) amine/Polyol *viz.* N-methyl diethanolamine / DEG (1:1)

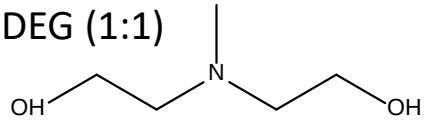

- 6 mmol $FeCl_2$
- 12 mmol $FeCl_3$
- 180g DEG
- 180g NMEDA
- 220°C 5h

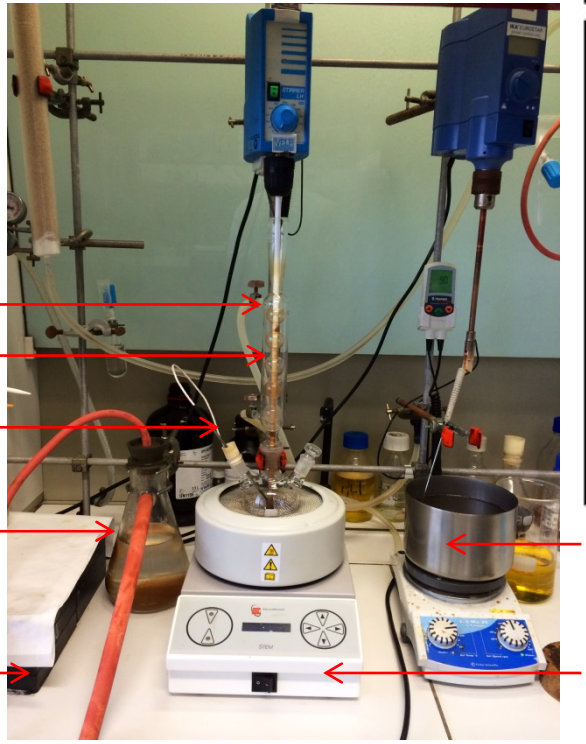

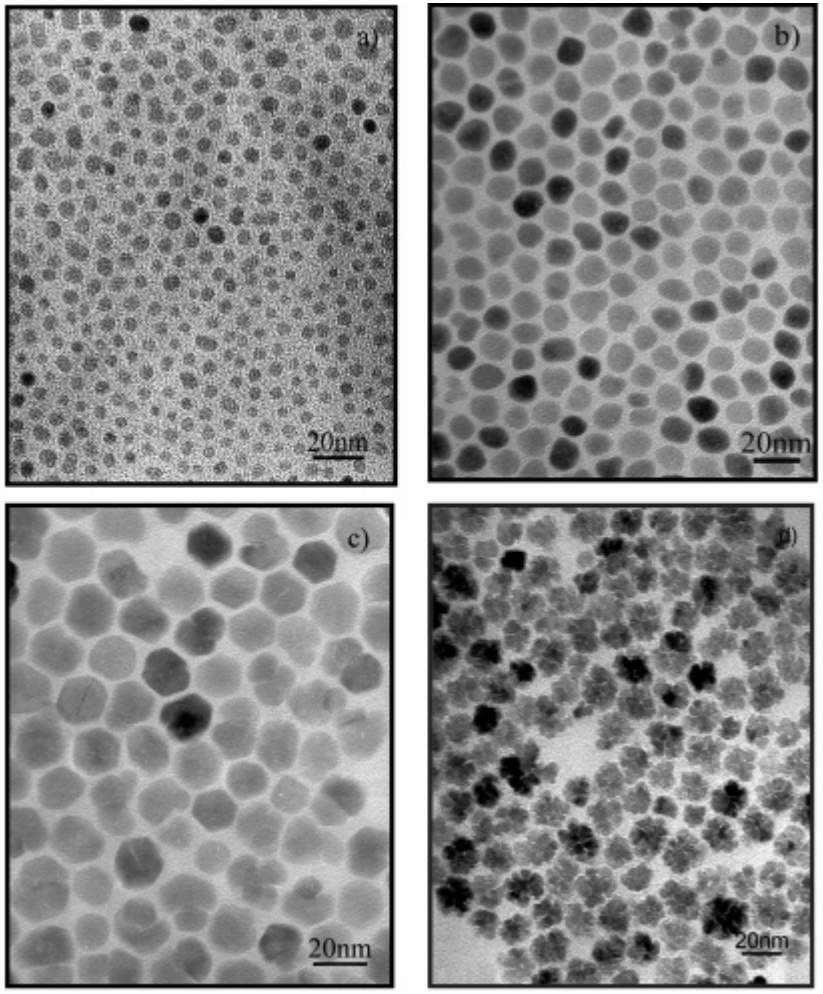

- Precursor
- Polyol composition
- Temp/Duration
- Water content

Variety of Fe_3O_4 NP batches synthesized in DEG:NMDEA

$$\langle d \rangle = d_0 e^{\sigma^2/2} \qquad var(d) = {d_0}^2 \left(e^{\sigma^2/2} - 1\right)$$

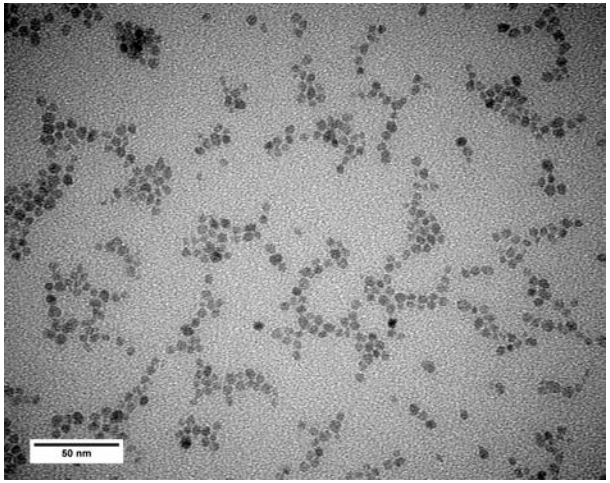

4FF: *d*=6.2±1.0 nm

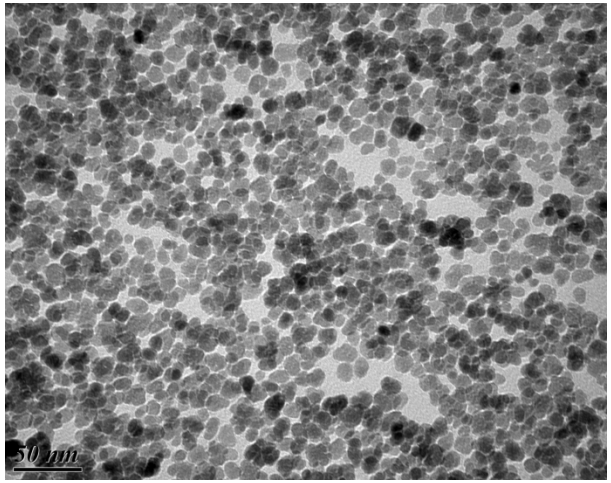

23FF: *d*=10.5±1.9 nm

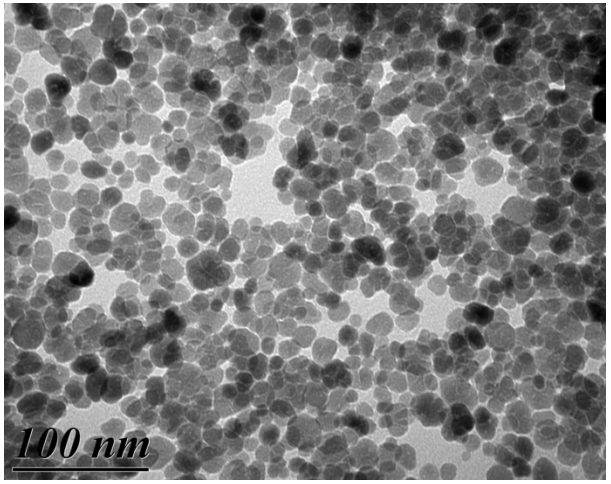

25FF: *d*=14.2±3.2 nm

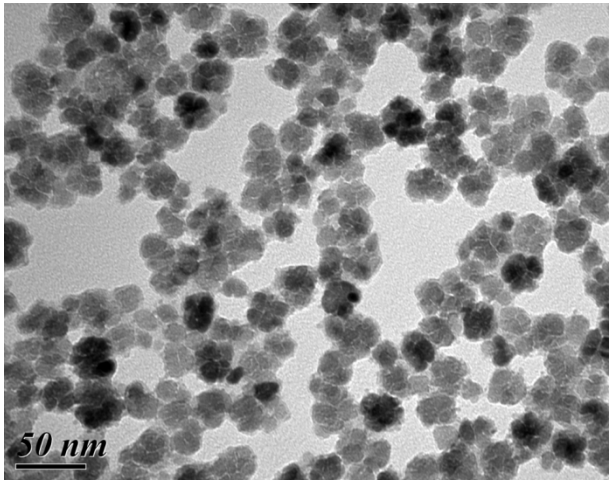

29FF: d_{out}=26.6±4.2 nm

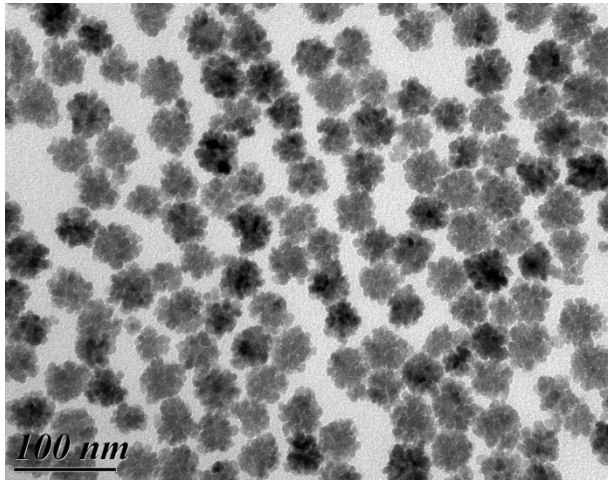

15FF: d_{out}=36.3±4.8 nm

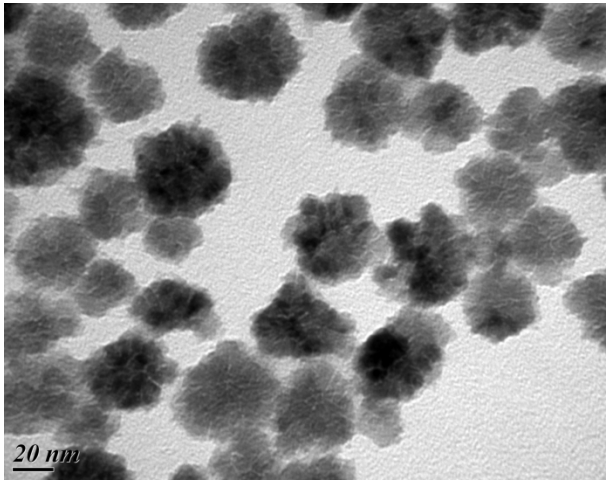

30FF: d_{out}=41.1±8.6 nm

Utmost importance of controlling water addition

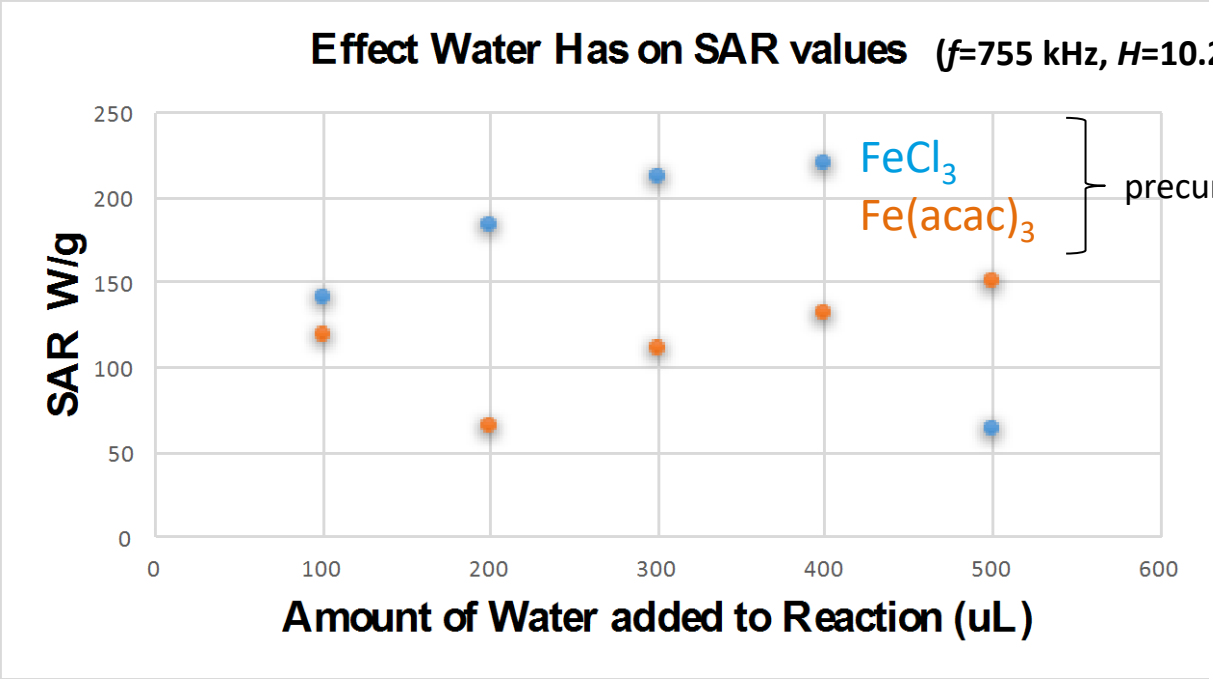

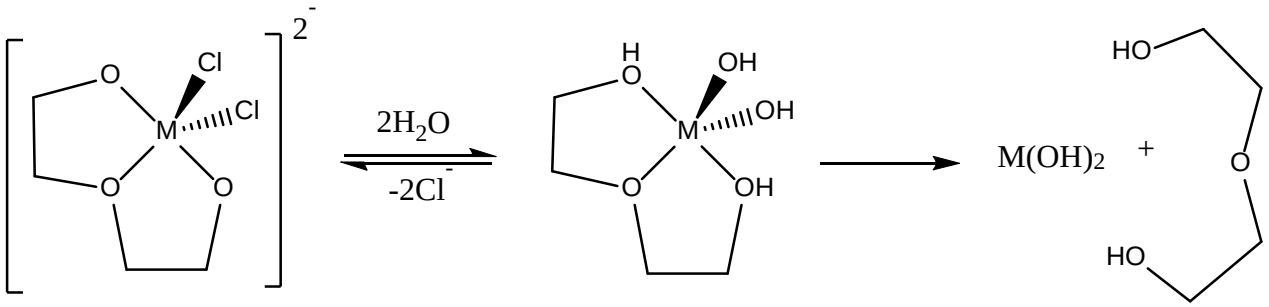

Chosen nanoflower sample: FF15

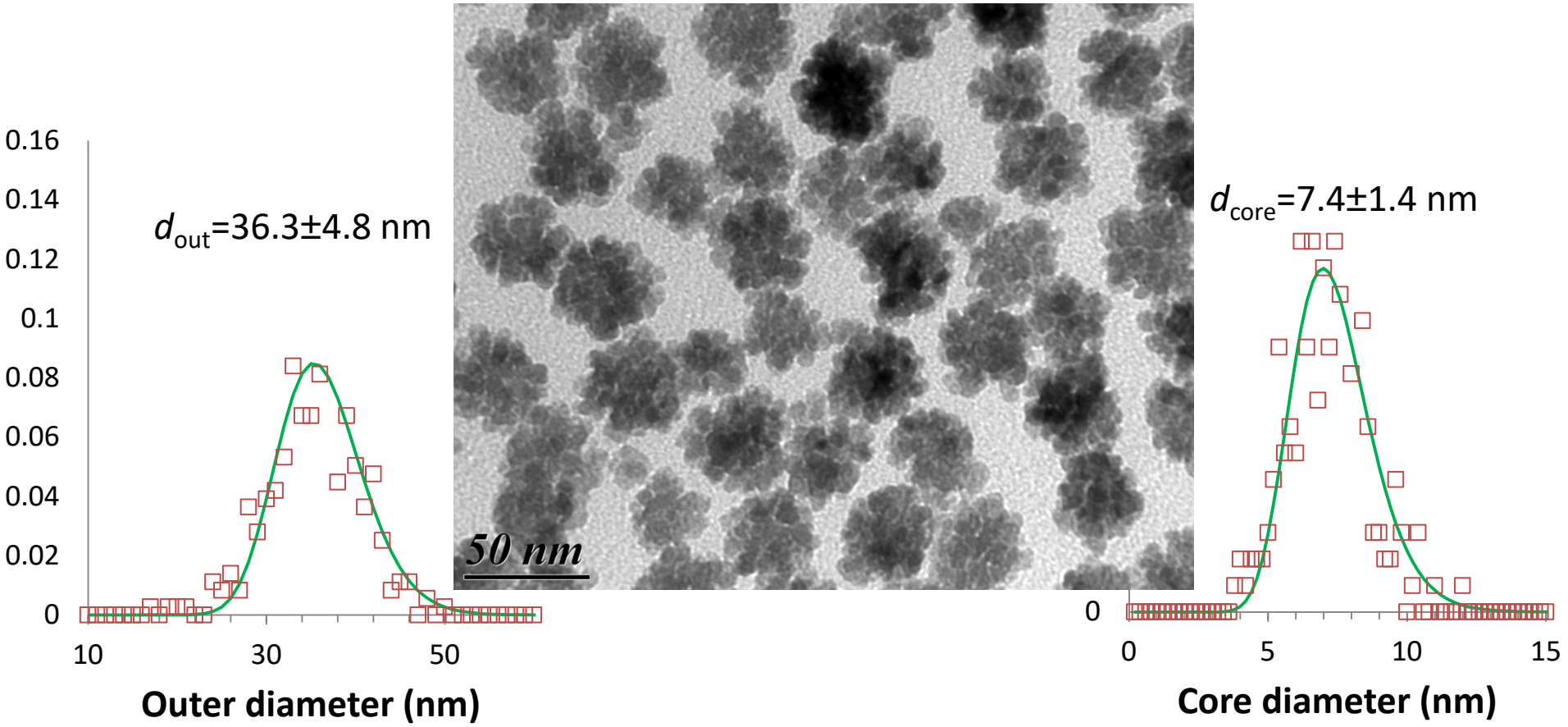

- Can be oxidized in boiling $Fe(NO_3)_3$: $Fe_3O_4 \rightarrow \gamma\text{–}Fe_2O_3$
- Washed and stabilized in water at pH~7 with citrate ligand

DC magnetization curves of FF15 nanoflowers

Room temperature M(H)

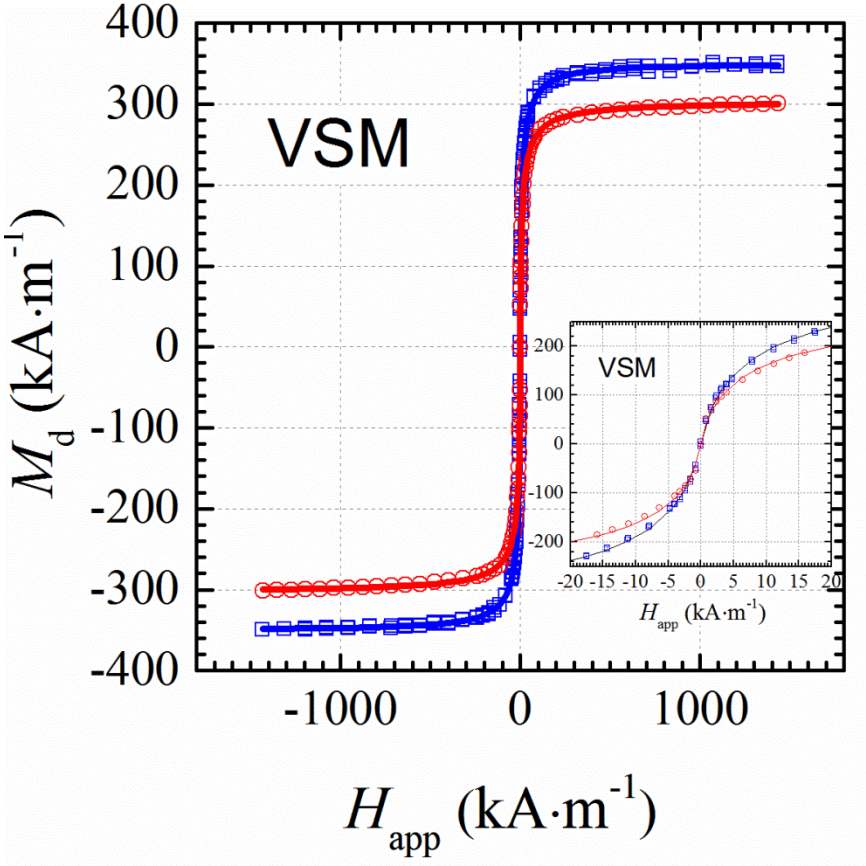

	Oxidized	Fe_3O_4
M_{spe} (kA/m)	300	350

Negligible coercitivity (H_c<0.5 kA/m) →

Field Cooled-Zero Field Cooled

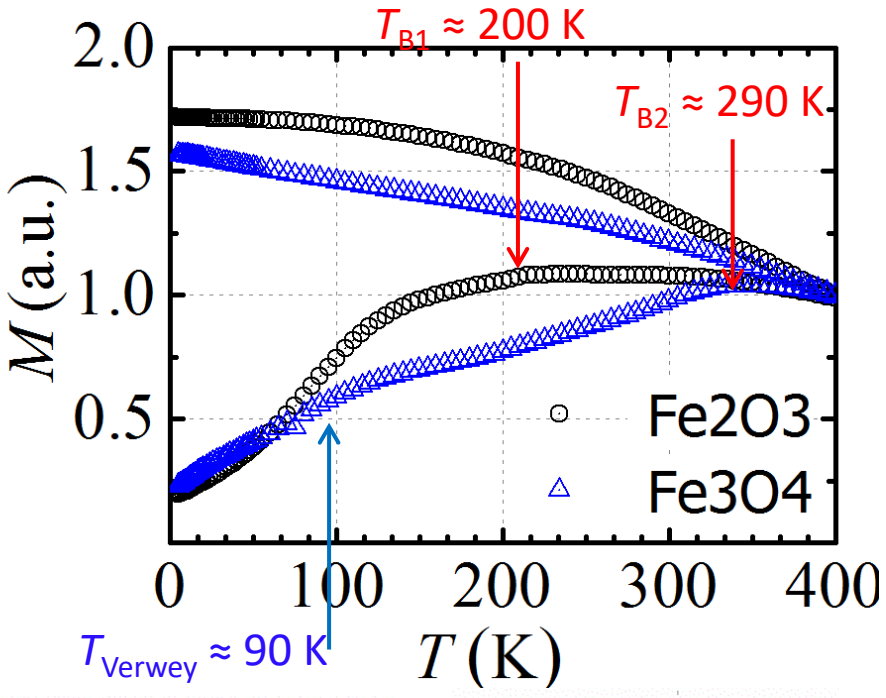

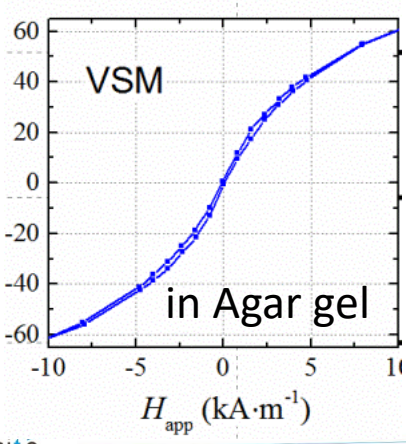

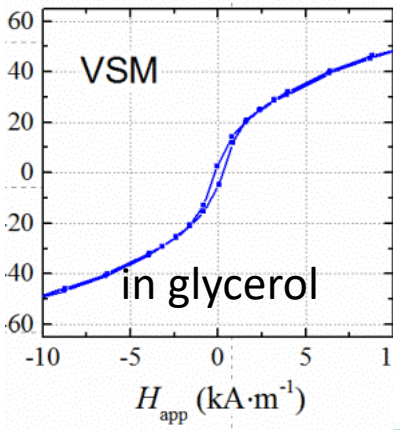

Peculiar Spin-Glass Dynamics of Nanoflowers

A. Kostopoulou, K. Brintakis, M. Vasilakaki, K. N. Trohidou, A. P. Douvalis, A. Lascialfari, L. Manna, A. Lappas, *Nanoscale* 6, 3764 (2014)

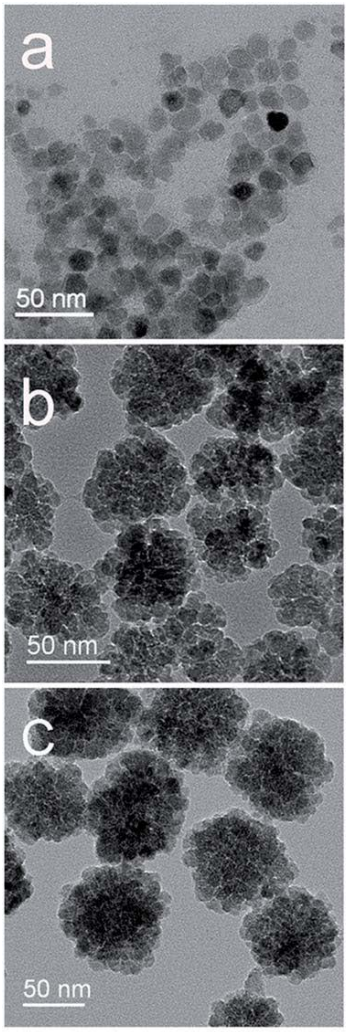

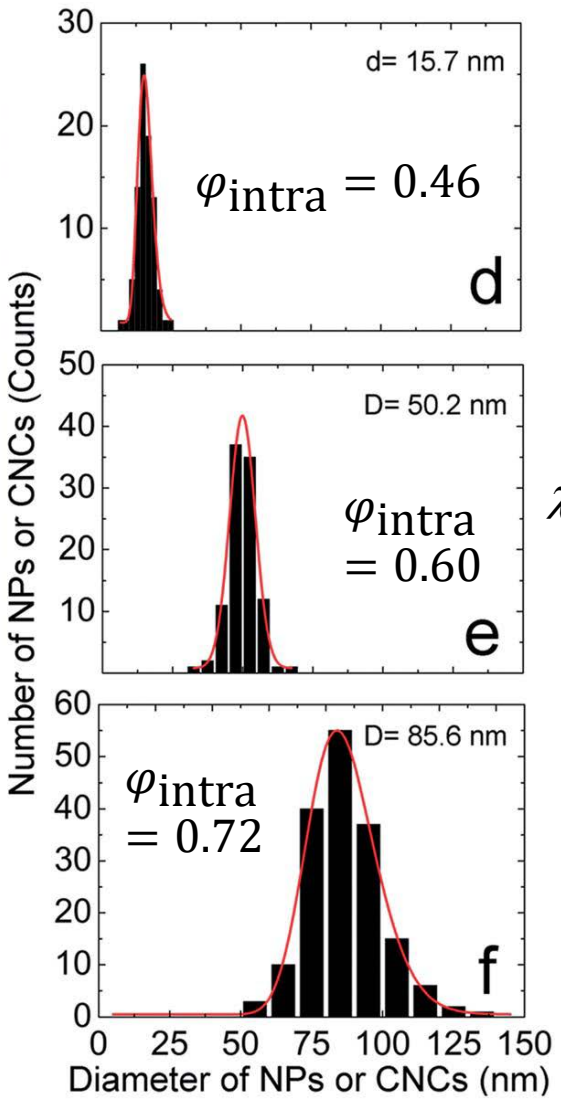

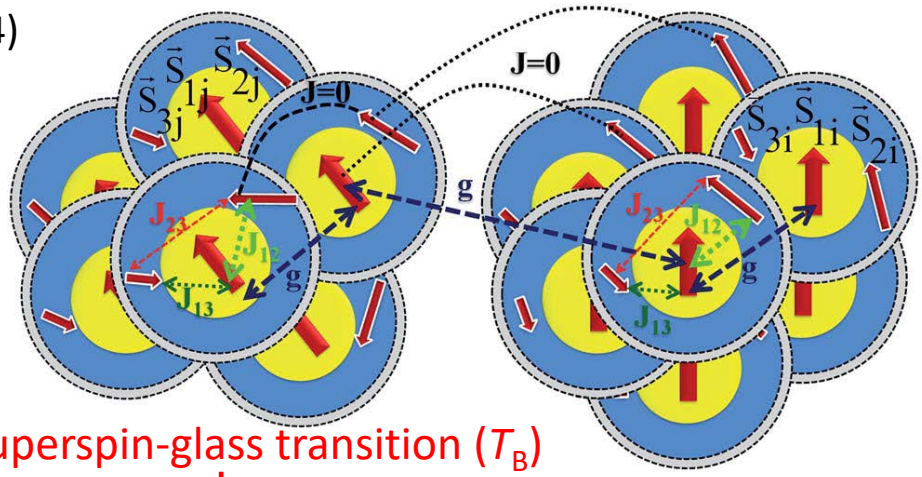

superspin-glass transition (T_B)

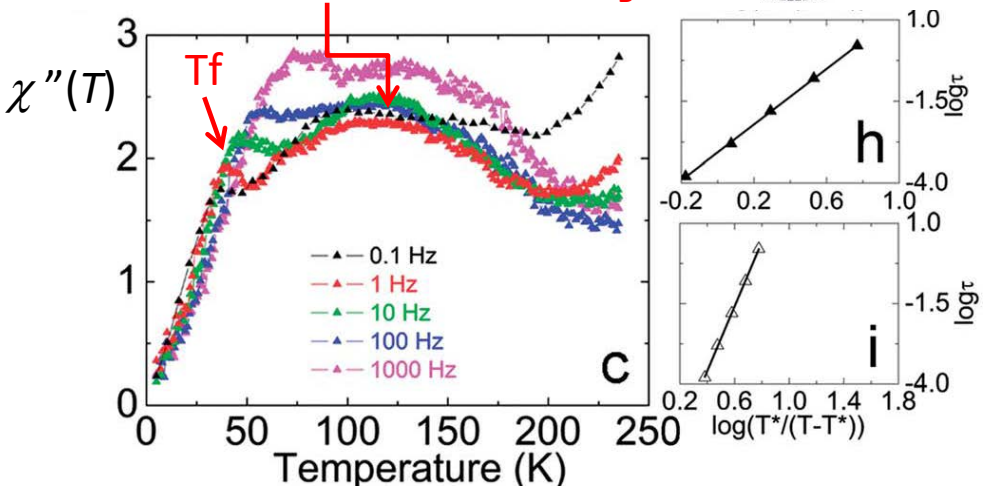

Different spin-dynamics / relaxation times τ

Interplay of dipolar interactions with spin disorder due to the defected surface coordination (PAA)

→ memory effects in the high T_B

AC hysteresis curves of FF15 nanoflowers

1.7 mg/mL Fe_3O_4

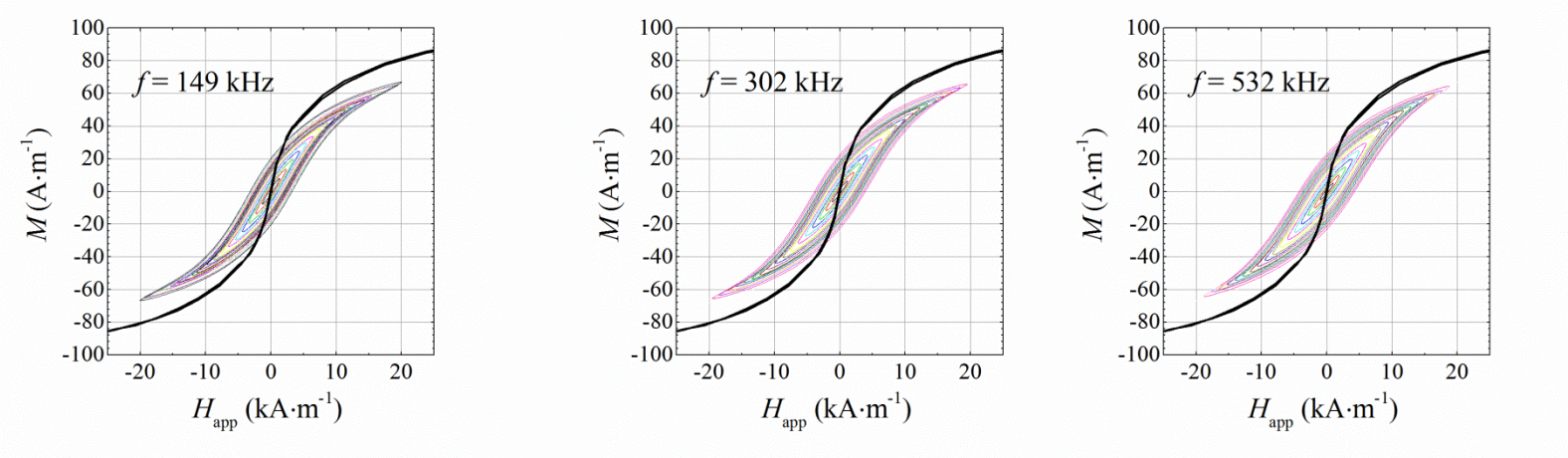

1.0 mg/mL γ–Fe_2O_3

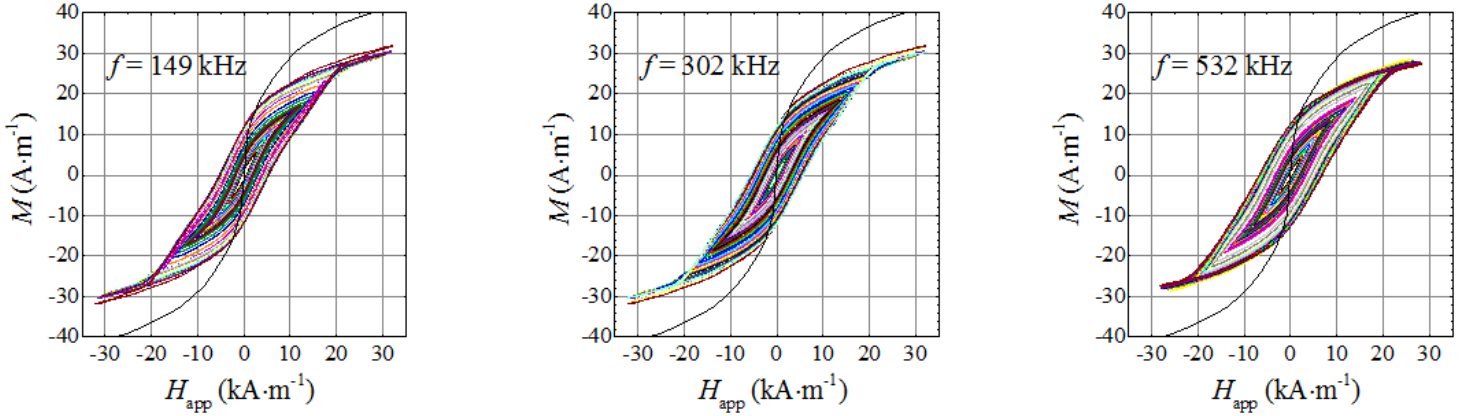

Measurements done by Eneko Garaio (UPV-EHU Bilbao)

SPM-FM transition depends on applied frequency!

Magnetite

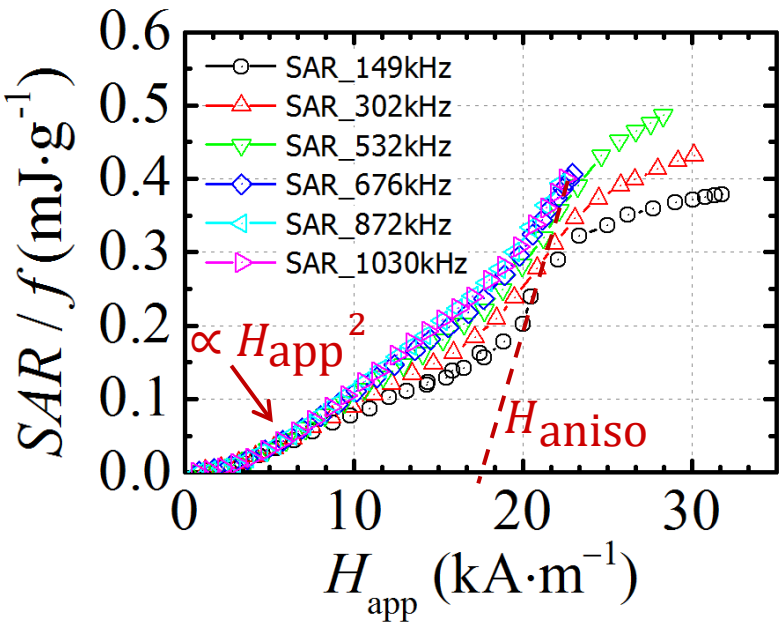

Oxidized

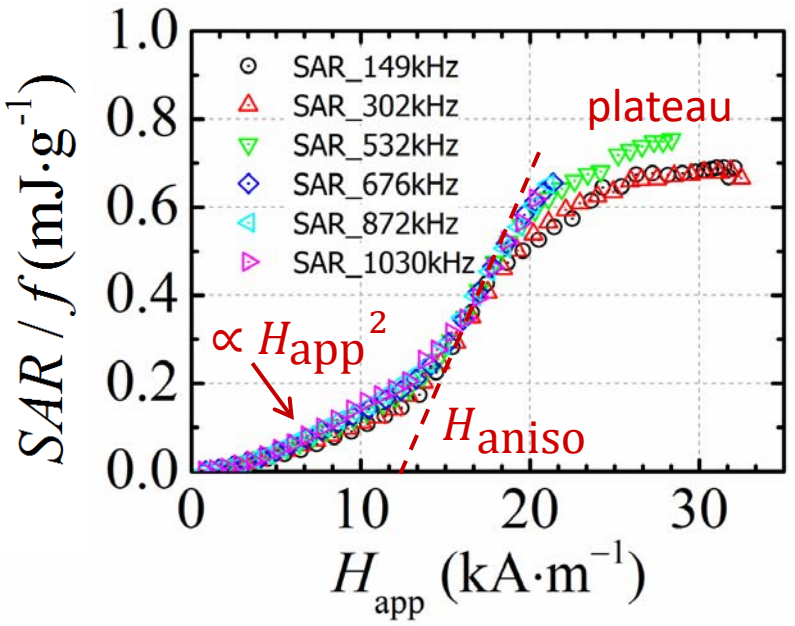

1. High *f*: SAR~H_{app}^2 scaling consistent with SPM state
(Néel relaxation main contribution to heating)

2. Low *f*: weak SAR below threshold field ($H_{max}<H_{aniso}$)
and scaling exponent >>2 for $H_{max}>H_{aniso}$ followed by plateau
→ so-called "Stoner-Wohlfarth behavior" by J. Carrey & G. Goya

Measurements done by Eneko Garaio (UPV-EHU Bilbao)

Modeling mag. moment dynamics by Fokker-Planck equation

Two-region modelling of nanoflower:

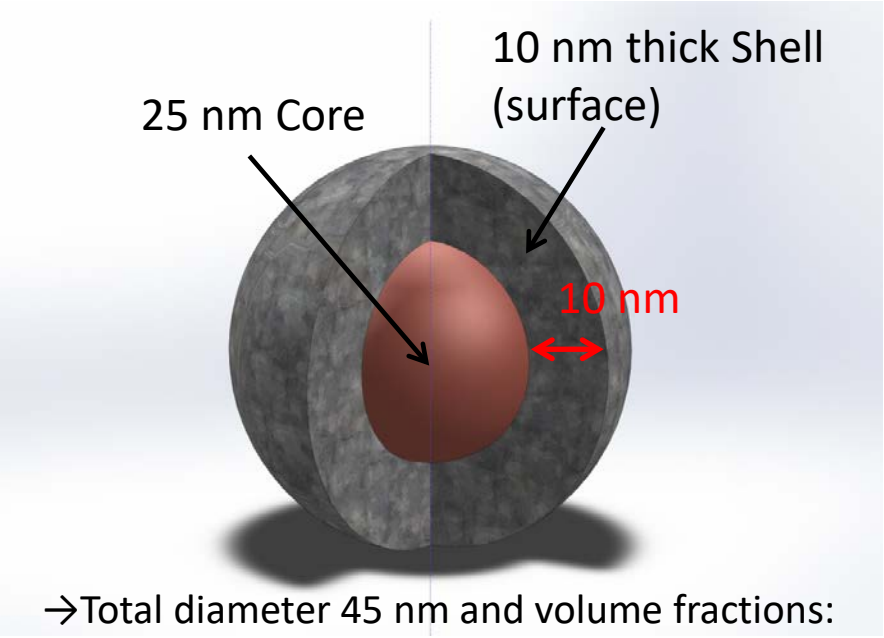

→Total diameter 45 nm and volume fractions:

$$\varphi_{Core} = \left(\frac{d_{Core}}{d_{core} + 2d_{surface}} \right)^3 \approx 0.17$$

$$\varphi_{Surface} = 1 - \varphi_{Core} \approx 0.83$$

$$M_{total} = \varphi_{surface} M_{surface} + \varphi_{core} M_{core}$$

Calculated hysteresis:

Maghemite:

M_{spe} = 300 kA/m

K_{eff}=8 kJ/m³

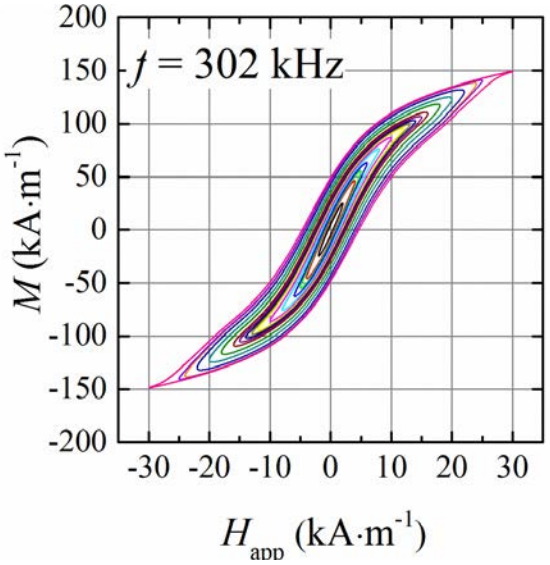

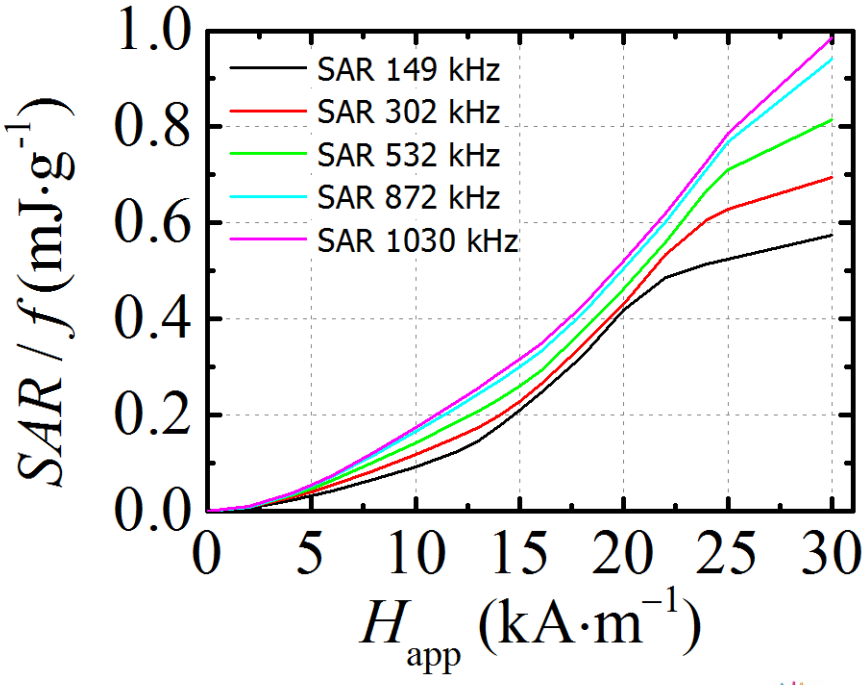

Simulation done by Eneko Garaio (UPV-EHU Bilbao)

The phase of M(H) harmonics enables measuring T !

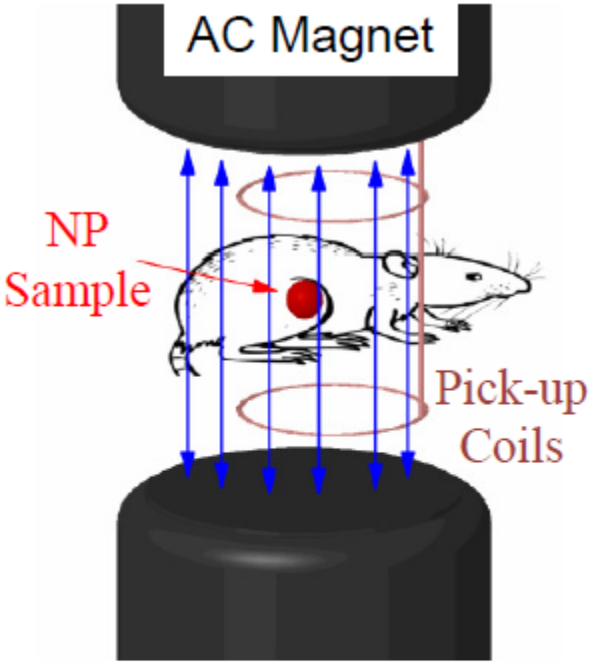

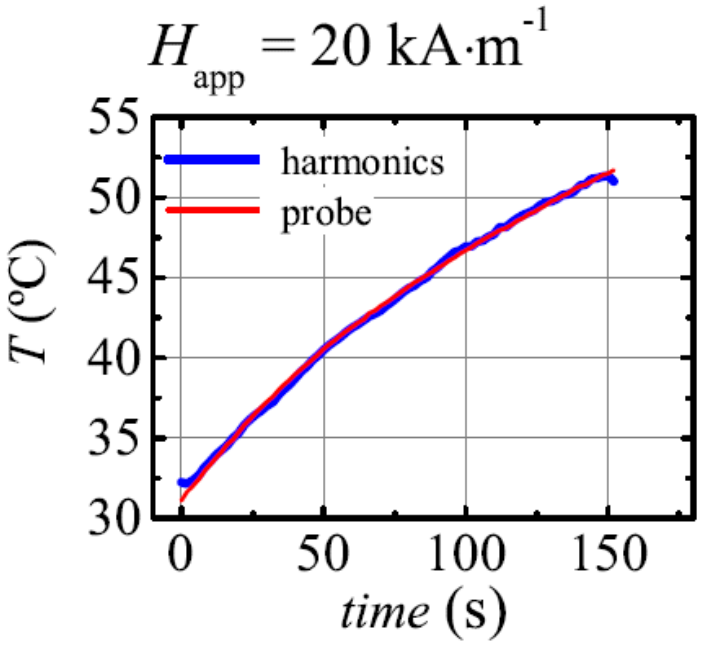

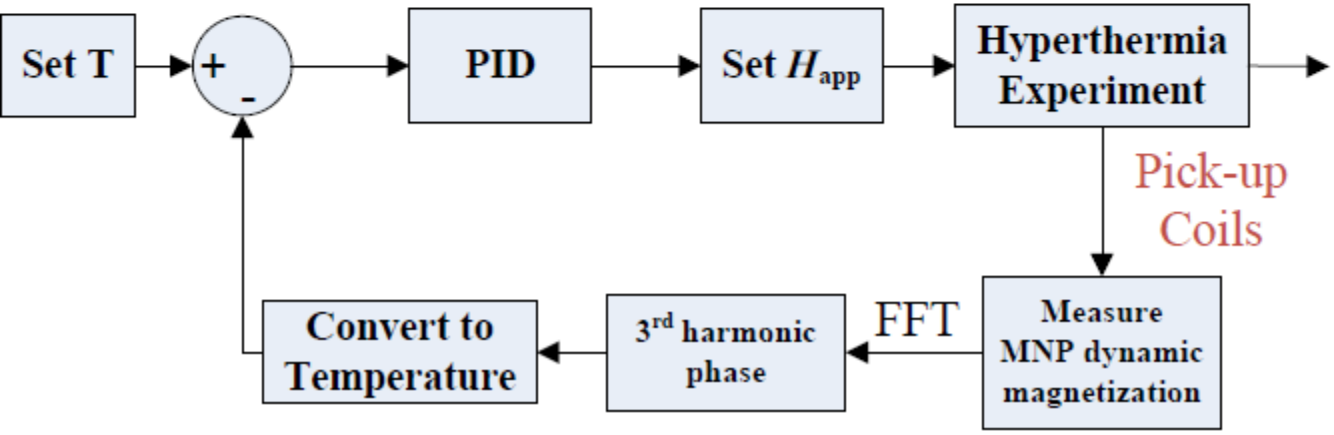

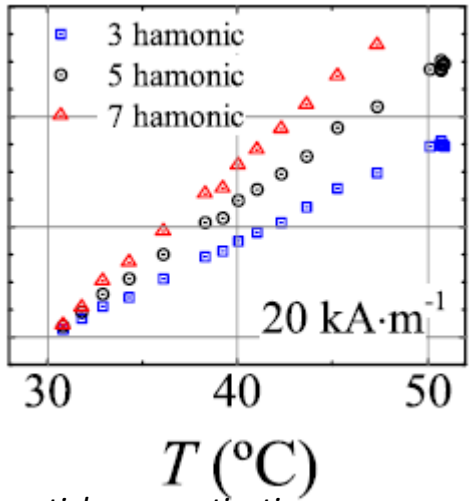

- E. Garaio, J-M. Collantes, J. A. Garcia, F. Plazaola, and O. Sandre, *Harmonic phases of the nanoparticle magnetization: an intrinsic temperature probe*, **Applied Physics Letters**, 2015. **107**: 123103

Magnetic hyperthermia works at macroscopic scale (tumor Ø~1cm), but what about the cellular or micro-metastasis level (Ø~10-100µm)?

LMDH (univ P6, P7) 1997

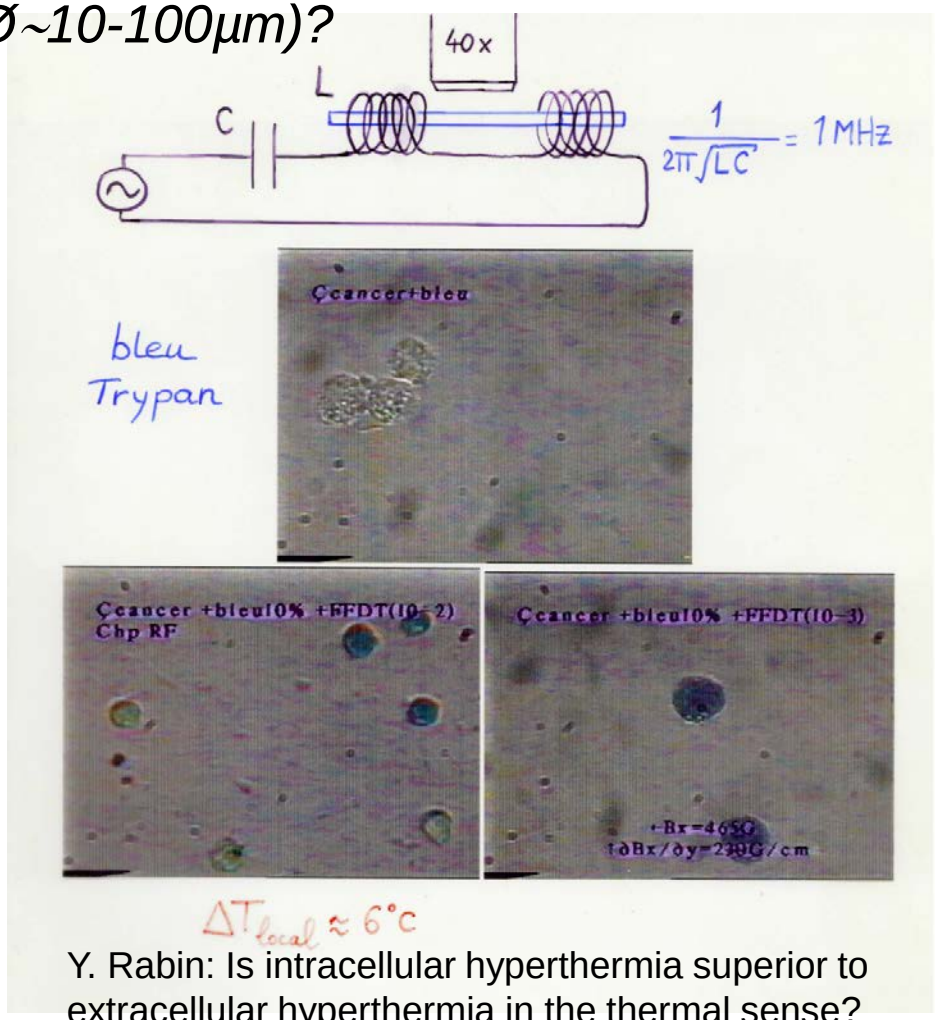

Y. Rabin: Is intracellular hyperthermia superior to extracellular hyperthermia in the thermal sense? *Int. J. Hyperthermia* 2002 18,194-202.

$$\frac{1}{r^2}\frac{\partial}{\partial r}\left(k_w r^2 \frac{\partial T}{\partial r}\right) + P = \rho C_p^w \frac{\partial T}{\partial t} \rightarrow \Delta T = \frac{P}{k_w R} \propto R^2$$

Cellular hyperthermia is still a very hot debate!

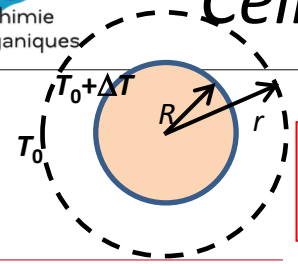

$$\Delta T_{max} = SAR \cdot C^{drop}_{\gamma Fe_2O_3} \cdot \frac{4\pi r^2_{drop}}{k_{medium}}$$

Validating subcellular thermal changes revealed by fluorescent thermosensors

To the Editor: In their recent Commentary arguing that a single cell cannot substantially raise its temperature by endogenous thermogenesis, Baffou *et al.* raised a critical issue[1] concerning the observations of temperature rise of ΔT in single cells and of subcellular thermal heterogeneities[2–4]. They argue that the observed ΔT (1–2 K) of a whole cell[2,3] would be much larger than the theoretical ΔT estimated from the relation

$$\Delta T = \frac{P}{\kappa L} \qquad (1)$$

where κ is conductivity, L is the diameter of the heat source and P is power.

This is derived from the macroscopic heat diffusion equation for continua

$$c\partial_t T(\mathbf{r},t) - \kappa\nabla^2 T(\mathbf{r},t) = p(\mathbf{r},t) \qquad (2)$$

where c is volumetric heat capacity and $T(\mathbf{r}, t)$ and $p(\mathbf{r}, t)$ are temperature and heat source density as a function of position $\mathbf{r}$ and time t.

We believe that the issue requires a deeper examination regarding the values of the parameters used in the calculation of ΔT from the relation (1) and the validity of the basic equation (2) for cellular systems.

Baffou *et al.* estimated ΔT within a cell to be around 10^{-5} K, assuming that the heat source size is 10 μm and that the average heat production per hour based on glucose production is 100 pW (360 nJ h^{-1}). Considering the transience and localization of actual heat production within intracellular organelles, they further estimated the energy required to increase 1 K over a 1-μm^3 volume during 1 s to be 1 μJ, which is still one or two orders of magnitude higher than the maximum energy produced by the total glucose contained within a cell[1]. In their estimation, they adopted κ = 1 W m^{-1} K^{-1}, representing a watery environment, for the medium surrounding the heat source. However, the interior of a cell is far different from a watery environment. For example, proteins, water and lipids all possess different κ values (0.6 and 0.1–0.2 W m^{-1} K^{-1} for water and proteins, respectively[5]). In addition, the typical size of the heat source in mitochondria is less than 100 nm.

Taking L = 100 nm and κ = 0.1 W m^{-1} K^{-1} to reflect the high concentration of the intracellular proteins, we reestimate the heat required for an increase of 1 K over the volume of the heat source within mitochondria (10^{-3} μm^3) during 1 s to be 10 nJ, in contrast to the 1 μJ calculated by Baffou *et al.* Notably, our value agrees well with the heat production of 3–5 nJ s^{-1} in brown adipocytes obtained using microcalorimetry[6,7]. We also note that the heterogeneity in the conductivity of intracellular components and the complexity of the membrane structures in intracellular organelles could contribute to the uneven temperature distribution. The complex and highly organized structure of the cells also strongly affects heat capacity c and may further elicit emergent behaviors (frequently described as "the whole is greater than the sum of the parts"), which disallow a simple adoption of equation (2), in subcellular heat diffusion. Therefore, we believe one must carefully consider this fact before employing equation (1) based upon steady-state and uniformity to interpret thermal properties of a real cell.

Additionally, we believe that the underlying assumption guaranteeing the validity of the macroscopic equation (2) may not hold for the actual conditions inside cells. Equation (2) assumes that the local equilibrium is preserved at every 'point' (in a macroscopic sense) in the surrounding medium under consideration, and therefore the point should correspond to a real volume of the order of 1 μm^3, according to ref. 8 (we interpret this reference to state that the threshold of applicability is true not only for the gas phase but also for liquid and solid phases). We also interpret ref. 8 to state that the size L of the heat source must be much larger than 1 μm for this equation to be applicable. Fluctuations of thermodynamic quantities will be significant and will violate the prerequisite homogeneity in small (<1 μm) systems, whereas they become completely immaterial at a larger length scale. The actual sizes of the heat sources, namely protein complexes and intracellular organelles, are 10–100 nm in size. Additionally, several heat sources exist in cells in a discontinuous manner. Therefore, we believe that it is necessary to adopt a heat diffusion equation with additional parameters.

We note that the active ion transport and the accompanying heat transport in Ca^{2+}-ATPase, or a temperature difference between the cytosol and endoplasmic reticulum (ER) and the corresponding heat flux across ER lumen, have been simulated by using the theory of mesoscopic nonequilibrium thermodynamics[9,10]. A similar approach may help interpret cellular thermal changes. We believe that equation (2) with appropriate values of κ and c is still valid for a nonuniform system such as a cell if the system may be properly represented by a coarse-grained continuum characterized simply by κ and c.

Furthermore, our experimental observations using tsGFP1-mito or tsGFP1-ER, targeted to the mitochondria or ER, respectively, clearly revealed the temperature changes in HeLa cells, brown adipocytes and differentiated myotubes, in contrast to tsGFP1 expressed throughout the cytosol[3]. This difference between tsGFP constructs supports the view that the generated heat was transferred directly to organelle-targeted tsGFP1s in the same compartment, for compartment sizes less than 100 nm, but reached the cytosolic tsGFP1 only after being diffused. This also might be the case in the observed higher temperature of the nucleus compared with the cytosol using fluorescent polymeric thermometers within the same compartment[2]. Inhibiting various biochemical processes in the nucleus should confirm this finding. We believe it will be critical to assess the effects of different subcellular environments through precise evaluation of the fluorescence properties of targeted thermosensors.

COMPETING FINANCIAL INTERESTS
The authors declare no competing financial interests.

Shigeki Kiyonaka[1,2], Reiko Sakaguchi[3], Itaru Hamachi[1], Takashi Morii[4], Takenao Yoshizaki[5] & Yasuo Mori[1,2]

[1]Department of Synthetic Chemistry and Biological Chemistry, Graduate School of Engineering, Kyoto University, Kyoto, Japan. [2]Department of Technology and Ecology, Hall of Global Environmental Studies, Kyoto University, Kyoto, Japan. [3]World Premier International Research Initiative-Institute for Integrated Cell-Material Sciences, Kyoto University, Kyoto, Japan. [4]Institute of Advanced Energy, Kyoto University, Uji, Japan. [5]Department of Polymer Chemistry, Graduate School of Engineering, Kyoto University, Kyoto, Japan.
e-mail: mori@sbchem.kyoto-u.ac.jp

1. Baffou, G., Rigneault, H., Marguet, D. & Jullien, L. *Nat. Methods* **11**, 899–901 (2014).
2. Okabe, K. *et al. Nat. Commun.* **3**, 705 (2012).
3. Kiyonaka, S. *et al. Nat. Methods* **10**, 1232–1238 (2013).
4. Sakaguchi, R., Kiyonaka, S. & Mori, Y. *Curr. Opin. Biotechnol.* **31**, 57–64 (2015).
5. Lervik, A., Bresme, F., Kjelstrup, S., Bedeaux, D. & Rubi, J.M. *Phys. Chem. Chem. Phys.* **12**, 1610–1617 (2010).
6. Clark, D.G., Brinkman, M. & Neville, S.D. *Biochem. J.* **235**, 337–342 (1986).
7. Hansen, E.S. & Knudsen, J. *Biosci. Rep.* **6**, 31–38 (1986).
8. Kondepudi, D. & Prigogine, I. in *Modern Thermodynamics: From Heat Engines to Dissipative Structures* 333–350 (Wiley, 1998).
9. Bedeaux, D. & Kjelstrup, S. *Phys. Chem. Chem. Phys.* **10**, 7304–7317 (2008).
10. Lervik, A., Bedeaux, D. & Kjelstrup, S. *Eur. Biophys. J.* **42**, 321–331 (2013).

The 10^5 gap issue between calculation and measurement in single-cell thermometry

To the Editor: In their recent Commentary, Baffou *et al.*[1] questioned the results of microscopy-based techniques for measuring endogenous heat production in single cells. First, following our and others' discussions on the '10^5 gap issue' (the difference between the measured temperature increase of 1 K in a single cell using cellular thermometry as compared to the theoretically calculated increase limit of 10^{-5} K)[2–4], they reached the same conclusion that the temperature of water with the same volume as a single cell delivering a power 100 pW is unlikely to have a temperature increase of 1 K in a water bath. In this regard, we agree with Baffou *et al.*

However, according to microcalorimetry studies, the amount of heat production varies among cell types. For example, brown adipocytes that are specialized in nonshivering thermogenesis can produce heat equivalent to ~1.6 nW per cell (ref. 5), which is 10^1 times larger than the 100 pW assumed in Baffou *et al.*'s calculation. Additionally, cells under stimulation and those without stimulation show substantial metabolic differences. Further explanations are needed for the gap pertaining to unstimulated cells (**Supplementary Discussion** and **Supplementary Table 1**). Although the 10^5 gap can be filled by one order of magnitude depending on the cell types and stimulation conditions, it is still insufficient to bridge the entire gap.

Site-specific nanothermometry (by positioning intracellular thermosensors at defined locations within a cell) has the potential to unmask the identities and quantities of the heat sources and fill the gap by another one or two orders of magnitude. Equation (2) in ref. 1 addresses temperature profile in relation to distance from the center of the heat source, L (units in meters) (**Supplementary Discussion**), and is as follows:

$$\Delta T = \frac{P}{\kappa L}$$

where ΔT represents the temperature difference (in kelvin), P represents the power of the heat source (in watts) and κ represents the thermal conductivity of the medium surrounding the heat source (in W m^{-1} K^{-1}). Yang *et al.*[2] argued that the deviation of measured ΔT originated from the distribution of L. In accordance with this idea, we detected no notable distribution in ΔT when our molecular thermometers targeted the endoplasmic reticulum (zero distance)—which is considered the major heat source in calcium shock measurements—without distribution of L (ref. 6 and **Supplementary Discussion**).

Second, Baffou *et al.* concluded that it is unlikely that the temperature of water with volume of 1 μm^3 can be sustained at 1 K higher than the surrounding medium for longer than a few seconds by means of the oxidation of stored glucose. However, most thermosensors used in intracellular thermometry are smaller than 1 μm^3 by two or more orders of magnitude (**Supplementary Discussion**). Also, Baffou *et al.* appear to have ignored glucose uptake in stimulated cells (**Supplementary Discussion**). Furthermore, their argument relies on general well-established equilibrium thermodynamics (historically developed for large steam engines) that do not take into consideration the realistic boundary conditions of heat transfer at the micro- or nanoscale in a cell. Thus, we believe that their argument does not necessarily invalidate the reported transient temperature dynamics.

Baffou *et al.*'s third point is that a single lipid bilayer is deficient in the thermal resistivity needed to result in a higher temperature value in an organelle than in cytosol[1]. Again, temperature discontinuity was calculated by assuming bulk-type heat flow. But we believe that this does not match the reality of the complex intracellular structure of a cell (**Supplementary Discussion**).

Finally, we agree with Baffou *et al.* that it is important to test the robustness of intracellular thermosensors with respect to environmental parameters other than temperature changes. Environmental impacts (inhomogeneous in space and time) need to be controlled in order to make progress in temperature imaging in single cells. Most studies cited by Baffou *et al.* have noted the utmost importance of deciphering potential sources of error in measurements (**Supplementary Table 1**). We therefore do not believe that all the data measured by means of completely different kinds of thermosensors can be attributed to factors other than temperature changes.

We expect that once the aforementioned uncertainties of variable heat sources in stimulated cells (10^1), length scales (10^1–10^2), and micro- and nanoscale thermal parameters (10^1–10^2) are clarified, the 10^5 gap issue may disappear. We envisage that these unknowns will be the next targets for investigation in this field.

Note: Any Supplementary Information and Source Data files are available in the online version of the paper (doi:10.1038/nmeth.3551).

ACKNOWLEDGMENTS
The authors acknowledge support from a Grant-in-Aid for Scientific Research on Innovative Areas (no. 2306) and Scientific Research (C) (to M.S.), Young Scientist (A) (to K.O.) and Specially Promoted Research and Scientific Research (S) (to S.I.) from the Ministry of Education, Culture, Sports, Science and Technology of Japan.

Detection of hyperthermia in micro droplets R=200µm/V=33nL

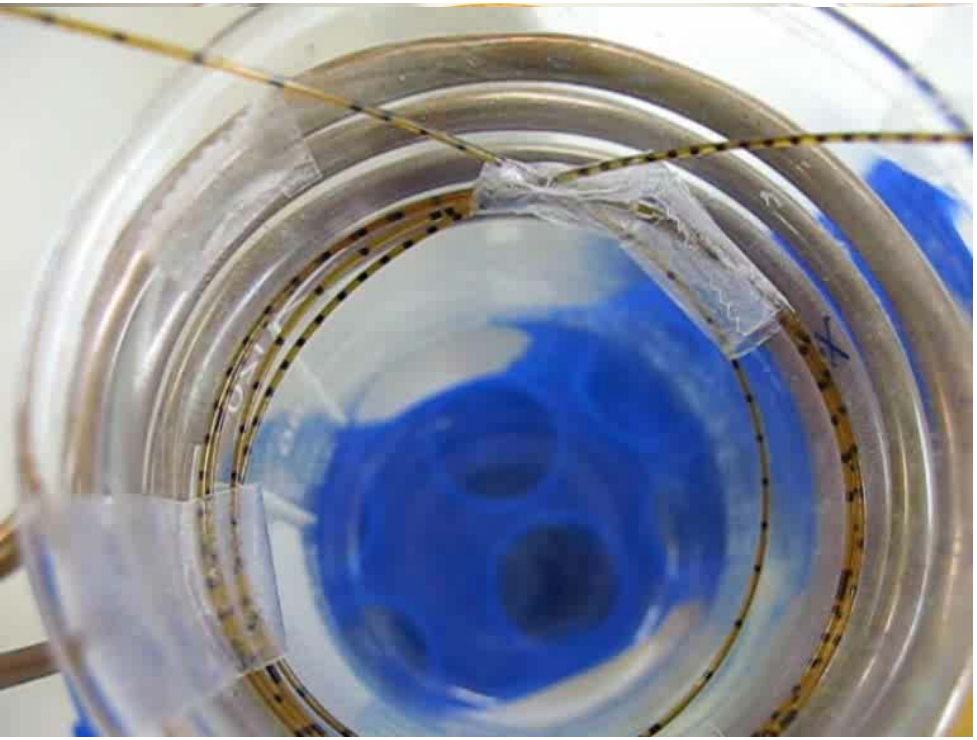

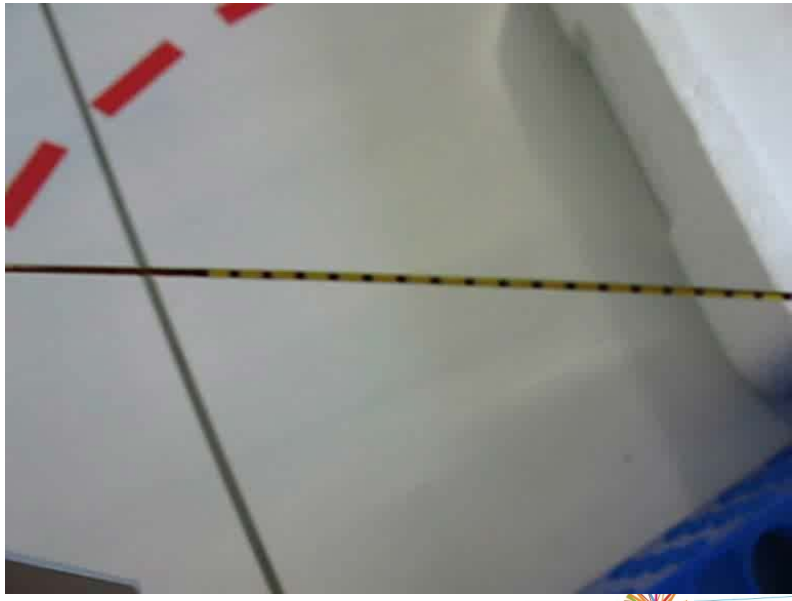

Q_{oil} (µL/mn)	Q_{FF} (µL/mn)	$t_{residence}$ (s)	$\Phi_{FF} = Q_{FF}/Q_{tot}$
90	15	85	14.3%
150	15	54	9.1%
150	50	45	25%

D. Habault et al, *IEEE Transactions on Magnetism* (2013) **49** 182-190, DOI: 10.1109/TMAG.2012.2221688

In situ measurement of the train of drops temperature

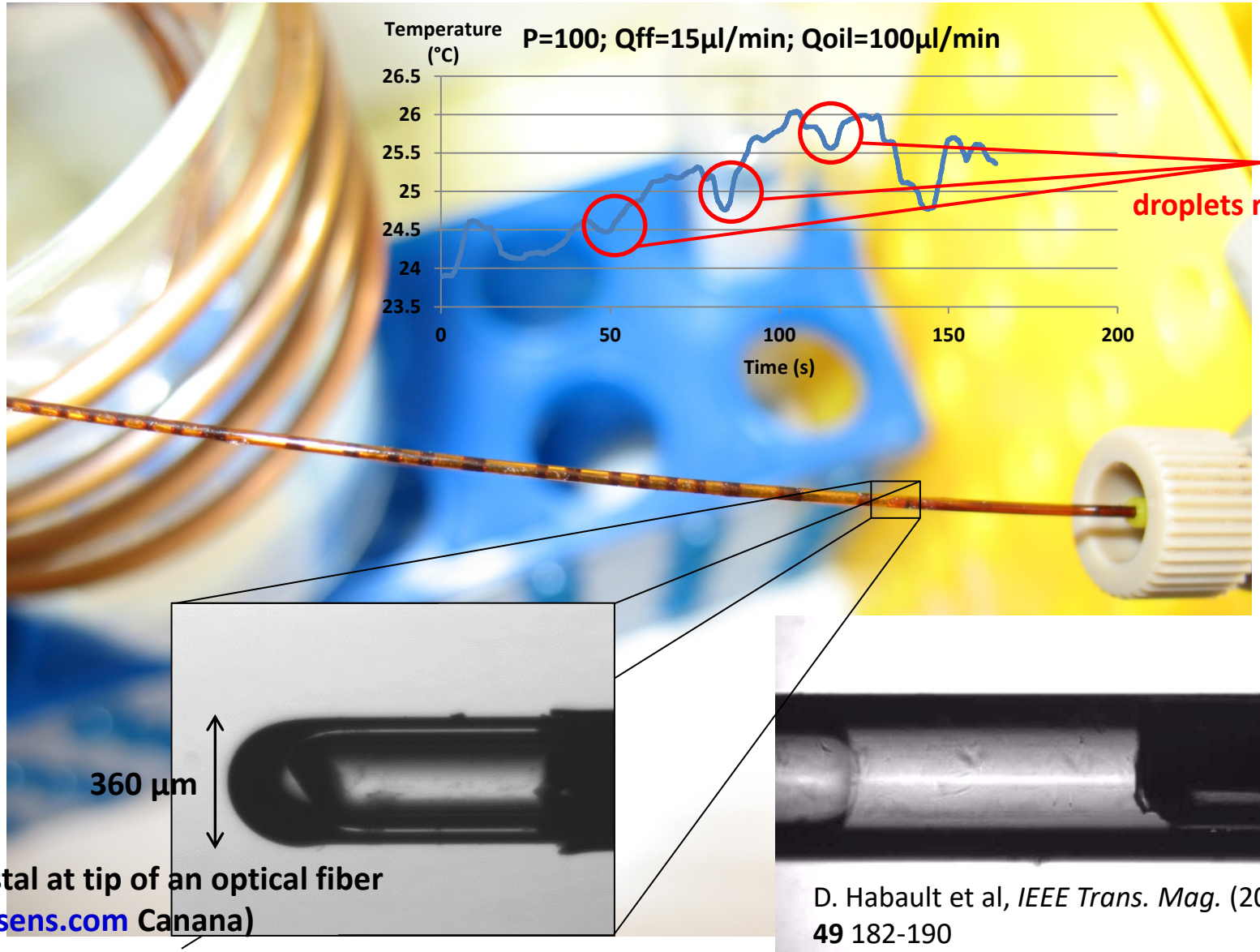

GaAs crystal at tip of an optical fiber (www.opsens.com Canana)

D. Habault et al, *IEEE Trans. Mag.* (2013) **49** 182-190

The dominant phenomenon is thermal conduction towards medium, here a fluorinated oil (C_6F_{14}) with $k_{oil} \sim k_{water}/10$

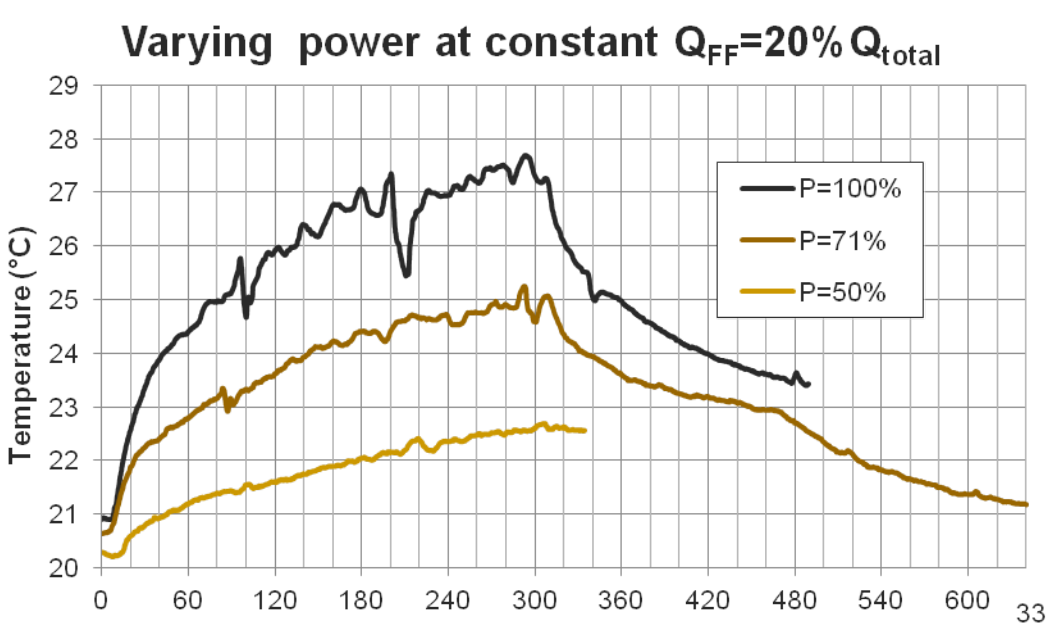

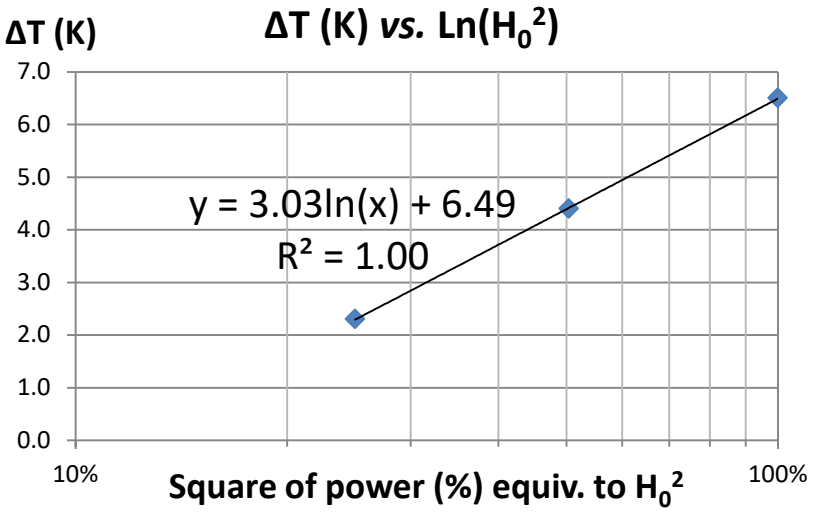

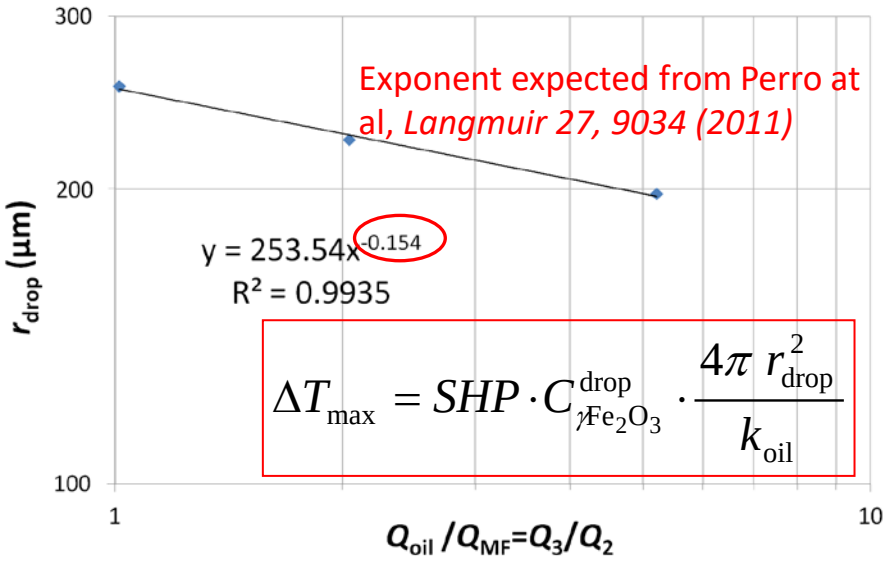

$$\Delta T_{max} = SHP \cdot C^{drop}_{\gamma Fe_2O_3} \cdot \frac{4\pi\, r^2_{drop}}{k_{oil}}$$

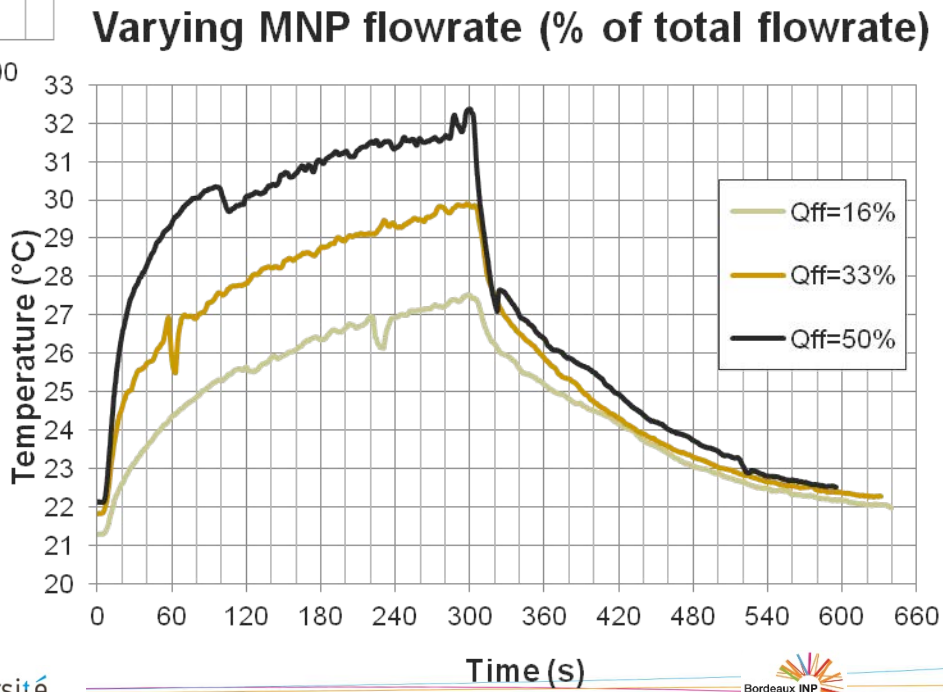

Detection of in vivo effects of magnetic hyperthermia: droplets Ø~1mm of fluorinated MF on mice skin

Genes 2017 **8**, 61

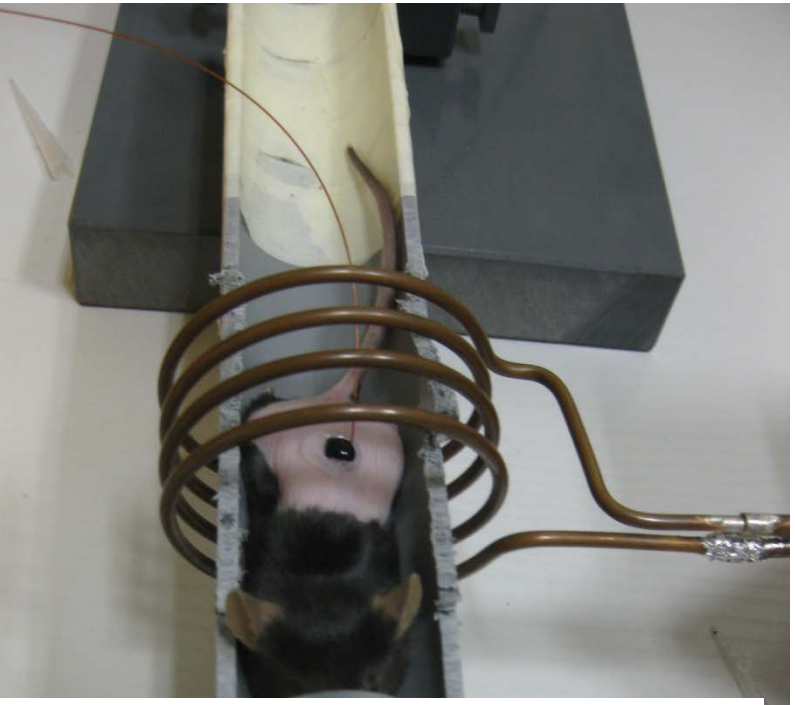

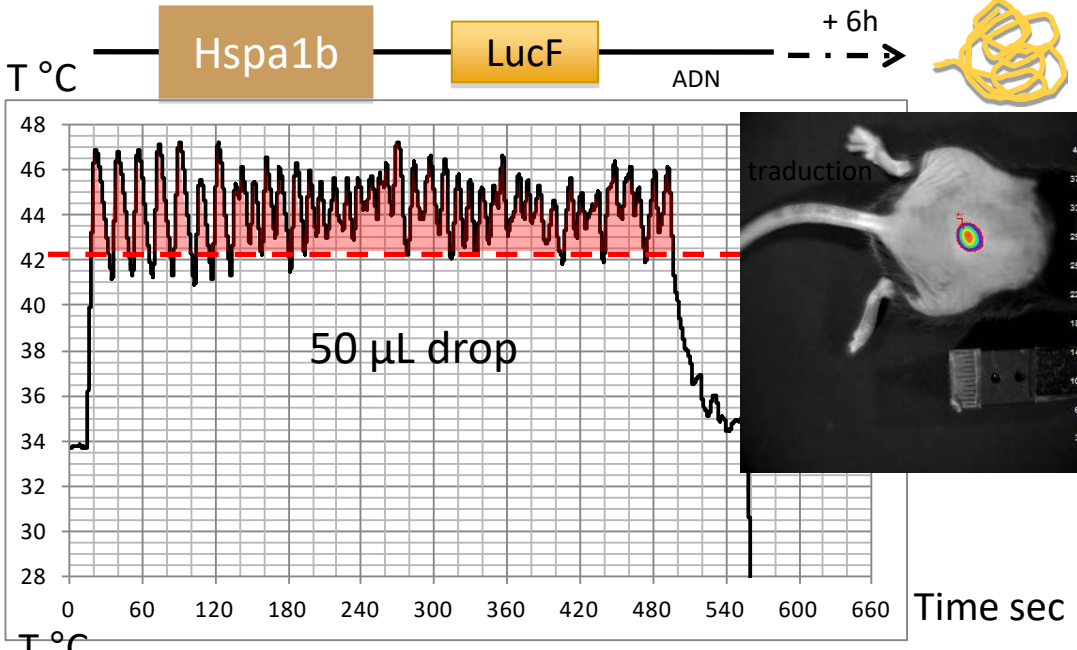

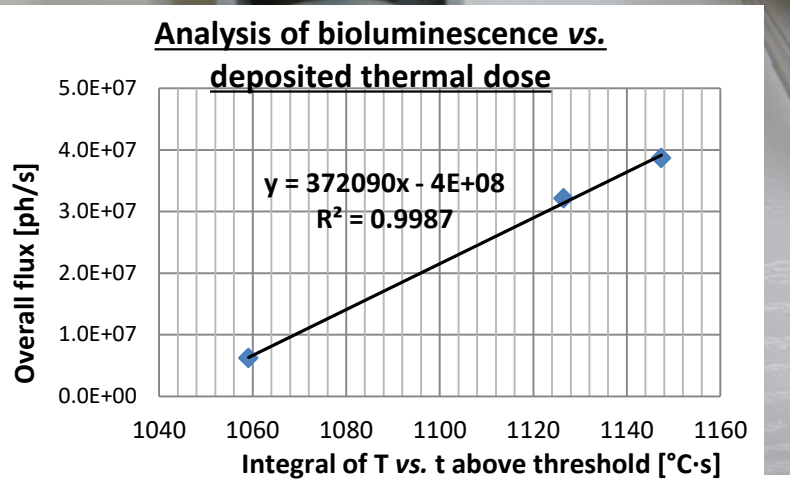

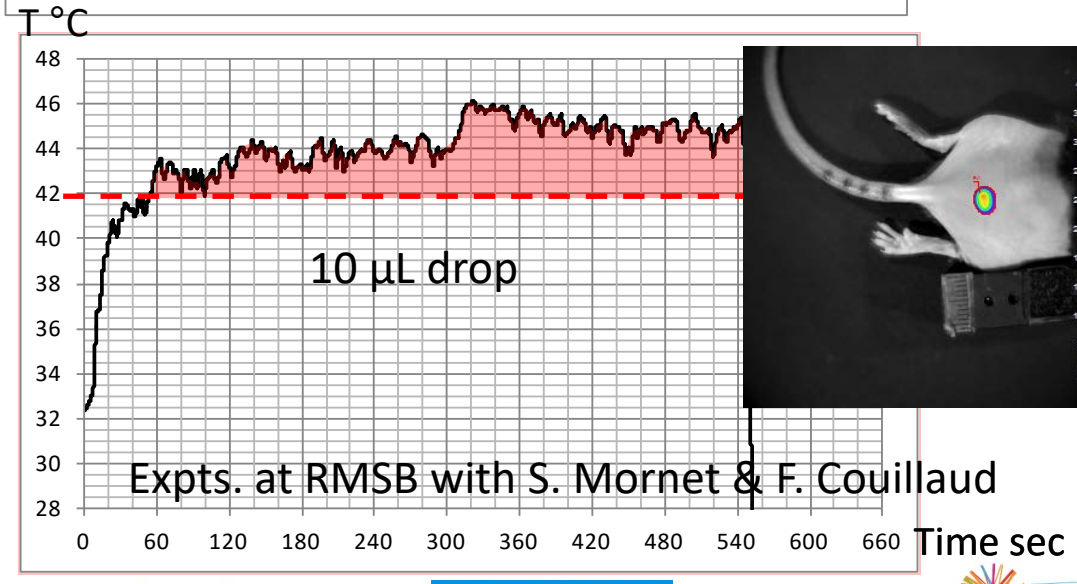

Expts. at RMSB with S. Mornet & F. Couillaud

In vitro and in vivo studies on tumor models to determine ΔT_{max} reachable after intra-tumor vs. intravenous injection of MNPs

Genes 2017 **8**, 61

- *In vitro*: magnetic bio-gels in a mouse model (agar gel)

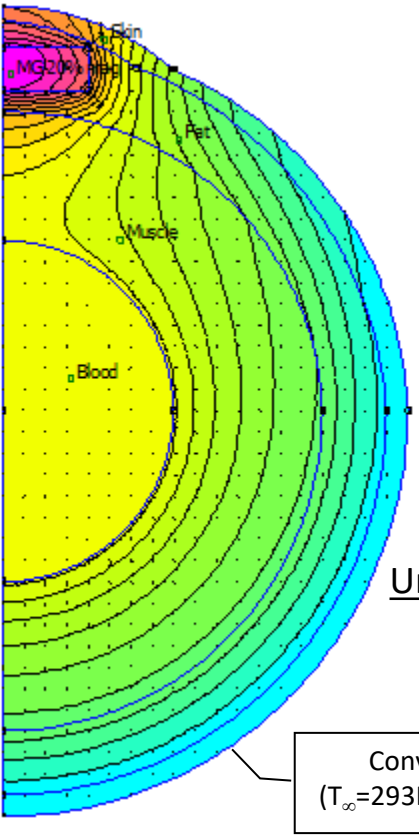

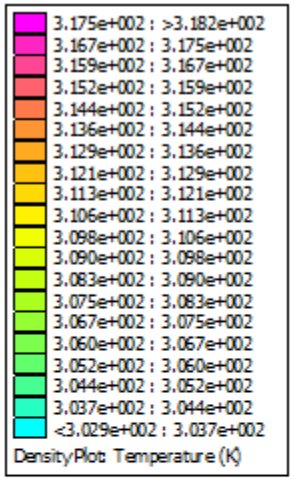

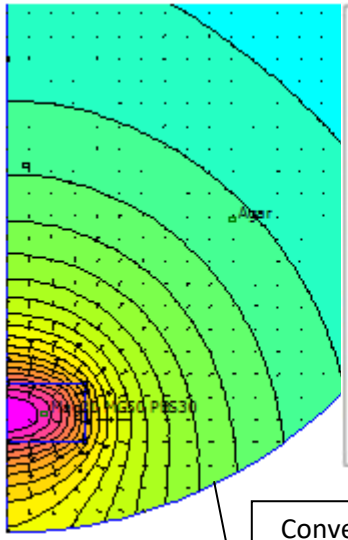

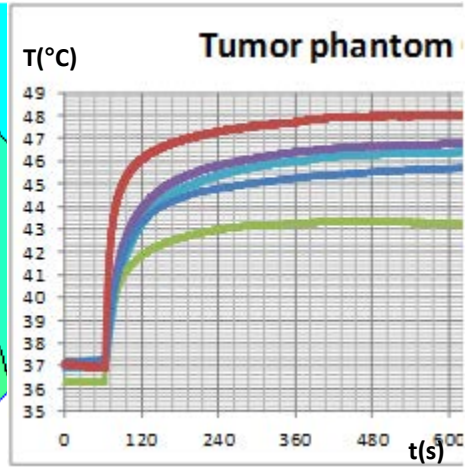

Convection in water-jacket
(T_∞=310K, h=100 W/m^2/K)

Undergoing experiments with S. Mornet (ICMCB), P. Durand and F. Couillaud (RMSB)

- *In vivo*: magnetic bio-gels injected subcutaneously

Convection in air
(T_∞=293K, h=10 W/m^2/K)

100 µL magnetic Matrigel™ placed in fat layer (3 mm thick) below skin (1 mm) and above muscles and blood (2 mL). Power density=1 W/cm^3. Tumor phantom heated at 45°C at center and 42°C in periphery.

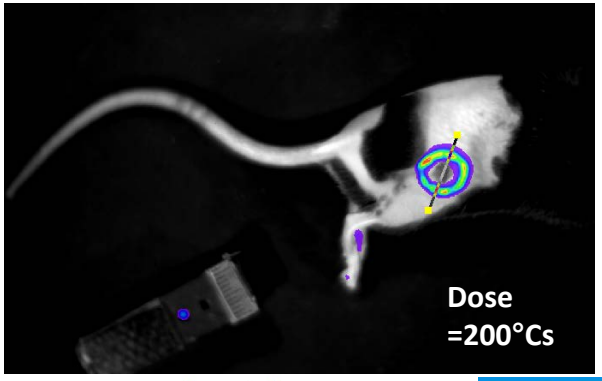

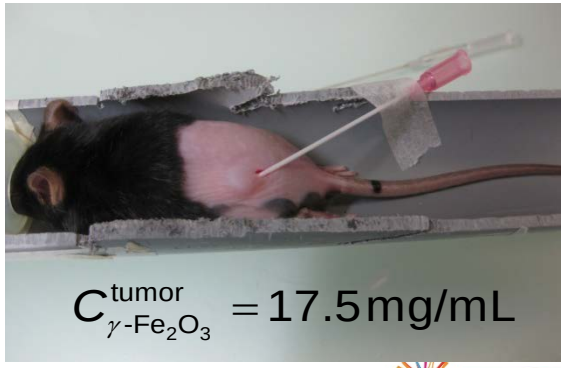

New commercial in vivo MFH setup (nB DM3)

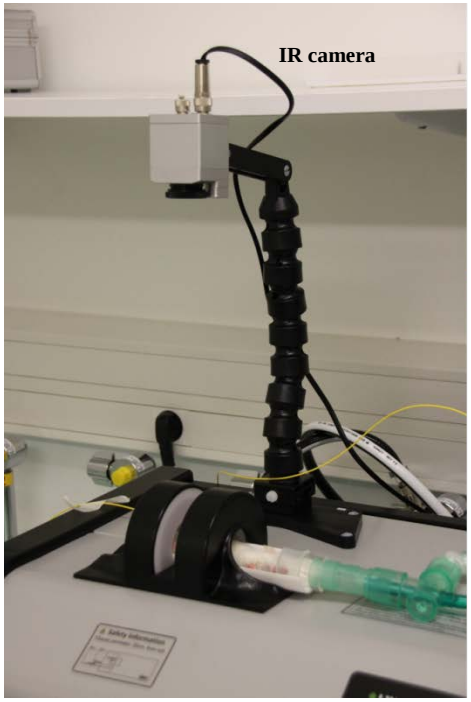

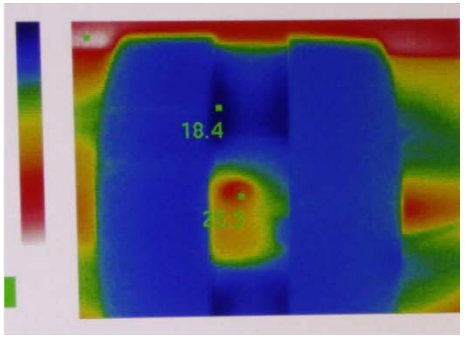

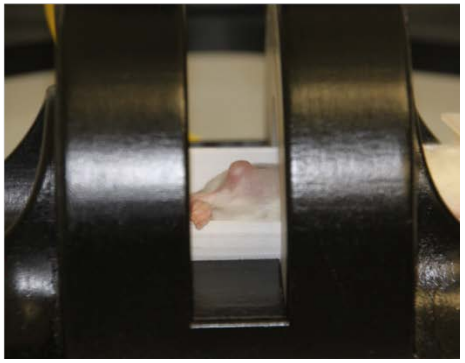

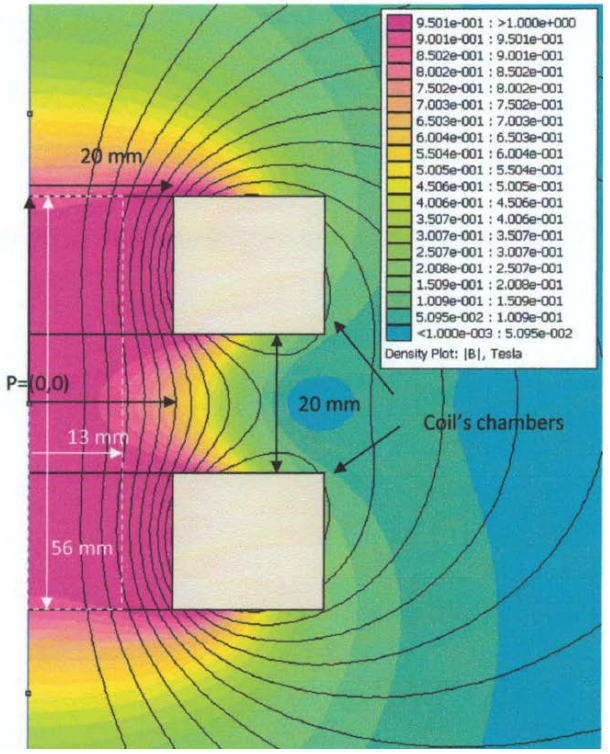

- 146 kHz, 27.6 mT
- 217 kHz, 26 mT
- 344 kHz, 20.4 mT
- 473 kHz, 16.8 mT

nB nanoScale Biomagnetics
Calle Panamá 2, Local 1
50012 Zaragoza
Spain
t. +34 976 741 714
contact@nbnanoscale.com
nbnanoscale.com

Mission interdisciplinarité
Centre national de la recherche scientifique

"défi nano 2014"

RF induction heating for magnetic drug release (magneto-chemotherapy): more gentle process than pure hyperthermia

Thermoresponsive polymer brush-functionalized magnetic manganite nanoparticles for remotely triggered drug release

S. Louguet.. S. Mornet, E. Duguet, S. Lecommandoux, C. Schatz

Polym. Chem., 2012,**3**, 1408

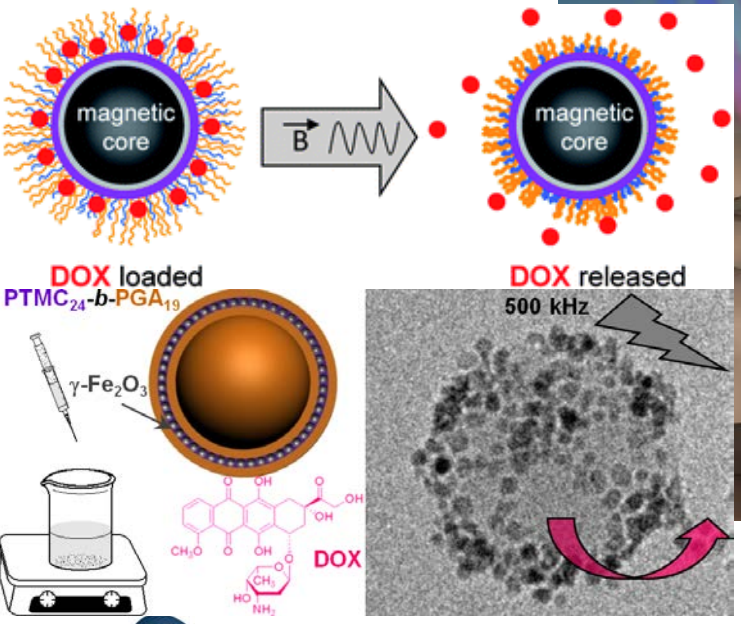

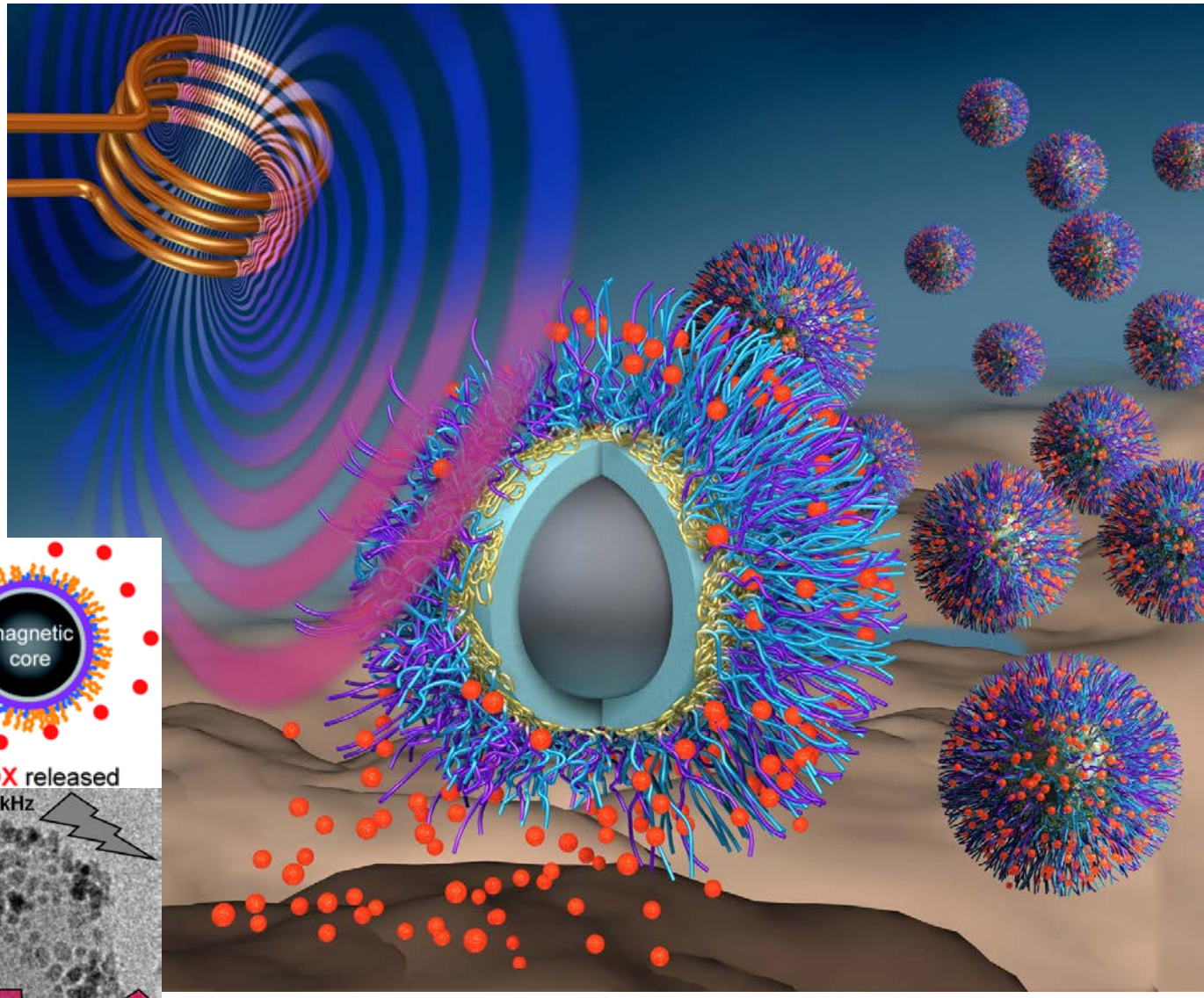

C. Sanson, O. Diou, O. Sandre, S. Lecommandoux, *ACS Nano* 2011, **5** 1122

Drug releasing nanoplatforms activated by alternating magnetic fields

BBA - General Subjects 2017
doi: 10.1016/j.bbagen.2017.02.025

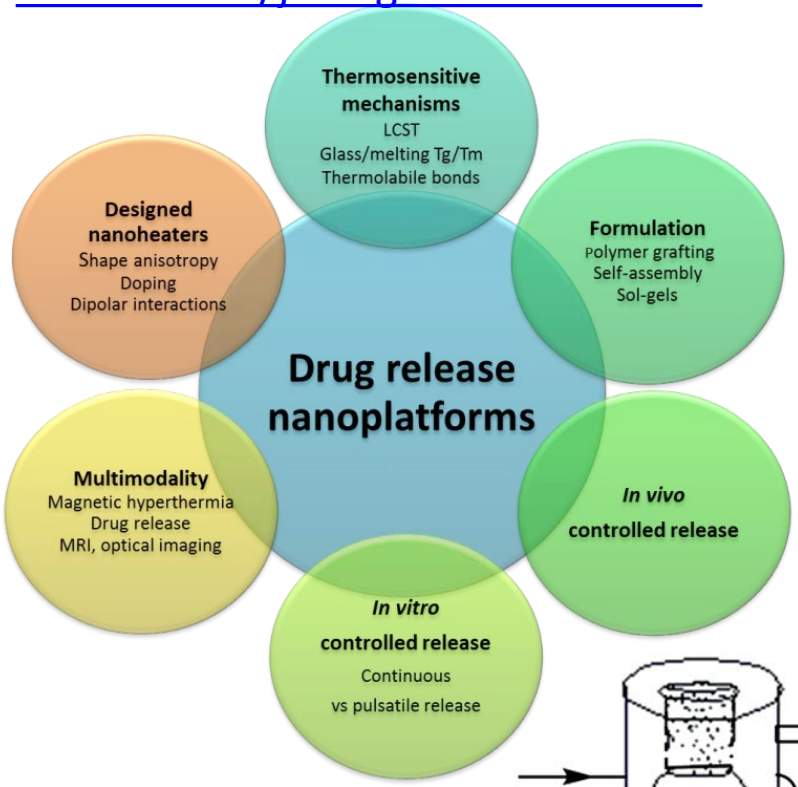

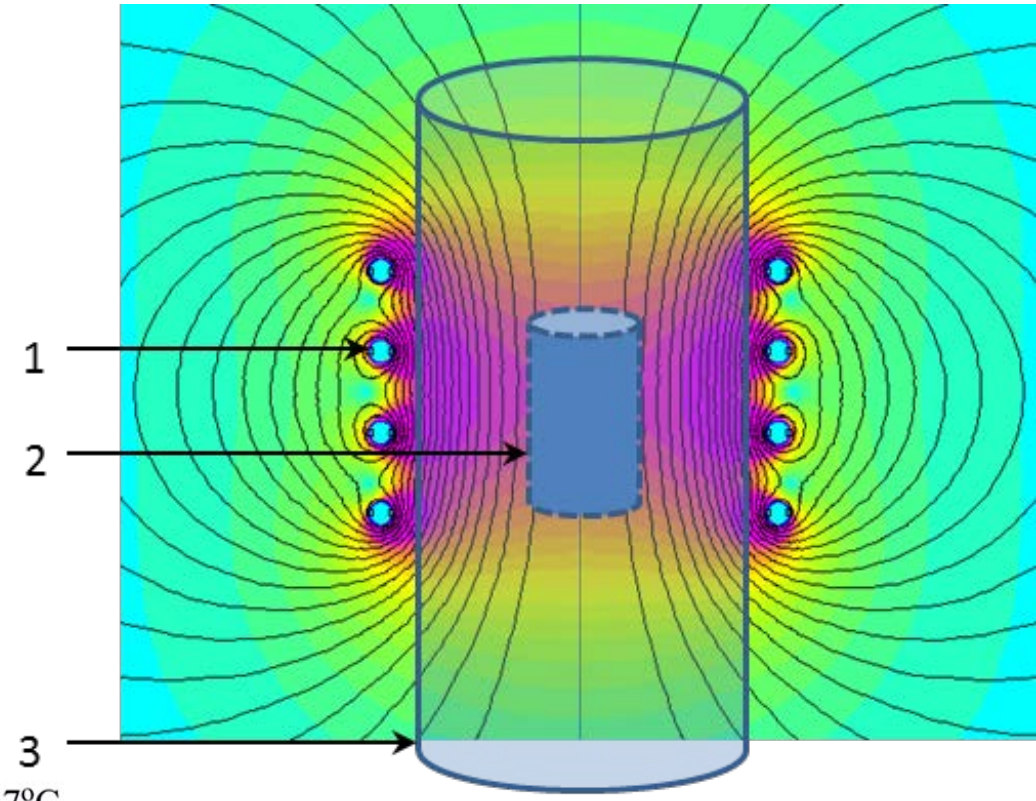

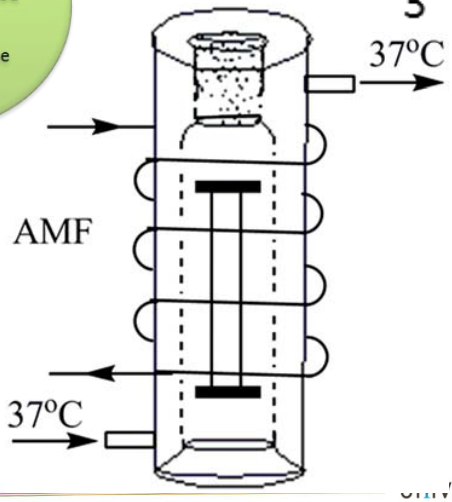

Liu et al, *Nanoscale* 2013, 5, 11464

Setup for model drug release experiment through drug diffusion across semi-permeable membrane

1: Solenoid and calculated magnetic field lines

2: Dialysis bag (e.g. Spectra/Por Float-A-Lyzer™, 50000 $g \cdot mol^{-1}$ MWCO, 10 mm diameter, 5 mL volume)

3: Cylinder (50 mL) filled with aqueous buffer

Usually the drug is titrated in the outer medium, in "sink" and thermostatic (37°C) conditions.

Preparation method of nanosized polymersomes from a rigid ($T<T_g$) or semi-crystalline ($T<T_m$) amphiphilic copolymer

Nanoprecipitation, *e.g.* PS-*b*-PEO, PLA-*b*-PEO, PCL-*b*-PEO…

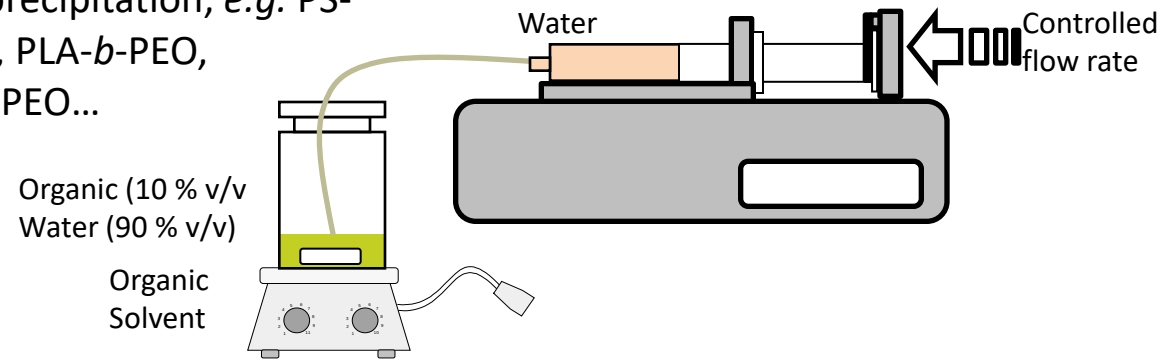

Vs. Direct dissolution (DD) for low T_g blocks: PBA-*b*-PAA, PBD-*b*-PEO, PDMS-*g*-PEO, PEO-*b*-PDMS-*b*-PEO …

(in buffered solution at 50 °C)

self-assembly mechanism called "nanoprecipitation" or "solvent displacement"*

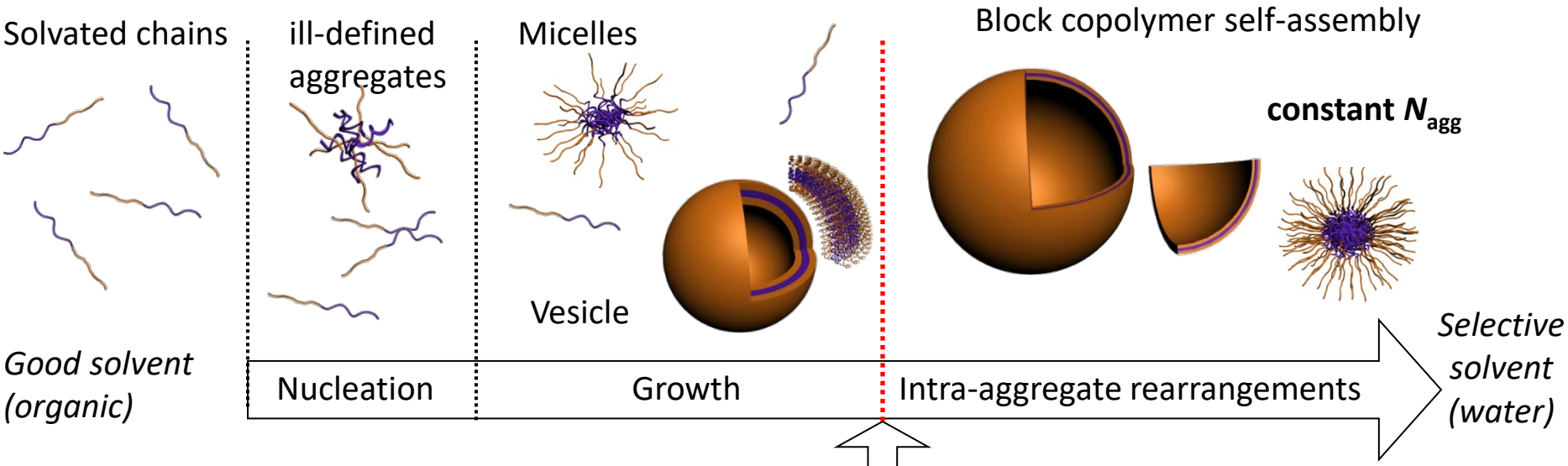

Critical water fraction
End of unimers diffusion

**Johnson et al. Phys. Rev. Lett. 2003*
Lince et al. J. Coll.& Interf. Sci. 2008

Sanson et al, *Langmuir 26 (2010) 2751*

Co-assembly in polymersomes for dual-loading

Self-assembly by “solvent displacement” method (nanoprecipitation)

DMSO*
(or THF/MetOH)
+
copolymer
+
Drug
+
γ-Fe_2O_3@Beycostat

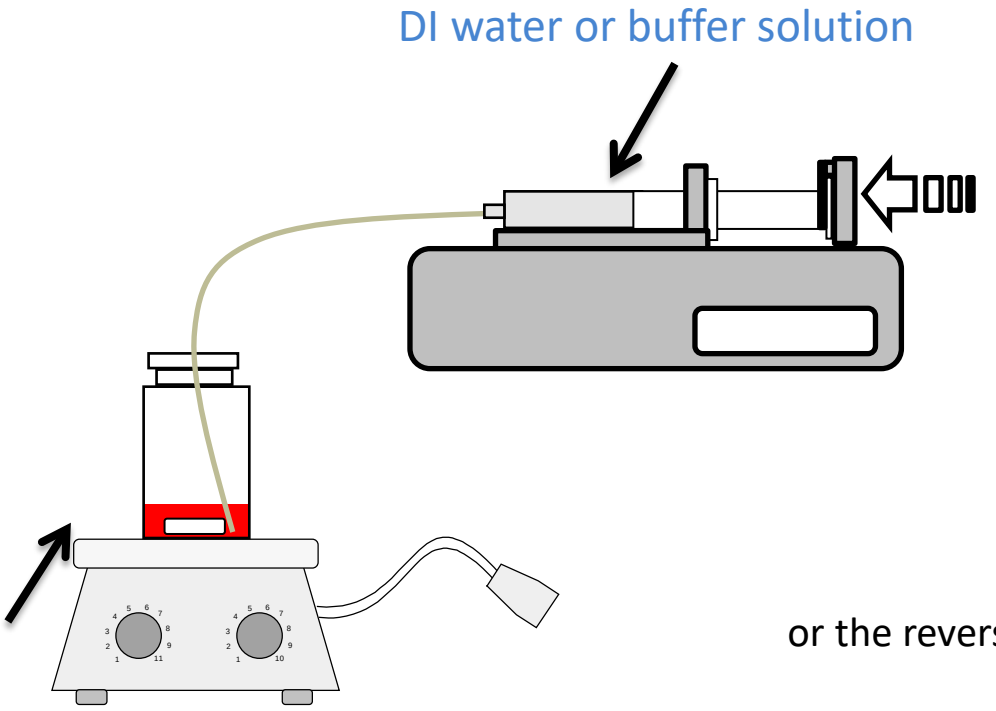

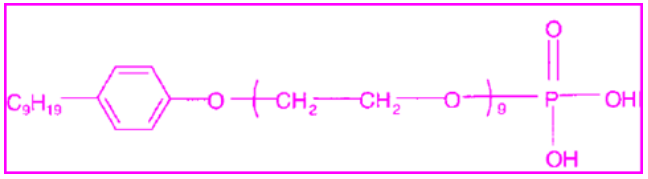

or the reverse (DMSO→H_2O)

+ extended dialysis

* LD_{50} by iv: 2.5-11g/kg (cats, dogs, monkeys, rabbits, mice, rats…)

Sanson et al. *Langmuir* **26**, 2751 (2010); *ACS Nano* **5**, 1122 (2011)

Magnetic micelles and vesicles self-assembled from MNPs and amphiphile diblock “rod-coil” copolymers

Poly(ethylene oxide)-*block*-poly(γ-benzyl-L-glutamate)

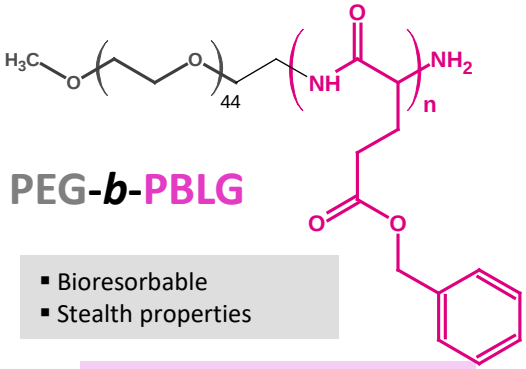

PEG-*b*-PBLG

- Bioresorbable
- Stealth properties

- Bioresorbable
- Synthetic polyaminoacid
- Rigid hydrophobic block
- Rod-like (helical) structure

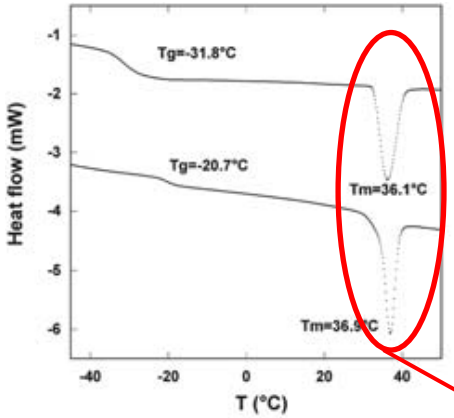

Poly(trimethylene carbonate)-block-poly(L-glutamic acid)

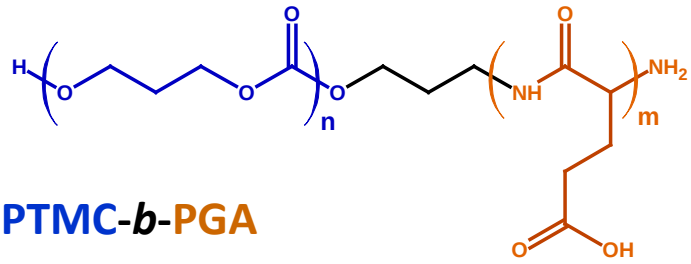

PTMC-*b*-PGA

- Bioresorbable
- Semi-crystalline for M_n < 12 000 g/mol :

Melting at $T_m \approx 37°C$

- Synthetic polyaminoacid
- Bioresorbable
- pH responsive
  → 2ndary structure transition

Sanson et al. *Langmuir* **26**, 2751 (2010); *Soft Matter* **6**, 1722 (2010); *J. Contr. Rel.* **147**, 428 (2010); *ACS Nano* **5**, 1122 (2011)

Micelles

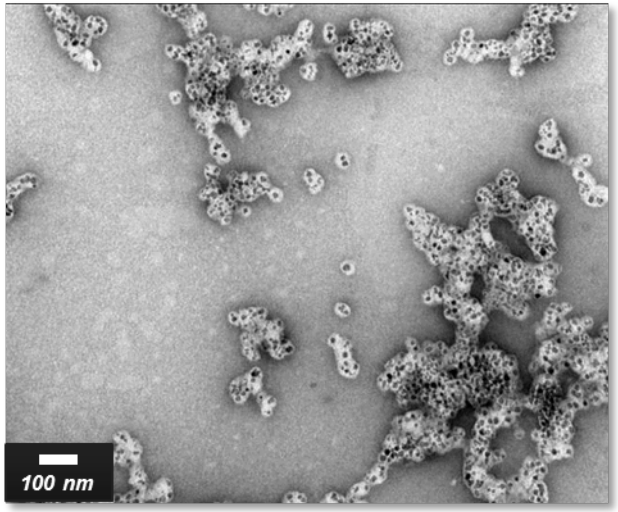

$$\Phi_{intra} = N^{USPIO}_{/object}\left(\frac{2R_G}{D_{USPIO}}\right)^3$$

$2R_G = 0.775 D_H$

Vesicles

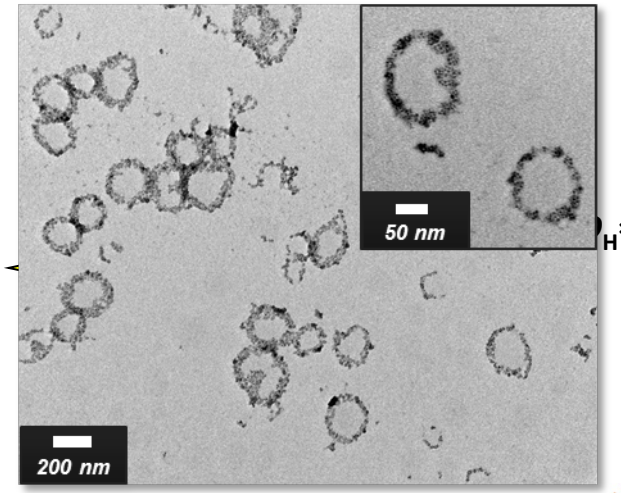

$D_H \approx 200nm$

P. Arosio et al. *J. Mater. Chem.* B 2013, 1, 5317-5328

Magnetic polymer vesicles: structural study

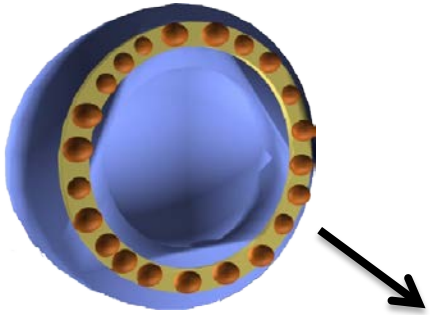

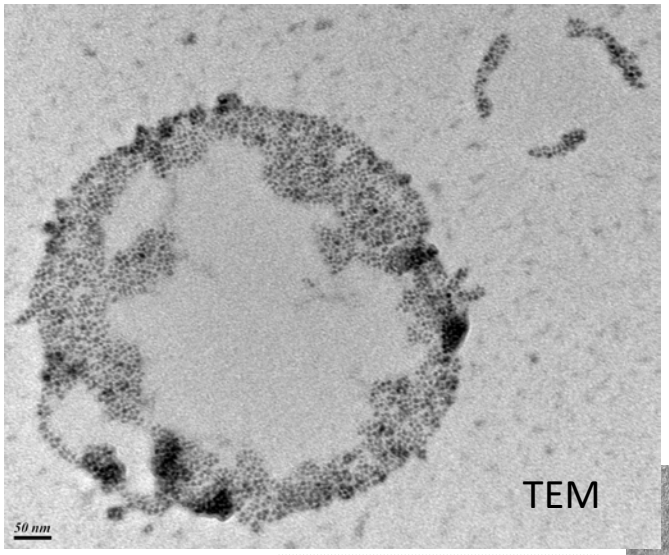

C. Sanson et al *ACS Nano* **5**, 1122 (2011)

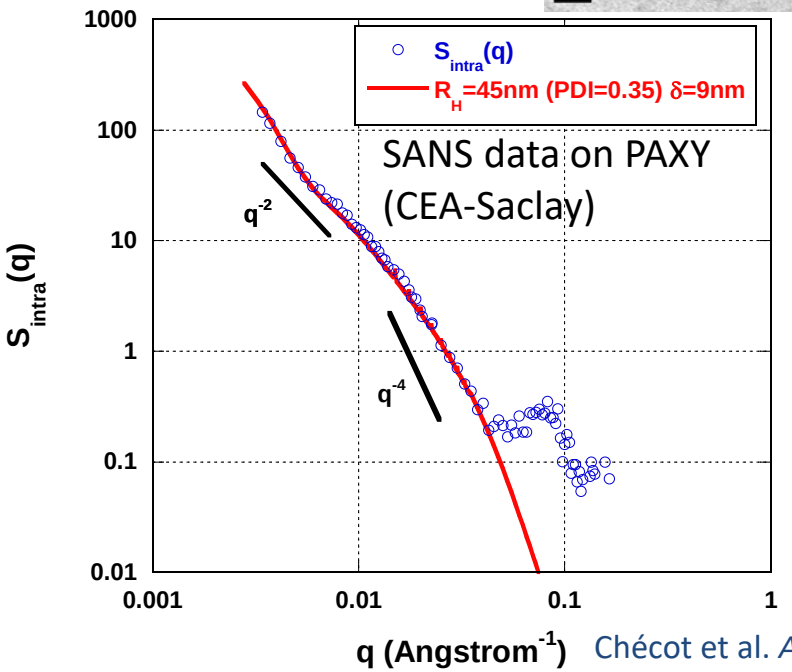

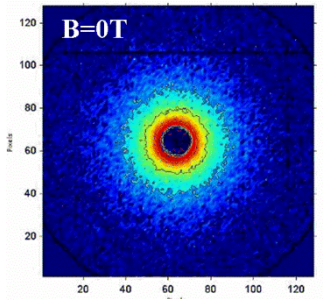

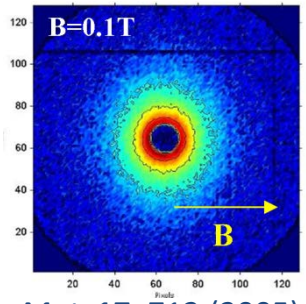

Chécot et al. *Adv. Mat.* **17**, 712 (2005)

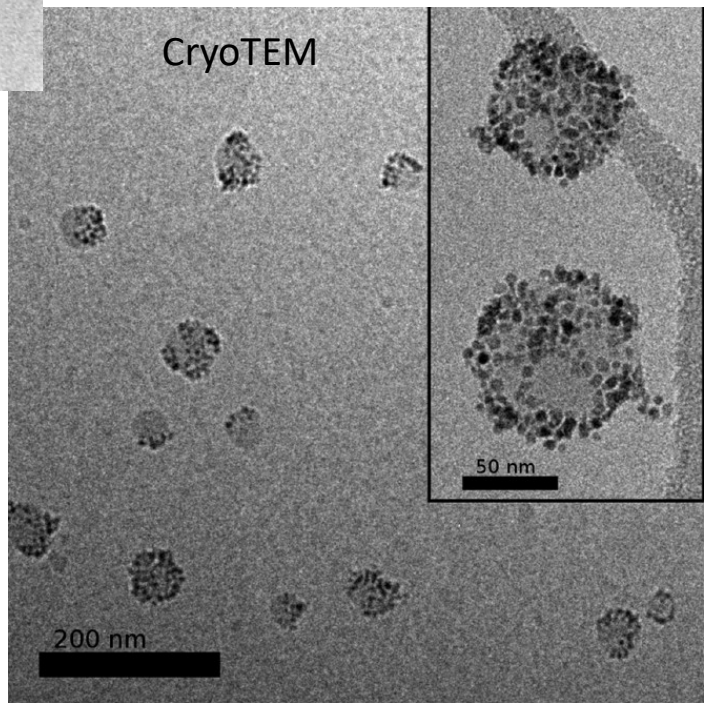

A. Brisson, CBMN

Magnetic guiding of PTMC-b-PGA vesicles under B gradient

Optical video microscopy under magnetic field gradient

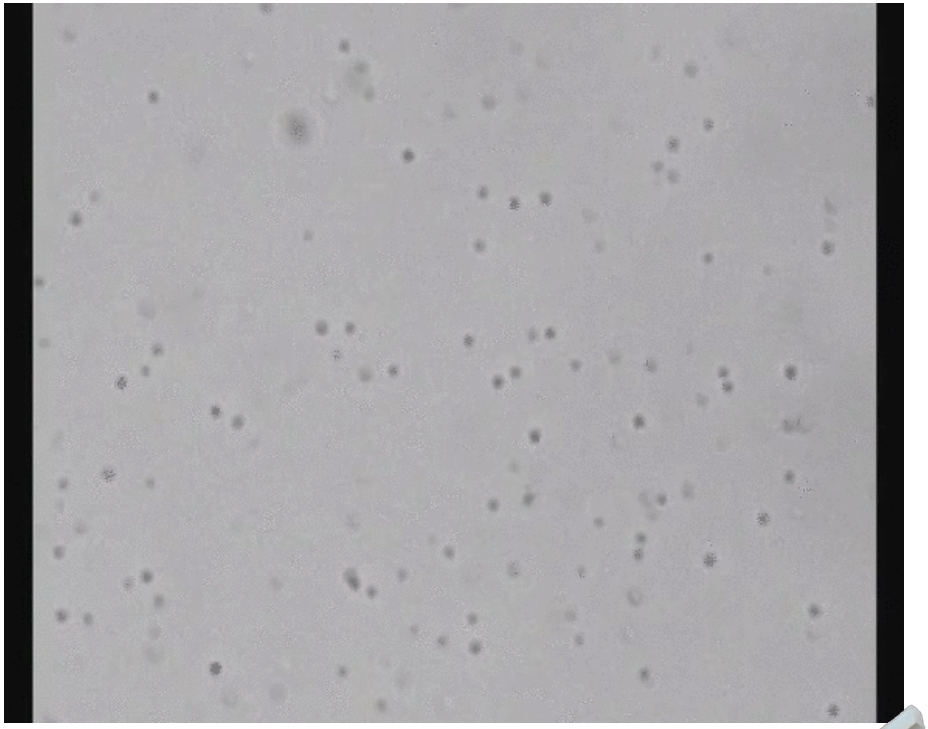

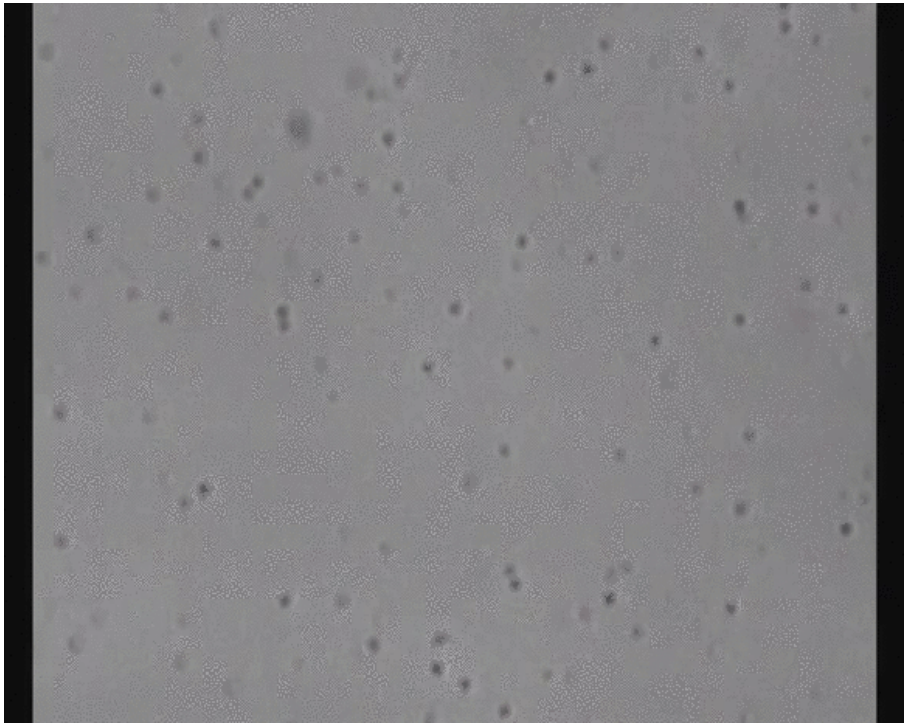

Magnetic guiding of PTMC-b-PGA vesicles under B gradient

Optical video microscopy under magnetic field gradient

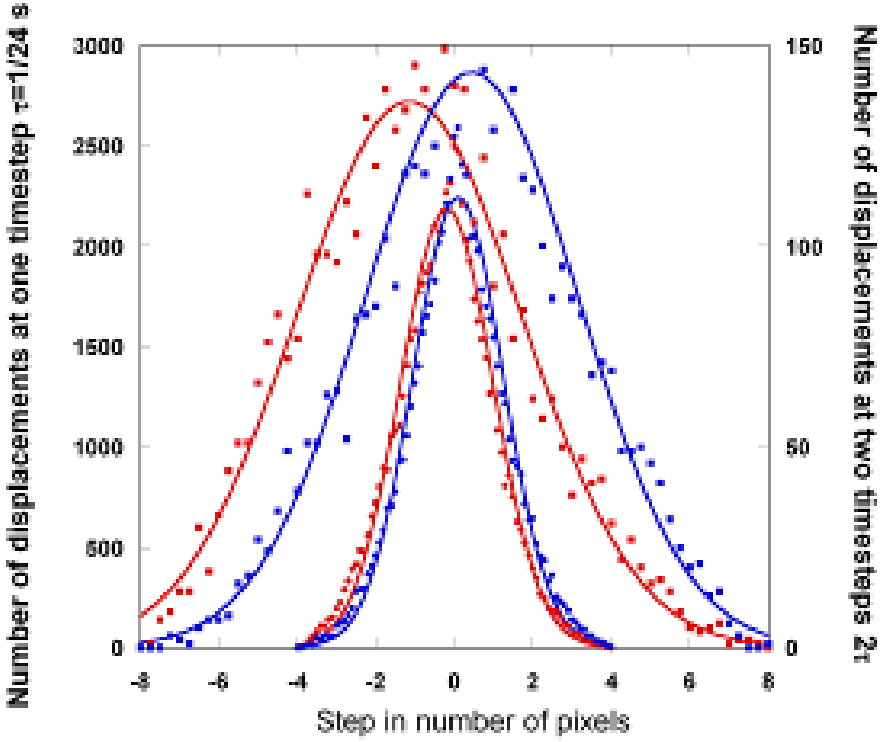

δx, δy increments every τ=40ms

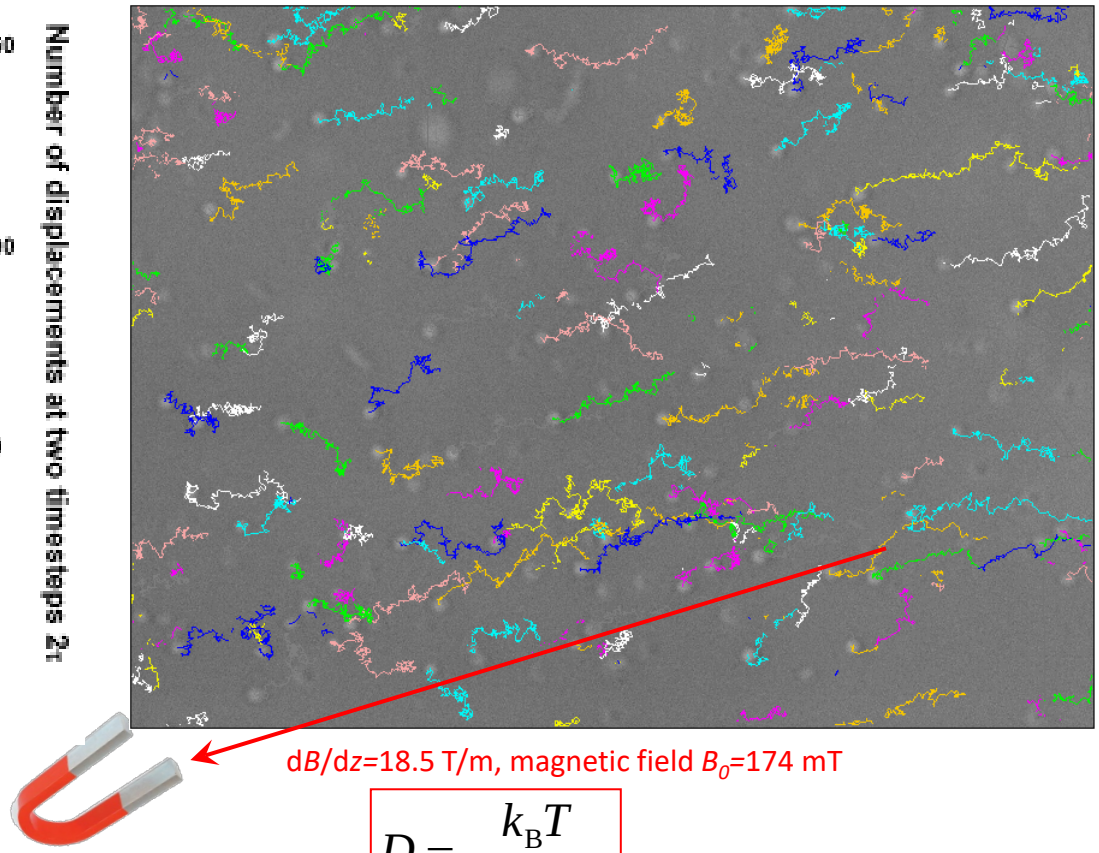

dB/dz=18.5 T/m, magnetic field B_0=174 mT

$$D = \frac{k_B T}{6\pi\eta R_h}$$ Stokes-Einstein

Brownian width: $\sigma_{x/y}(\tau) = \sqrt{2D\tau}$ ➲ Diffusion constant $D_x = D_y = 1.11\,\mu m^2/s \longrightarrow R_h = 196\,nm$

Linear drift motion: $V_{x/y} \times \tau$ ➲ Experimental magnetophoretic mobility ***V* = 1.09 µm/s**

SPIONs particles for all bio-related properties: MRI, tumor homing & hyperthermia / magnetic drug release

T_2 relaxivity

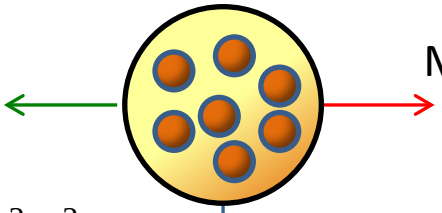

Magnetophoretic mobility

$$r_2\,\Phi_{intra} = \frac{R_2}{[Fe]} = \frac{2}{405}\,\frac{M_{Fe_2O_3}}{\rho_{Fe_2O_3}}\,\frac{\gamma^2\mu_0{}^2 M_v^2 d^2}{D}$$

$$\vec{F}_v = 3\pi\,\eta\,d\,\vec{v}$$

$$\vec{F}_m = \mu_0\,\chi\,\vec{\nabla}_z\left(\tfrac{1}{2}H_0^2\right)\tfrac{\pi}{6}\,d^3$$

$$M_v = \Phi_{intra} M_{spe}$$

at high field: B_0>0.94T (f>40MHz)

$$\chi = \frac{\mu_0\,\pi}{18 k_B T}\,\Phi_{intra} M_{spe}^2\, d_{core}^3$$

at low field: B_0<0.1T
but high field gradient: ∇B_0=10-100T/m

$$r_2 = 11.6\times10^{-12}\,\Phi_{intra} M_{spe}^2\, d^2$$

$$\frac{v_{mag}}{\vec{\nabla}_z\left(\frac{1}{2}B_0^2\right)} = \frac{\pi\, d_{core}^3}{(18)^2\,\eta\, k_B T}\,\Phi_{intra} M_{spe}^2\, d^2$$

For a given batch of USPIOs (M_{spe} and distribution of d_{core} sizes), the design of clusters of controlled geometry (Φ_{intra} and d) enables to tune both MRI contrast and guiding properties

Both parameters (r_2 and v_{mag}) can be measured by MRI, as in A. Ionescu et al. *Nanotechnology* 19 (2008) 395102: d_{core}=9.6nm, d=12µm, Φ_{intra}=0.6, M_{spe}=2.35×10^{5}A/m, η=10^{-3}Pas, T_2*=50µs, [Fe]=48g/L≡600mM→r_2=33s^{-1}/mM$_{Fe}$, B_0=7T, ∇B_0=1.21T/m, v_{mag}=5×10^{-4}m/s

Magnetic vesicles as negative MRI contrast agents

Relaxation rates (r2=(1/T2)) versus iron concentration

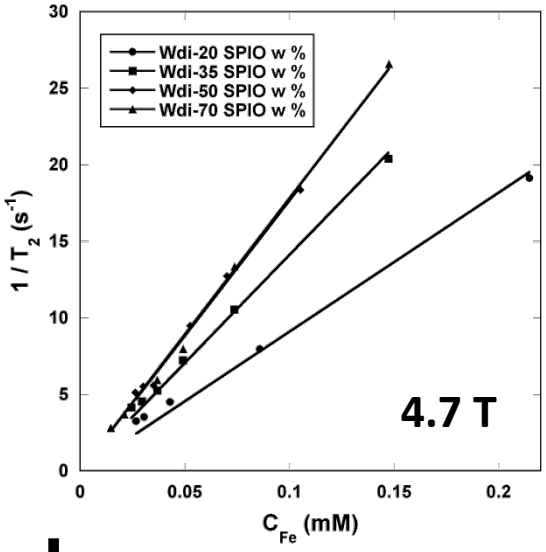

Wt % SPIO	r2 (Fe.mM^{-1}.s^{-1})
20	85
35	141
50	177
70	178

Vesicles with 70 wt % SPIO at different dilution factors

[Fe] (µM)	H_2O	21	37	49	74	148
[copo] (µg/mL)	H_2O	2.9	5	6.7	10	20
	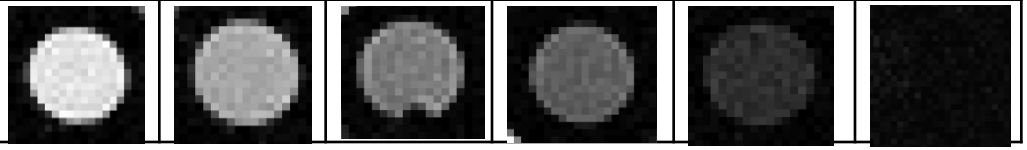					

MR detection limit: copolymer concentration at which the MRI signal intensity decreases to 50 % of that of pure water

➲ 0.6 nM vesicle concentration

For comparison, threshold for PCL-*b*-PEG micelles loaded with 16 nm Fe_3O_4 NPs
→ 5 nM (***Gao et coll. Adv. Mat. 2005)***

➲ **r2 increases with SPIO loading content**

➲ **Good T2 contrast agent for MRI**

Collaboration with RMSB:
Line Pourtau, Sylvain Miraux, Eric Thiaudière

C. Sanson et al, *ACS Nano* 5, 1122 (2011)

Antibody-functionalized magnetic polymersomes: in vivo targeting and imaging of bone metastases using high resolution MRI

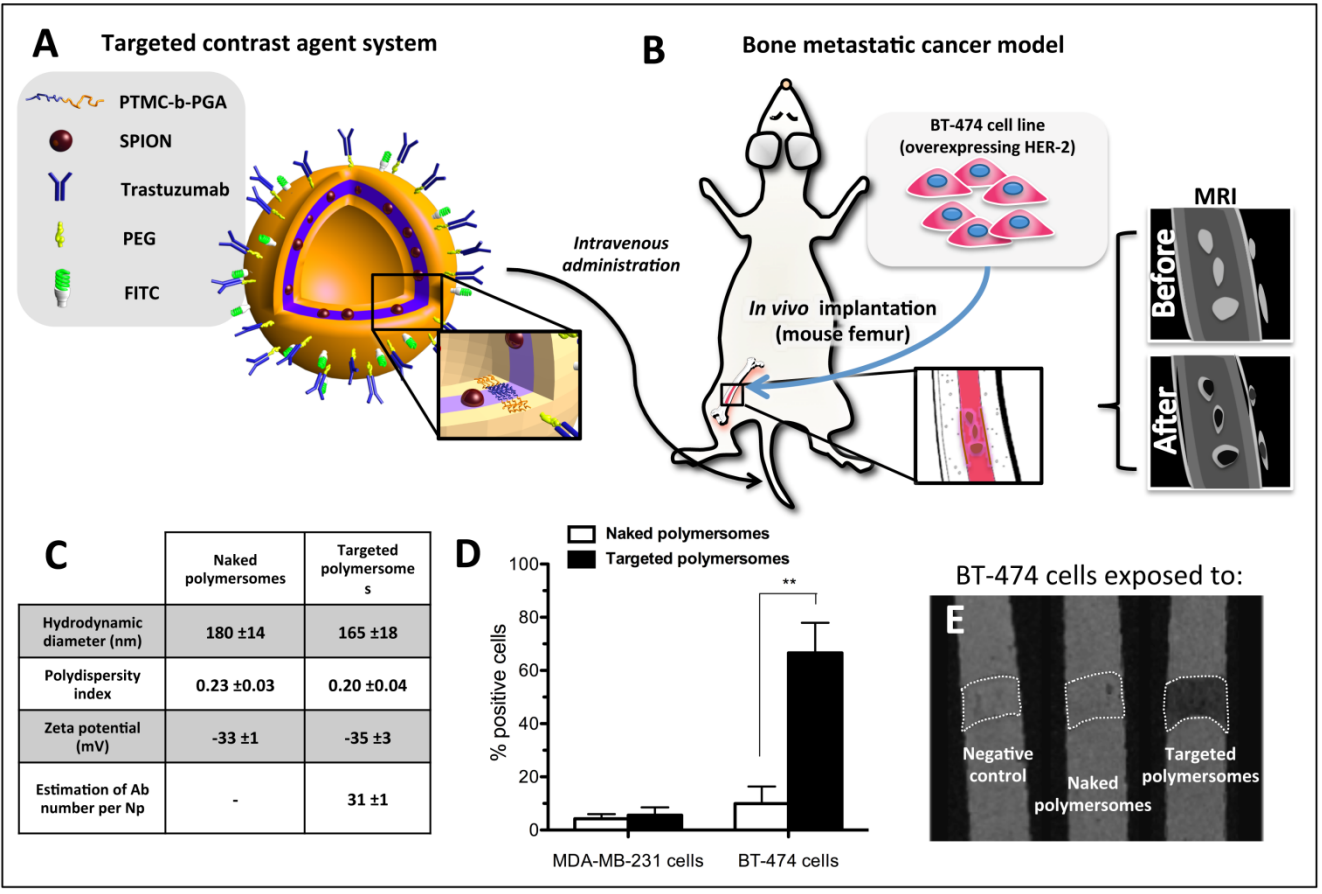

C

	Naked polymersomes	Targeted polymersomes
Hydrodynamic diameter (nm)	180 ±14	165 ±18
Polydispersity index	0.23 ±0.03	0.20 ±0.04
Zeta potential (mV)	-33 ±1	-35 ±3
Estimation of Ab number per Np	-	31 ±1

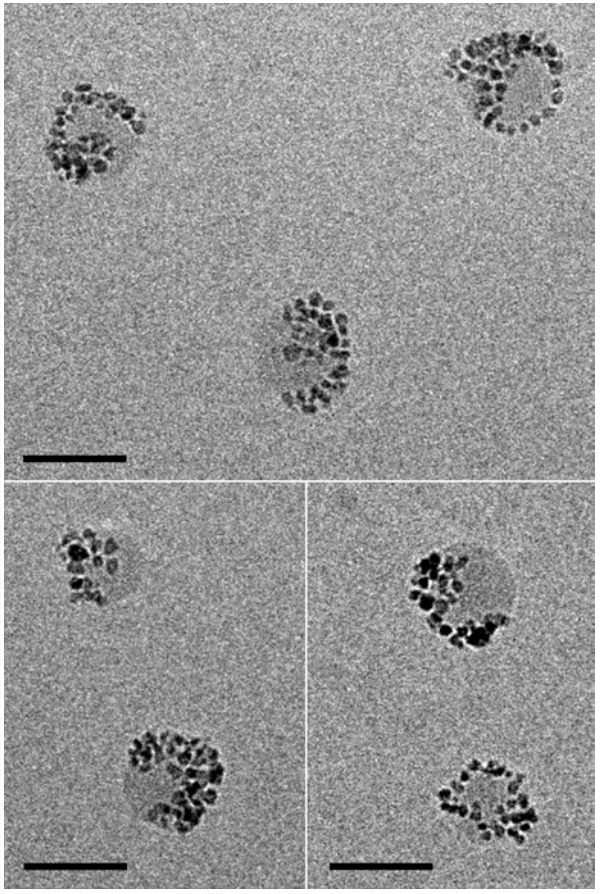

L. Pourtau, H. Oliveira, J. Thévenot, Y. Wan, A. Brisson, O. Sandre, S. Miraux, E. Thiaudière, and S. Lecommandoux, *Advanced Healthcare Materials*, 2013, 2, 1420–1424

In vitro tumor targeting efficacy

Cell internalization by FACS

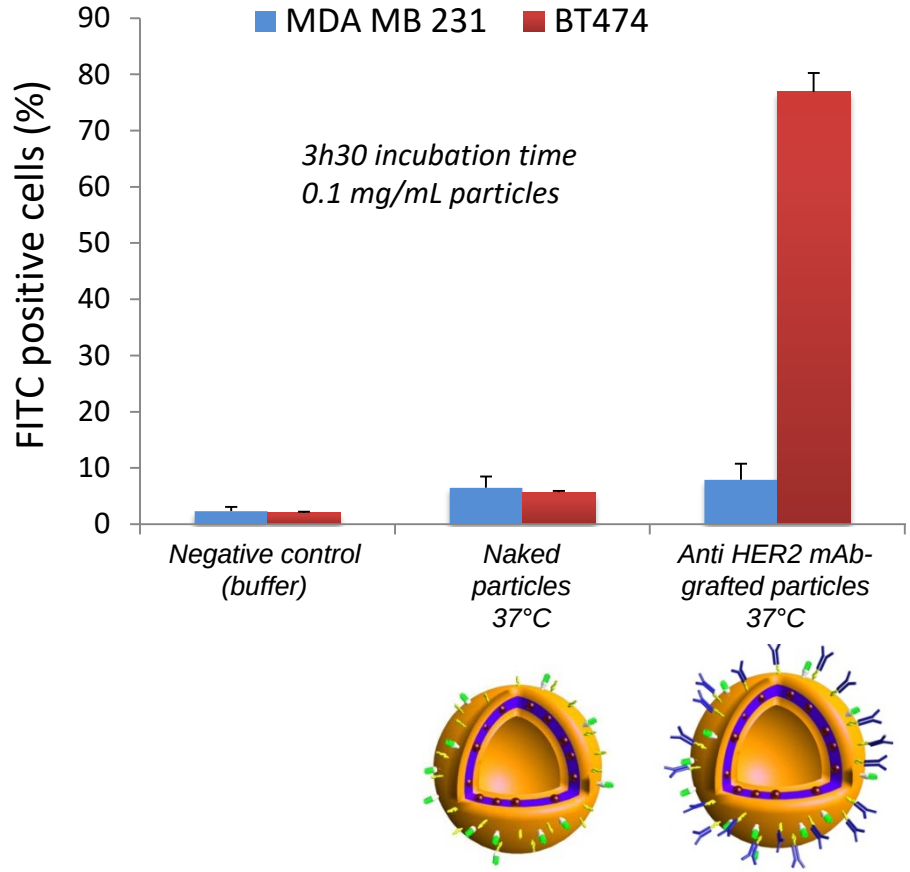

Breast cancer cell lines:

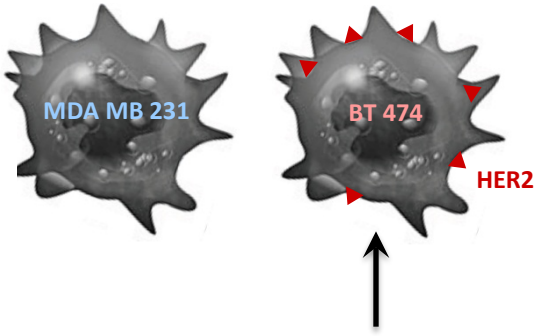

Overexpress HER2
(Human Epidermal Growth Factor Receptor-2)

Internalization ↗ by targeting in HER2 positive cells

In vitro tumor targeting efficacy

Cell internalization by MRI

24h incubation time
0.2 mg/mL particles

↓

washing

↓

Cells embedded into a gel and imaged by MRI

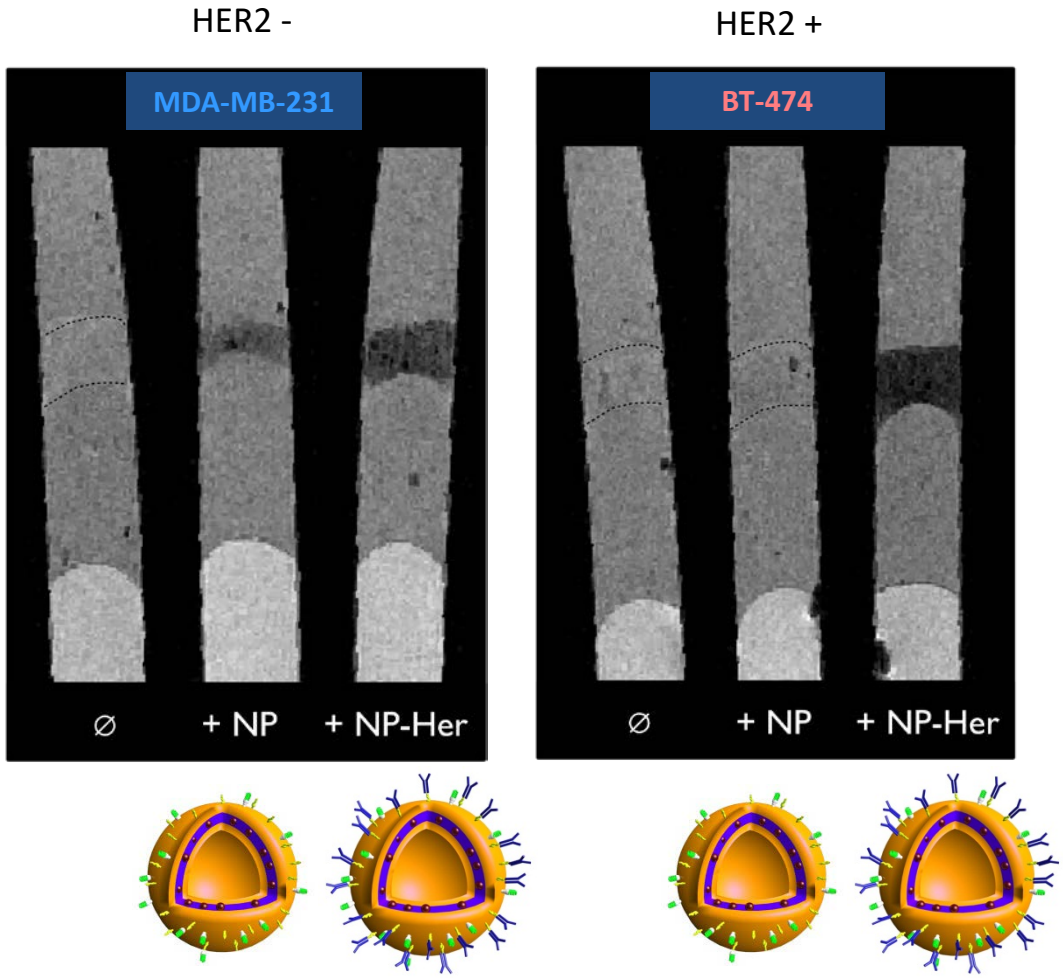

⇨ **Both methods (FACS and MRI) confirm the specific internalization of antibody-bearing polymersomes in HER2 positive cells**

Bio-distribution / Pharmacokinetics of magnetic polymersomes by MRI

L. Pourtau, H. Oliveira, J. Thévenot, Y. Wan, A. Brisson, O. Sandre, S. Miraux, E. Thiaudière, S. Lecommandoux, *Advanced Healthcare Materials*, 2013, 2, 1420–1424

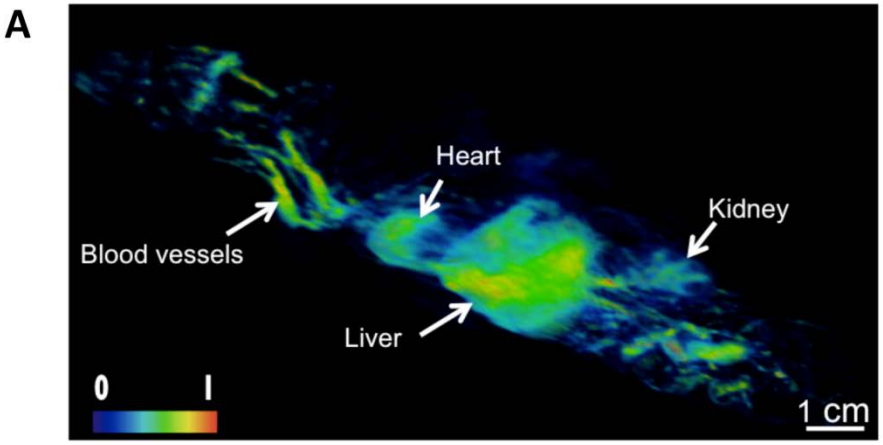

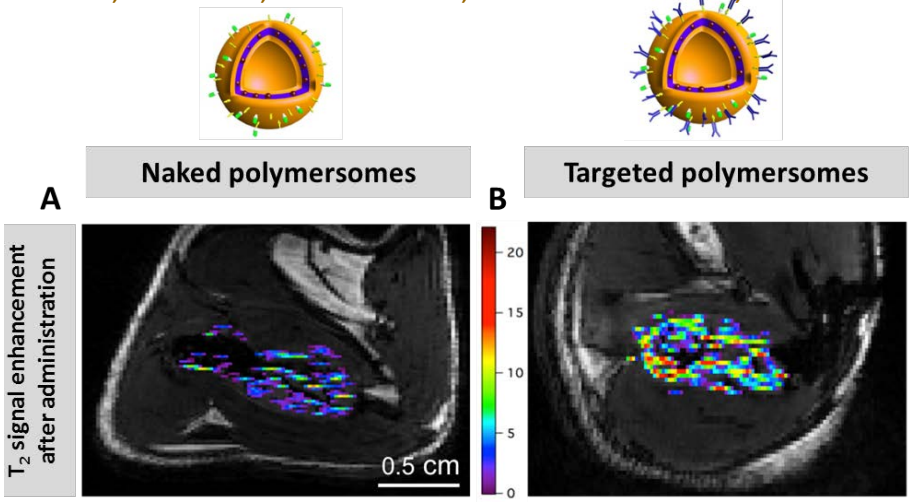

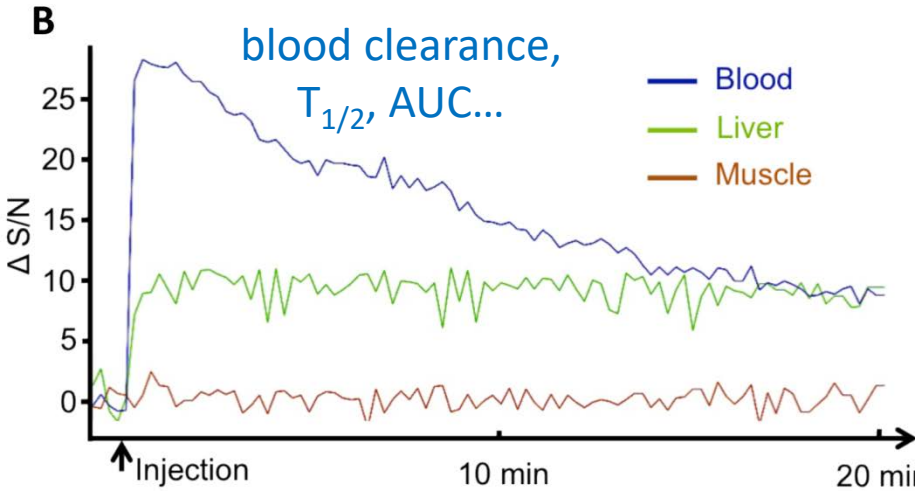

Real time 3D MR imaging at 4.7 T of the distribution of hybrid polymersomes after *iv* injection of a 100 µL bolus of contrast agent at a dose of 250 µmol Fe/kg (15 mg/mL copolymer) injected in the mouse tail vein.

Targeting of bone metastasis.

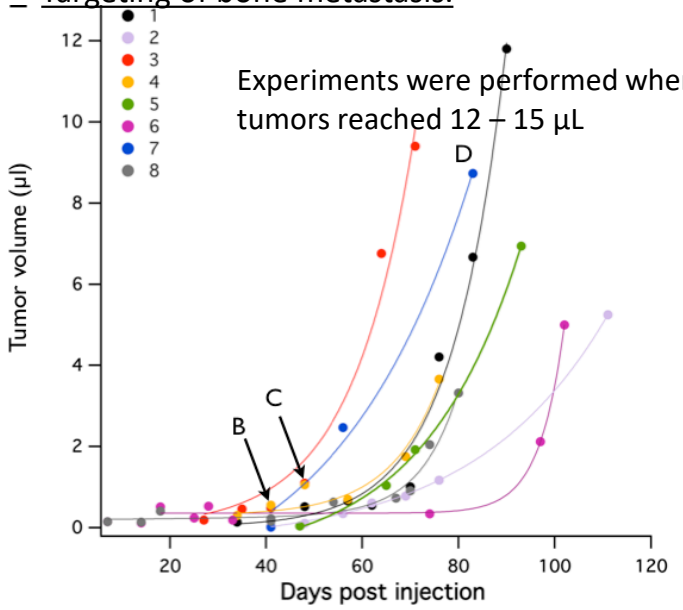

Dual loaded polymers with the anthracycline anticancer drug doxorubicin (up to 30 wt%) and USPIOs (up to 70 wt%)

Doxorubicin-loaded PTMC-b-PGA polymersomes

- **Incorporation during the nanoprecipitation process (DOX in DMSO)**
- **Optimal loading with carbonate buffer pH 10.5**

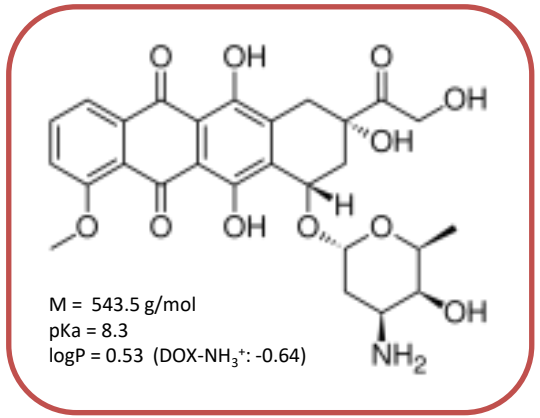

hematological cancers, carcinoma, sarcomas…
free drug or as liposomal formulation (Doxil™)

$PTMC_{24}$-*b*-PGA_{15}
+ 6-7nm γ-Fe_2O_3 USPIOs

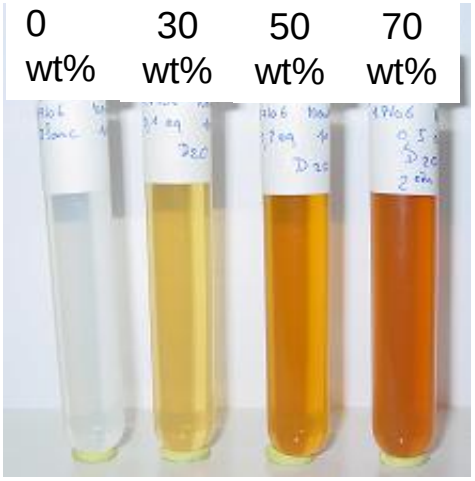

Loading content (LC) up to 70 wt% (12 vol%) USPIOs without size change

$PTMC_{24}$-*b*-PGA_{15}
+ 50 wt% 6-7nm USPIOs
+ DOX

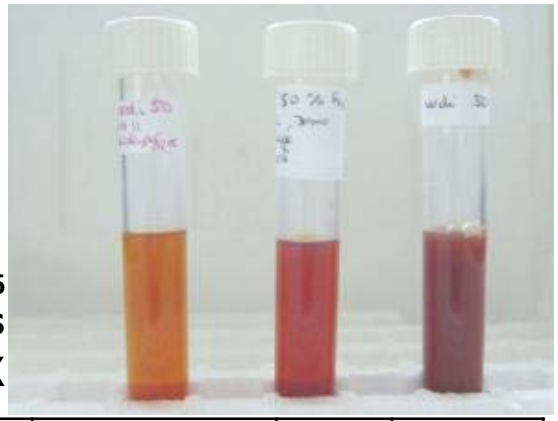

wt_{dox}/wt_{copo} (%)	D_h^{Contin}(nm)	PDI	Zeta (mV)
0	113	0.22	-40.8
20	122	0.15	-42
30	274	0.20	NA

RF induction heating for drug release (magnetochemotherapy): latest assays "in cellulo" (magneto-cytotoxicity)

H. Oliveira et al, *J. Contr. Rel.* 2013 169(3), 165-170

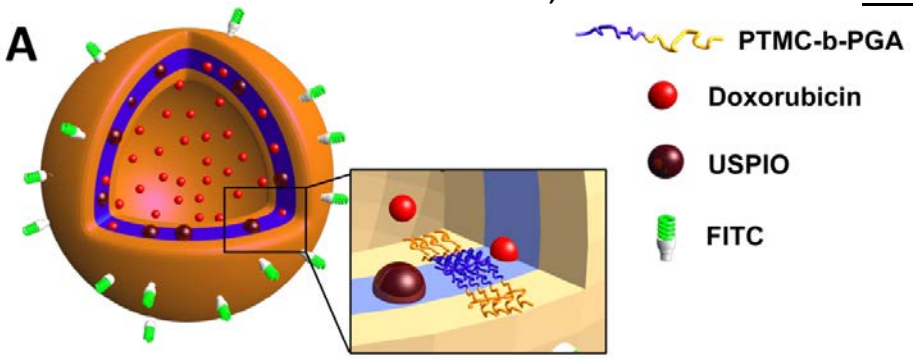

Vesicles loaded at 6±1% doxorubicin, size: 192 nm (pdi=0.1)

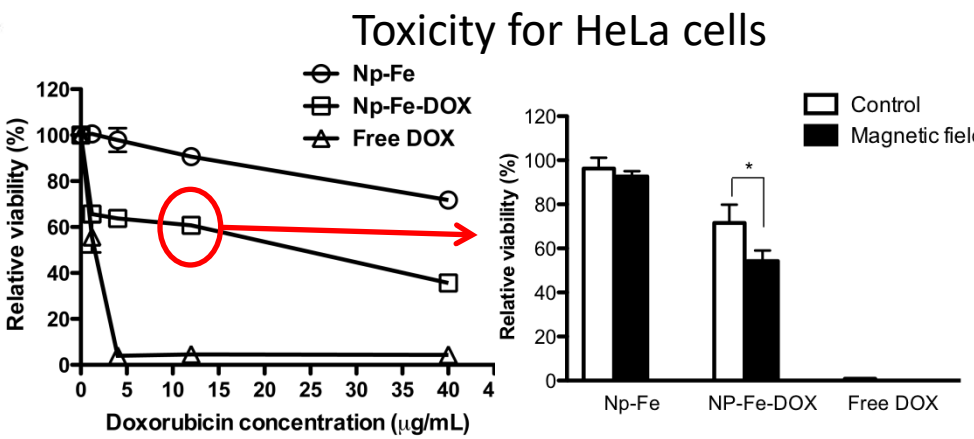

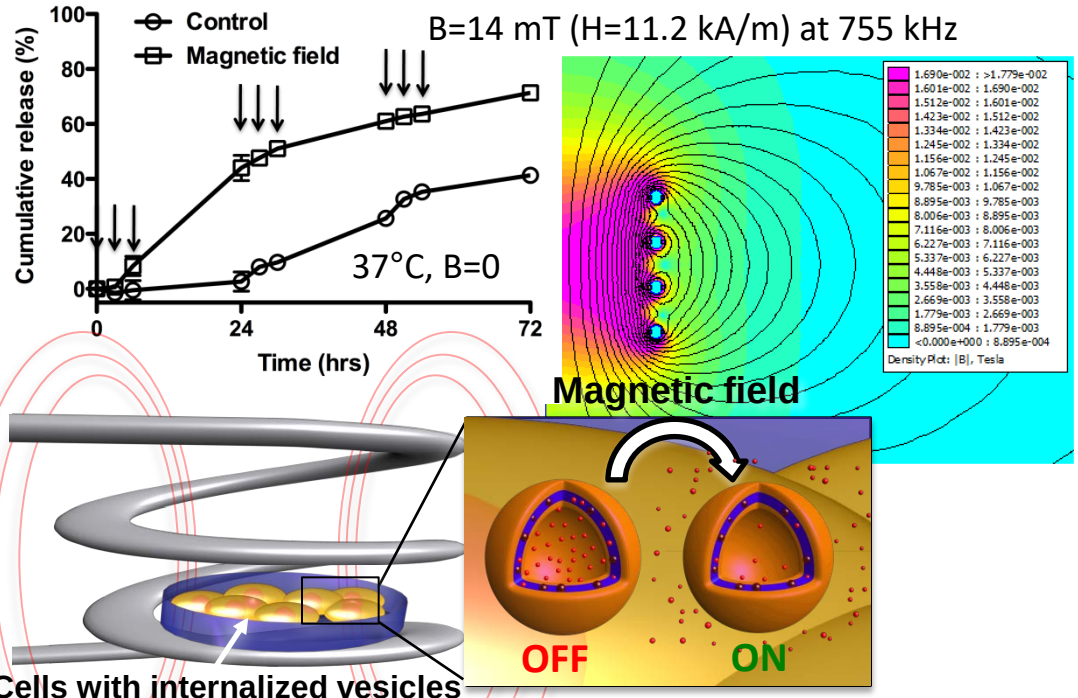

H. Oliveira (postdoc) in front of the "magnethermon" at CIC biogune (Bilbao)

LCPO
Laboratoire de Chimie des Polymères Organiques

Thank you for you attention

o CNRS-MI

Mission interdisciplinarité
Centre national de la recherche scientifique

"défi nano" (2012, 2014-2015)

o Cancéropôle GSO

Cancéropôle Grand Sud-Ouest

Bordeaux ● Limoges ● Montpellier ● Nîmes ● Toulouse

o C'Nano GSO

NanoSciences GRAND SUD - OUEST

€

o National Science Foundation

NSF

France/Belgium iREU in Translational Chemistry

Louis Stokes Alliances for Minority Participation

o Agence Nationale de la Recherche

"MagnetoChemoBlast" (2013-2017)

AGENCE NATIONALE DE LA RECHERCHE
ANR

o Europe

http://cost-radiomag.eu/

cost
TD1402 - RADIOMAG

"Multifunctional Nanoparticles for Magnetic Hyperthermia and Indirect Radiation Therapy"

EU networking: COST Action TD1402 RadioMAG

"Multifunctional Nanoparticles for Magnetic Hyperthermia and Indirect Radiation Therapy"

http://cost-radiomag.eu/

21 countries

Management Committee

Core Group

WG 5
Public relations

WG 1
Physical chemistry:
fabrication
coating / targeting

WG 2
Physical MH aspects:
standardisation
testing

WG 3
Radiosensitation & MH:
pre-clinical / clinical aspects

WG 4
Instrumentation:
thermometry & development of MH devices

Roadmap:

- Better design of nanoparticles for *in vivo* hyperthermia
- Standardize SAR measurement
- *In vivo* assays: pre-clinical and towards clinical trials
- Temperature mapping (intra-tumoural)